

https://dspace.org/

PD characteristics of typical MV XLPE power cable termination defects at VLF and power frequency test voltages

Fynes-Clinton, Daniel

2016-10-11
http://hdl.handle.net/10539/21149

Downloaded from a DSpace repository. https://dspace.org/

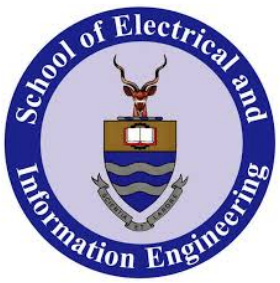

MSc (Engineering) Research Report

PD Characteristics of Typical MV XLPE Power Cable Termination Defects at VLF and Power Frequency Test Voltages

Daniel Fynes-Clinton

A research report submitted to the Faculty of Engineering and the Built Environment, University of the Witwatersrand, in fulfilment of the requirements for the degree of Master of Science in Engineering.

The financial assistance of the National Research Foundation (NRF) towards this research is hereby acknowledged. Opinions expressed and conclusions arrived at, are those of the author and are not necessarily to be attributed to the NRF.

Johannesburg, June 1, 2016

DECLARATION

I declare that this research report is my own unaided work. It is being submitted for the Degree of Master of Science to the University of the Witwatersrand, Johannesburg. It has not previously been submitted for any degree or examination to any other university.

Daniel Fynes-Clinton	Date

ABSTRACT

It has been reported in literature that newly installed cable accessories can pass typical commissioning tests and yet show significant PD activity leading to premature failure in the long term. This research report details the partial discharge (PD) characterisation of three artificial defects in MV cable terminations, at both power and very low frequency (VLF). The defects included a semi-conductor feather, a tram line in the cross-linked polyethylene (XLPE) insulation and an XLPE ring cut. The experimental methodology involved subjecting the terminations to a standard overvoltage withstand test, after which the PD activity was monitored, at 0.1 Hz and at 50 Hz excitation frequencies. All the defects passed the overvoltage test, despite some showing significant discharges. The defects gave distinct phase-resolved PD patterns that are effectively invariant of excitation frequency. The PD magnitudes at power frequency were typically bigger than at VLF, while the PD inception voltages tended to be lower at VLF. The PD magnitudes of the semi-conductor feather defect surface discharges were found to increase with increasing applied voltage, while no increase was observed for the tram line and ring cut void discharges. The results show that common installation defects in MV cable terminations can be suitably characterised using VLF PD measurements.

To my parents, family and girlfriend, without whom this work would not have been possible.

ACKNOWLEDGEMENTS

The author would firstly like to acknowledge and thank Prof. Cuthbert Nyamupangadengu for his supervision and support given to this project, despite many other commitments.

Gratitude is given to Eskom for their support of the High Voltage Engineering Research Group at Wits University through TESP. The author would also like to express gratitude to the Department of Trade and Industry (DTI) for THRIP funding and to thank the National Research Foundation (NRF) for direct funding of the research group and this project. Furthermore, the author would like to acknowledge funding received from SITA, through their corporate social responsibility programme investment in the University of the Witwatersrand.

In terms of support for this particular research, the author would like to thank Powertech System Integrators and Aberdare Cables for their contribution to this work, in terms of training, donations of terminations and cables, as well as technical support throughout this research. In particular, the author would like to thank Khakhane Motaung, Henni Scholtz and Isak Hattingh for their individual contributions in assisting this work.

Furthermore, the authors would like to acknowledge the donations of cables by B&W Instrumentation and Electrical, RWW Engineering and training provided by HV Test. Particular mention should be given to Mr Ron Goodwin (HV Test) for his advice regarding this research.

Contents

DECLARATION i

ABSTRACT ii

ACKNOWLEDGEMENTS iv

LIST OF FIGURES viii

LIST OF TABLES x

LIST OF SYMBOLS xi

1 INTRODUCTION 1

1.1 Problem Statement 3

1.2 The Research Methodology 4

1.3 Research Report Structure 4

2 BACKGROUND AND LITERATURE REVIEW 6

2.1 Electric Fields in Power Cables 6

2.2 Partial Discharges 10

2.2.1 Void Discharges 11

2.2.2 Surface Discharges 12

2.2.3 Corona Discharges 12

2.2.4 PD Testing 15

2.3 Cable Accessory Defects 17

2.4 PD Testing of Cable Accessory Defects 17

2.5 Summary 23

3 EXPERIMENTAL WORK METHODOLOGY 25

3.1 Sample Preparation 25

3.1.1 Type of Defects 26

3.2 PD Measurement Experimental Setup and Procedure 29

3.2.1 Overvoltage and PD Testing 29

3.2.2 Comparative PD Testing at 0.1 Hz and 50 Hz Test Voltages 34

3.3 PD Data Analysis Techniques 35

3.4 Electric Field Simulations in the Cable Terminations 36

3.5 Summary 38

4 RESULTS, ANALYSIS & DISCUSSION 39

4.1 Simulation Results: Electric Fields in the Terminations 39

4.1.1 Healthy Terminations Electric Field Distribution 39

4.1.2 Semi-conductor Feather Defect Electric Field Distribution . 41

4.1.3 Tram Line Defect Electric Field Distribution 43

4.1.4 Ring Cut Defect Electric Field Distribution 47

4.1.5 Effect of Frequency on Electric Field Simulations 50

4.1.6 Simulated PD Inception Electric Field Strength 51

4.2 Experimental Results: Frequency Comparative PD Test Results . . 53

4.2.1 PD Magnitude as a Function of Defect Type & Test Voltage Frequency 53

4.2.2 PD Magnitude as a Function of Supply Voltage Magnitude . 58

4.2.3 PD Inception/Extinction Voltage as a Function of Defect Type & Test Voltage Frequency 59

4.2.4 PD Phase Resolved Pattern Variations as a Function of Defect Type and Frequency 62

4.2.5 Positive & Negative half-cycle PRPDP 70

4.3 Summary of the Experimental Findings 71

5 CONCLUSION & RECOMMENDATIONS FOR FUTURE WORK 73

REFERENCES 75

A ISH 2015 PUBLICATION **82**

B IEEE Electrical Insulation Magazine Paper **89**

LIST OF FIGURES

1.1 Typical Defects and Failure Mechanisms in Cable Joints 2

2.1 Typical Construction of an XLPE Power Cable 7
2.2 Electric field of a coaxial electrode configuration [13] 9
2.3 Electric field strength versus radial distance in a power cable [13] . 10
2.4 Dielectric-bounded Square Cavity Void [13] 11
2.5 Electric Field Stress Enhancement around the Semi-conductive/Insulation layer Interface with and without Stress Control adapted from [21] © 2001 IEEE 13
2.6 Corona Discharges of a Rod-plane Configuration [13] 14
2.7 Characteristic Corona Discharge Pattern 14
2.8 Basic PD Measurement Circuit [16] 16

3.1 The Major Components of a Medium Voltage Heat-Shrinkable Three-Core Cable Termination System 26
3.2 Semi-conductor Feather Defect 27
3.3 XLPE Tram Line Defect 28
3.4 XLPE Ring Cut Defect 28
3.5 Test Setup for Cable Terminations 30
3.6 Photos of the Test Setup; Cable under test (top left) and VLF supply & PD Detector (bottom left) 31
3.7 Photos of the Test Setup; Blocking Resistor & Coupling Capacitor . 32
3.8 The Experimental PD Test Procedure 33

4.1 Electric Field Plot of a Planar Termination Model at 0.1/50 Hz . . 40

4.2 Electric Field Strength versus Radial Length Plot for Planar Model 40
4.3 Electric Field Plot of an Axisymmetric Termination Model at 0.1 Hz (above) and 50 Hz (below) 42
4.4 Electric Field Plot of the Semi-conductor Feather Defect at 0.1 Hz . 44
4.5 Electric Field Plot of the Semi-conductor Feather Defect at 50 Hz . 45
4.6 Electric Field Plot of the Tram Line Defect at 0.1/50 Hz 46
4.7 Electric Field Strength versus Radial Distance from the Centre of the Cable for the Tram Line 47
4.8 Electric Field Plot of the Ring Cut Defect at 0.1 Hz 48
4.9 Electric Field Plot of the Ring Cut Defect at 50 Hz 49
4.10 Partial Discharge Magnitude Distribution Histograms; (a) Semicon Feather, (b) Tram Line and (c) Ring Cut 57
4.11 Gap Overstress Phenomenon due to Delayed Availability of Seed Electron to Initiate PD 58
4.12 Average Apparent Charge versus Test Voltage for Different Defect Types 59
4.13 The Influence of Statistical Time Lag on Partial Discharge Inception for Varying Voltage Test Frequencies 61
4.14 Space Charge Dynamics in a Partial Discharge Event 63
4.15 Semi-conductor Feather PD Patterns at 50 Hz and 0.1 Hz for the Pulses Test 66
4.16 Tram Line PD Patterns at 50 Hz and 0.1 Hz for the Cycles Test . . 67
4.17 Cross-section of the Tram Line 68
4.18 Ring Cut PD Patterns at 50 Hz and 0.1 Hz for the Pulses Test . . . 68
4.19 Cross-section of the Ring Cut 69
4.20 Average Apparent Charge versus Phase Graph of a Ring Cut at 11 kV 70

LIST OF TABLES

2.1 Major Failure Modes of Cable Accessories 18
2.2 PD Testing of Cable Accessories; A review of the literature 20

3.1 Electrical Properties of Materials used in Simulations 37

4.1 Maximum Simulated Electric Field Strength for the Defects at 50 and 0.1 Hz 50
4.2 Simulated versus Measured Inception Voltages of the Artificial Defects at 50 and 0.1 Hz 52
4.3 PD Characteristics of the Terminations tested at 50 and 0.1 Hz . . 54
4.4 Measured PD Inception/Extinction Voltages of the Terminations tested at 50 and 0.1 Hz 60
4.5 The Interaction of Various Electric Fields in the Discharge Area as a Function of the Phase Position and the Resultant Effect on PDs . 64

LIST OF SYMBOLS

Description	Symbol	Units
Electric field strength	E_{max}	volts/metre [V/m]
Applied voltage difference	V	volts [V]
Distance between two electrodes	d	metres [m]
Radius of Outer Electrode	R	metres [m]
Radius of Inner Electrode	r	metres [m]
Distance between Electrodes	x	metres [m]
Test Object	C_a	coulombs [C]
Coupling Capacitor	C_k	coulombs [C]
Impedance	Z	ohms [Ω]
Measuring Instrument Impedance	Z_{mi}	ohms [Ω]
Electrical Conductivity	σ	siemens/metre [S/m]
Relative Permeability	ϵ_r	-
PD Inception Voltage	$PDIV$	volts [V]
PD Extinction Voltage	$PDEV$	volts [V]
Average Apparent Discharge	Q_{av}	coulombs [C]
Maximum Apparent Discharge	Q_{max}	coulombs [C]
Background Electric Field	E_0	volts/metre [V/m]
Vector sum of Electric Fields	E_{total}	volts/metre [V/m]
Inception Electric Field Strength	E_{inc}	volts/metre [V/m]
Statistical Time Delay	Δt_{inc}	seconds [s]
Space Charge due to Positive	$E_{res(P)}$	volts/metre [V/m]
& Negative Half Cycles	$E_{res(N)}$	volts/metre [V/m]

Chapter 1

INTRODUCTION

The mining industry in South Africa is one of the biggest in the world, accounting for about 20% of the country's gross domestic product (GDP) annually [1]. As a result, there is a large demand for medium voltage (MV) equipment such as motors, transformers, circuit breakers and cables, for use in the mining infrastructure. A consequence of this, is a demand for a reliable power network supported by its cable system. Typically cross-linked polyethylene (XLPE) cables are employed due to their superior electrical and thermal characteristics [2] in the South African mining industry and other power utilities [3].

Insulation failures in a cable network are typically caused by ageing processes leading to lower dielectric strength of the cables, internal defects in the insulation system and/or external factors such as poor installation workmanship [4]. In particular, MV networks with increasingly popular extruded power cables are experiencing insulation failures largely due to their low partial discharge (PD) tolerance [5]. These insulation failures are most commonly caused by the failure of the weakest parts of the cable insulation system, namely cable accessories such as joints and terminations [6, 7]. The main reasons for weaknesses in joints and terminations include [7]:

- Inadequate manufacturing, such as internal contaminants or an air gap. An illustrative example of contaminants (metal particles) in the insulation of a power cable is shown in Figure 1.1(a) [7].

- Poor workmanship during installation, which may include dimension errors in installation, introducing contaminants into the cable accessory such as metal particles and damaging of cable insulation layers, in particular the semi-conductor layer. In Figure 1.1(b) [7], an example of insulation damage during installation is shown by an incision into the XLPE layer of a power cable.

- Interface defects between joint/termination insulation and cable insulation, for example inadequate clasp force leading to an air gap. An air gap defect between two layers of a power cable is shown in Figure 1.1(c) [7].

- Ageing of cable accessory insulation, which may be the result of a combination of electrical, thermal and chemical stressing. A failed joint due to ageing is shown in Figure 1.1(d) [8]. The ageing processes were accelerated by water ingress leading to the corrosion of the joint's metal sheath [8].

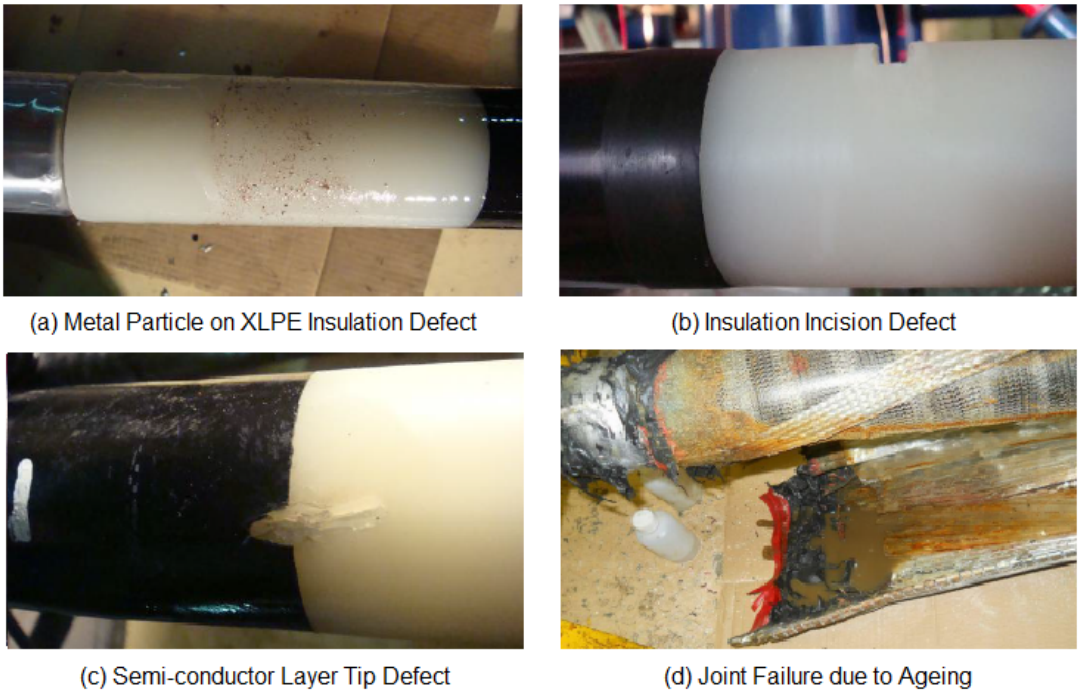

Figure 1.1: Typical Defects and Failure Mechanisms in Cable Joints [7], [8] © 2010, 2012 IEEE.

Continued research into the condition assessment of cable systems is important because it is known that XLPE cables typically have a very low PD tolerance level. It has been reported in the literature that some XLPE joints with very high PD levels did not lead to a failure for up to 6 years of operation [9]. Furthermore, new dry type joints and terminations can withstand PD activity of up to 2000 pC, but they will eventually fail [5]. Further research is therefore needed into PD testing and recognition of cable accessory defects. Investigating PD patterns of different defects can be used to establish a database of PD fingerprints of typical defects for on-site PD measurements [7]. A PD fingerprint database of defects will be beneficial for cable maintenance decisions and experience accumulation. By understanding a component's response to PD activity, material selection, geometries, and interfaces of the cables and their accessories, can be optimized to increase both endurance and reliability [10]. This research is therefore aimed at improving the quality control of MV cable terminations, as motivated mainly by the needs of the South African mining industry.

In PD diagnosis of power cables, a common challenge is the relatively large test voltage sources needed for energising long cables at power frequency (50 Hz). One of the alternative and more viable technologies in this regard, is the use of very low frequency (VLF) test voltage sources [11]. However, the use of VLF test sources may result in different electric stress conditions to those of normal operating conditions, resulting in different PD test results. Thus it is important to compare and verify the PD results of different test sources.

1.1 Problem Statement

There is a problem that newly installed cable terminations on XLPE MV cables can pass typical commissioning tests, in particular an overvoltage withstand test, and yet may show significant PD activity that leads to premature failure in the long term. These MV cable systems suffer from cable accessory failures and cause costly disruptions in South African mining operations. Use of VLF PD test techniques is now a common practice and yet there still remains a lack of understanding and knowledge regarding partial discharges occurring under VLF compared to power frequency. It is desired that as an after installation/commissioning test, the

type of defects that may be present in the cable accessory under investigation, be accurately identified. This research project therefore aims to investigate answers to the following research questions;

- Are there any specific characteristics in the partial discharge measurements that uniquely distinguish different defects in MV cable terminations tested at VLF HV?
- How do the characteristics in MV XLPE cable termination defects compare and contrast at VLF & power frequency excitation voltages?

1.2 The Research Methodology

This research report investigates methods to characterise partial discharge activity in cable accessory defects at different frequencies of excitation voltage. The cable accessories of interest in this case are MV cable terminations, while the frequencies of interest are very low and power frequencies. Therefore the PD characteristics of artificial defects in MV cable terminations were monitored at both VLF and 50 Hz.

The following methodology was devised to answer the research questions. The basic method was to monitor the PD parameters of interest over a specific test duration. The PD parameters were then analysed to form characteristic profiles for each defect. The test data was then compared and contrasted between different defects and test frequencies, to extract trends and important information from the results.

1.3 Research Report Structure

Chapter 2 details the background literature review on PD testing in general and specifically for cable accessory defects. This is followed by the research experimentation and procedure in Chapter 3. Chapter 4 contains the results of the physical testing and simulations, as well as a comprehensive discussion of these results. Finally, the research report is concluded in Chapter 5, along with suggestions for

future work and directions this research could take. Appendix A is a paper which covers part of this work, published at the International Symposium of High Voltage Engineering (ISH) 2015. Appendix B is another paper from this MSc research work, that has been accepted to be published in the July/August 2016 issue of the IEEE Electrical Insulation Magazine.

Chapter 2

BACKGROUND AND LITERATURE REVIEW

This chapter reviews the basics of electric fields in power cables, partial discharge testing, and cable accessory defects. Different defects in cable accessories are discussed, as well as the resulting damage to the cable systems. Furthermore, the literature on partial discharge research of cable accesory defects is summarised and discussed.

2.1 Electric Fields in Power Cables

The study of electric fields is fundamental in understanding the behaviour of electrical insulation used in power cables. A power cable is typically made up of several layers; from the inner conductor, to the outer polyvinyl chloride (PVC) outer sheath. The construction of a typical XLPE power cable is illustrated in Figure 2.1.

These major layers consist of:

- Conductive layers- typically the copper/aluminium conductor and the earth screen.

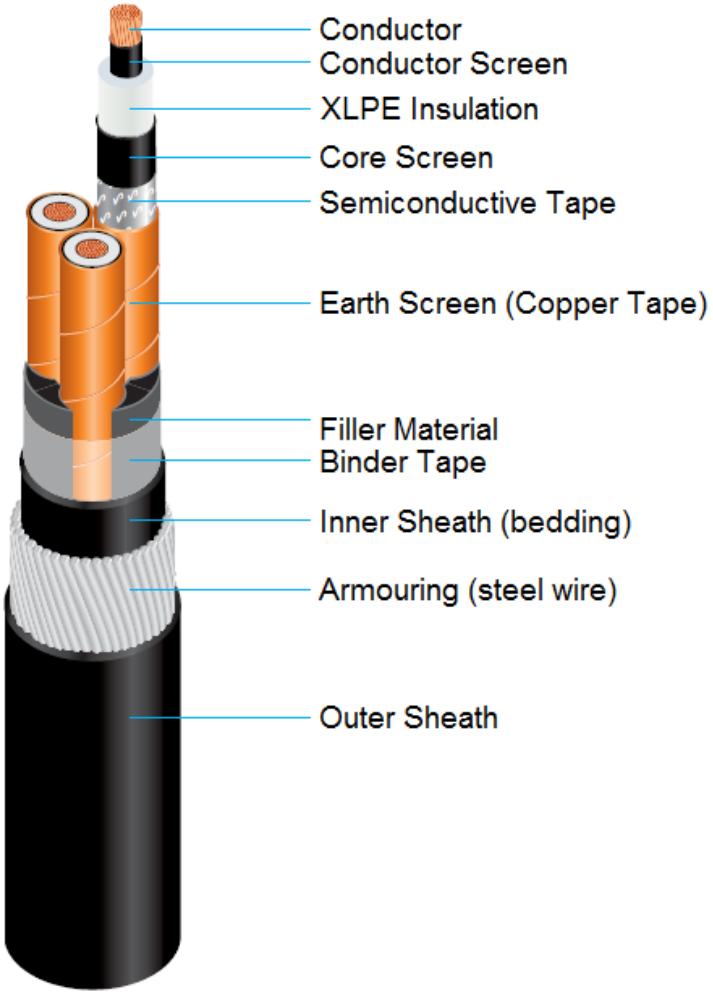

Figure 2.1: Typical Construction of an XLPE Power Cable [12] reproduced with permission from © Aberdare Cables

- Electric field control layers also termed the screening/shielding materials, made up of the inner (conductor screen) and outer (core screen) semi-conductive layers.
- Insulation layers such as cross-linked polyethylene (XLPE) or Oil-impregnated paper insulation.
- Mechanical strength and environmental protection layers, i.e. the bedding, armouring and outer sheath layers.
- Other layers such as water blocking fillers.

The electric field within a power cable is largely governed by the conductive, insulative and field control layers. A coaxial electrode configuration, as shown in Figure 2.2, provides a useful representation of the electric field distribution in a power cable. This configuration is indicative of a capacitor, and as a result power cables are often considered as capacitors, for example in tanδ testing. In the case of an XLPE power cable, as in Figure 2.1, the inner electrode takes the form of the conductor and its screen, with the outer electrode being the core and earth screens and the solid dielectric being the XLPE insulation. The electric field for a coaxial configuration is nonlinear, with the strength of the field represented by Equation (2.1).

$$E = \frac{V}{xln(\frac{R}{r})} \tag{2.1}$$

Where V represents the RMS voltage in Volts [V] applied between the electrodes. R represents the inner radius of the outer electrode (core and earth screens), while r represents the radius of the inner electrode (conductor and screen). x is the radial distance between the electrodes, expressed in metres [m]. E is the electric field strength measured in Volts per metre [V/m], and in the case of a power cable, it is the specific field strength at insulation thickness x. The parameters of Equation (2.1) are the same as those presented in Figure 2.2. For a fixed voltage, the electric field distribution in terms of field strength (E) versus radial distance between electrodes (x) follows an inversely proportional curve, with the rest of the variables being fixed. The distribution is graphically illustrated in

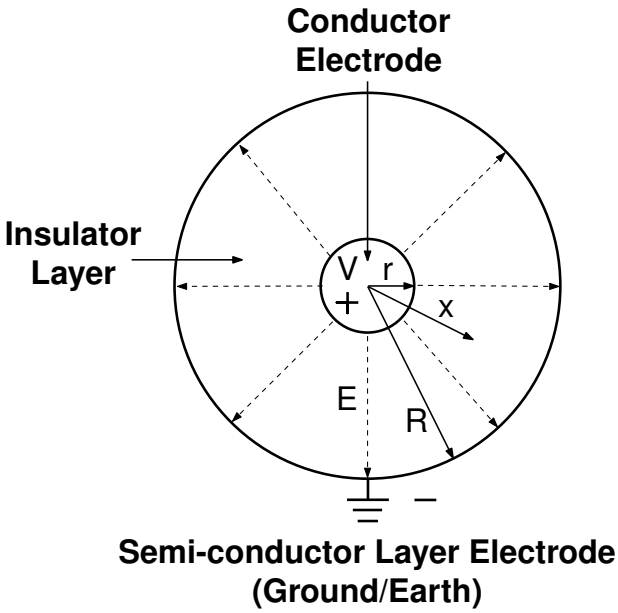

Figure 2.2: Electric field of a coaxial electrode configuration [13]

Figure 2.3, which show the maximum and minimum field strengths occurring at r and R respectively. Therefore, electric field strength is maximum at the conductor screen/insulation interface and minimum at the insulation/core screen interface.

An important aim of HV insulation coordination is to ensure that the electric fields of HV equipment (including power cables) are less than the withstand values of the insulation to avoid discharge phenomena, which may have long term consequences on the performance of the equipment. Although power cables as well as their accessories are designed to ensure their electric fields are within the withstand levels of the insulation as much as possible, failure to correctly apply these accessories may result in regions of highly divergent, enhanced electric fields. These localised regions of highly divergent electric fields are termed defects. This is of particular concern because once the electric field strength has exceeded a certain value determined by the material's permittivity, in a localised region of the insulator, this region changes into a conductor momentarily allowing localised breakdown of the insulation [14, 15]. This conductive region formed by an enhanced non-linear electric field and localised breakdown may not bridge the gap between the two electrodes (insulation/cable failure). However, the resulting current flow damages the insulation and reduces its electrical breakdown strength,

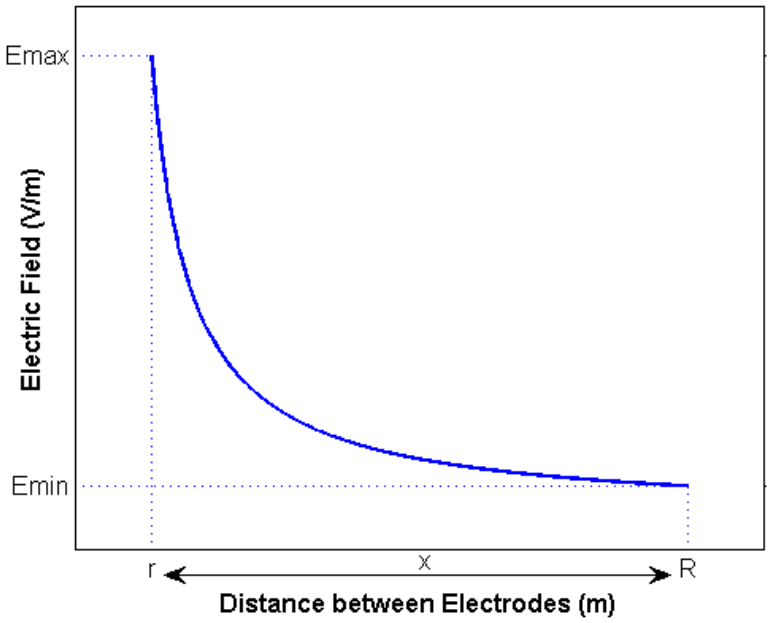

Figure 2.3: Electric field strength versus radial distance in a power cable [13]

therefore leading to further breakdowns and eventually complete bridging of the insulation. These discharge events are expanded upon in the following section.

2.2 Partial Discharges

Partial discharges (PD) are localized electrical discharges that do not completely bridge the gap between the electrodes of an insulation system [16]. Typically, a discharge event results from the electrical breakdown of a gas such as air, contained within a void extruded in insulation or in a highly non-uniform electric field [17]. Partial discharges produce ozone (and other gaseous by-products), a powerful oxidizing agent, which in the presence of moisture may yield corrosive nitric acid and other chemicals, thereby leading to chemical erosion of the insulation [10]. If the void is within an organic medium such as in the insulation (oil, paper, polyethylene) of a power cable, the PD breakdown processes will degrade the organic material, eventually leading to the insulation reaching its breakdown stress level or in localized thermal breakdown [17]. Partial discharge events can generally

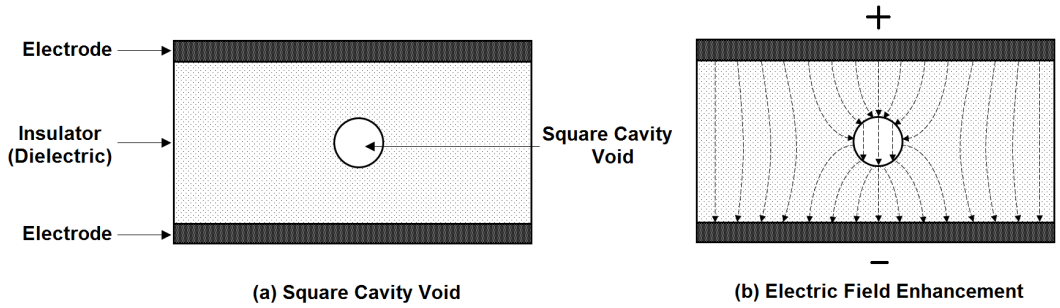

Figure 2.4: Dielectric-bounded Square Cavity Void [13]

be classified into three general categories as presented in the next subsections.

2.2.1 Void Discharges

A void partial discharge is an internal PD, which occurs in an air-filled cavity in insulation. These gas-filled voids are typically the consequence of manufacturing flaws, but may also result from ageing of the insulation system. An example of a dielectric-bounded, spherical cavity void is illustrated in Figure 2.4a. Void discharge events occur due to the difference in permittivity between the gas in the void and the surrounding material (insulator/conductor), leading to electric stress enhancement in the void as shown in Figure 2.4b. If this enhancement reaches an electric field strength exceeding that of the PD inception field strength, a discharge may occur.

Cavities/voids may be classified according to their geometry (spherical, flat, narrow), as well as according to their position in the insulation material (dielectric-bounded, electrode-bounded). These characteristics of void discharges influence PD parameters such as the discharge patterns, inception/extinction voltages and other statistical parameters, thereby making them distinguishable [18]. In power cables, void defects commonly occur in cable accessories due to imperfections introduced during manufacturing, incorrect installation techniques, environmental ageing which can for instance lead to cracking of insulation and a lack of maintenance.

2.2.2 Surface Discharges

A surface discharge is a PD event which occurs along the surface of solid insulation, whereby the electric field at the surface of the electrode/insulation exceeds the breakdown strength of the surrounding gas. Ionisation of air near the surface of the electrode occurs as a result of the tangential field on the insulation surface being high enough to cause PDs along its surface [19]. Therefore, a requirement for surface discharges is that of a non-linear, highly enhanced electric field at the electrode/insulation boundary. The electric field strength typically depends on the cable's geometry, the applied voltage and the material combination (ratio of permittivity and resistivity) [20]. In an unterminated power cable, there is a large electric field concentration around the semi-conductor (core screen) layer/insulation interface, particularly at the end of the semi-conductor layer. This electric field stress of an unterminated power cable is illustrated in Figure 2.5a. This area of stress enhancement is typically mitigated by special screening/shielding materials of the cable accessories, known as stress control products, as shown in Figure 2.5b. These products aim to manage or lessen the electric field strength within dielectrics [20]. The design of cable accessories, specifically the stress control, must ensure that the electric field strength is always below the dielectric strength of insulating materials to avoid intrinsic breakdown. Forms of stress control include conductive paint, stress control mastic tape/tube, void filling tape, crutch void filler and self amalgamating tape [20]. Therefore, surface discharges are likely to occur at the semi-conductor/insulation interface as a result of defects in the screening/shielding materials of the cable or its accessories.

2.2.3 Corona Discharges

Corona discharges are a type of partial discharge and can be defined as the localised breakdown of a gas or liquid [19]. Corona most commonly occurs in air, when a sharp point results in high electrical stress about the point. The typical electrode configuration for corona discharge is similar to that of surface discharges, with the insulator/dielectric being a gas/liquid. The electric field is typically modelled as a rod-plane configuration, with the rod electrode being a needle/pin or some other very sharp object. A simple illustration of this configuration is displayed

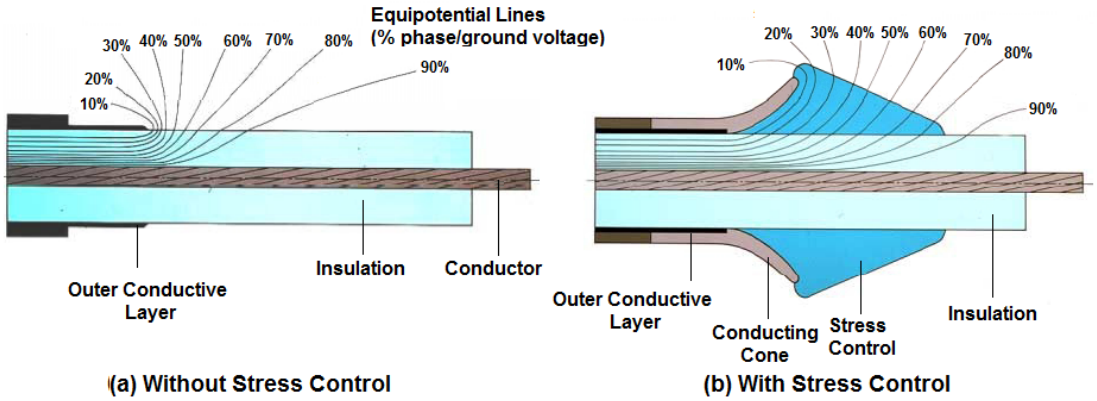

Figure 2.5: Electric Field Stress Enhancement around the Semi-conductive/Insulation layer Interface with and without Stress Control adapted from [21] © 2001 IEEE

in Figure 2.6, when the applied voltage at the sharp point electrode exceeds the breakdown strength of the gas/liquid, ionisations of the gas/liquid occur near the sharp point, forming positive and negative streamers depending on the voltage polarity [19]. The electrical stress is a function of the point's tip radius, the voltage difference between the electrodes and the distance between the electrodes (insulation thickness).

The phase resolved discharge patterns of corona are quite distinct from those of void and surface discharges, with discharges clustering about the peaks and troughs of the applied voltage, and an absence of discharges around the zero crossing [15]. Corona pattern discharges are further distinguished from those of surface discharges by larger amplitude pulses on one peak and uniform, smaller amplitude pulses (Trichel) on the opposite polarity's peak. An example of a corona discharge pattern is given in Figure 2.7.

In power cables the interest in identifying corona is in reducing its undesirable effects such as:

- electromagnetic interference
- audible noise
- associated power losses reducing the inefficiency of the electrical system
- possible damaging of insulation over extended periods of exposure to corona.

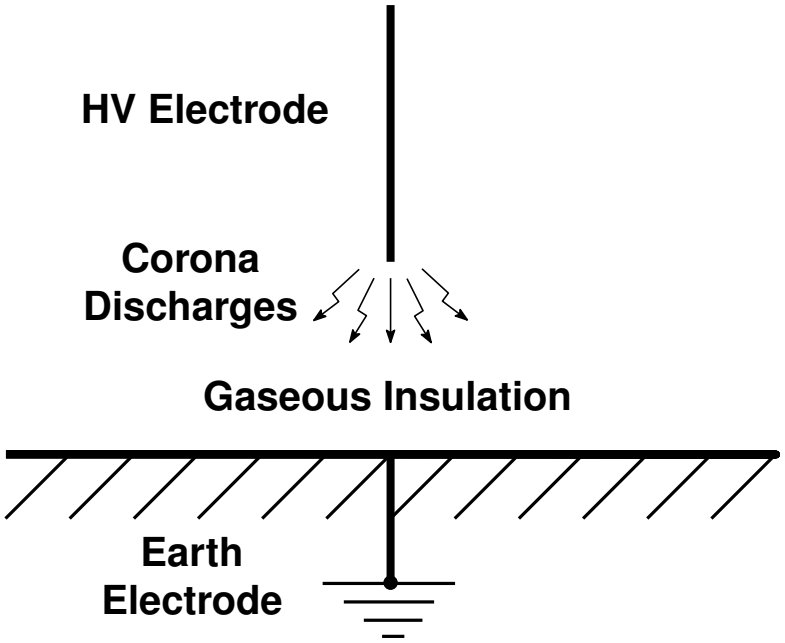

Figure 2.6: Corona Discharges of a Rod-plane Configuration [13]

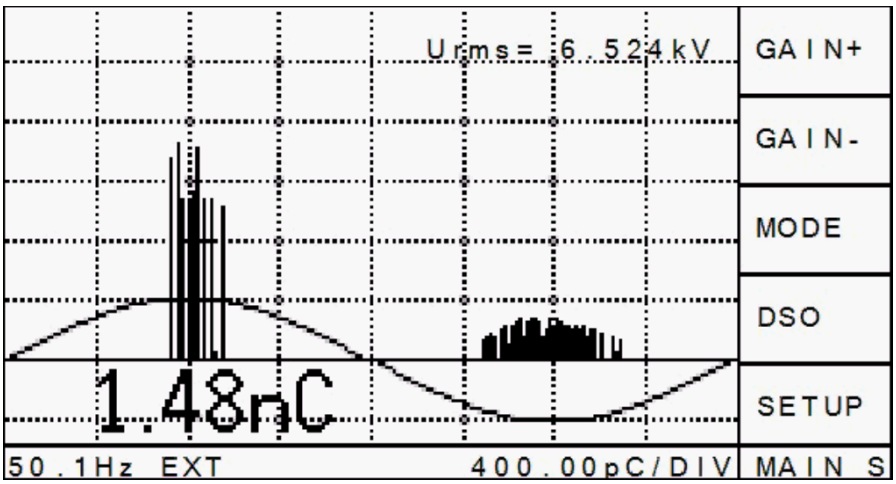

Figure 2.7: Characteristic Corona Discharge Pattern

2.2.4 PD Testing

Since the presence of PD is usually an indication of an undesired condition of the insulation, electrical equipment needs to be tested for PD as a condition assessment criterion. A popular diagnostic parameter in power cable testing is therefore that of partial discharge (PD) activity [11]. PD detection and measurement is a field of study which dates back to 1924, when a loss factor bridge was first used to detect PD events [22]. Since then many electrical and non-electrical procedures have been developed for PD recognition. The detection of partial discharges is important because the major breakdown mechanisms leading to insulation failures are either thermal or a slow deterioration of the material's dielectric strength due to PD [10]. Therefore, PD testing is commonly employed throughout the lifetime of a power cable; from design to installation and finally for diagnostics to assess whether the condition of the cable warrants possible repairs or replacement.

PD is a stochastic process where an electron is required to initiate the electron avalanche leading to the voltage breakdown across a localised part of the insulation [11]. Variations in the time required for this free electron to appear in the void are known as the statistical time lag. A delay in the appearance of an initiating electron will result in the applied voltage rising above the intrinsic breakdown voltage of the discharge gap, until an initiating electron becomes available. As a result, phase variations of the PD pulse positions relative to an applied sinusoidal voltage wave may occur, indicating changes in the breakdown voltages and resultant PD pulse magnitudes [22]. This unpredictable behaviour can result in interpretation difficulties in PD pattern recognition and thus PD measurements require multiple readings for reproducibility and validation [22].

The current or voltage pulses resulting from partial discharge activity occurring within insulation, are measured using suitable detection circuits in terms of a variety of quantities related to the PD pulses [16]. These quantities typically include PD charge magnitude, phase angle, repetition rate, discharge current/power, as well as the inception and extinction voltages of the PD pulses. Some of these quantities are commonly presented as a function of another, such as charge magnitude plotted versus phase angle to form a phase-resolved-partial discharge pattern (PRPDP). An example of a PRPDP is shown in Figure 2.7.

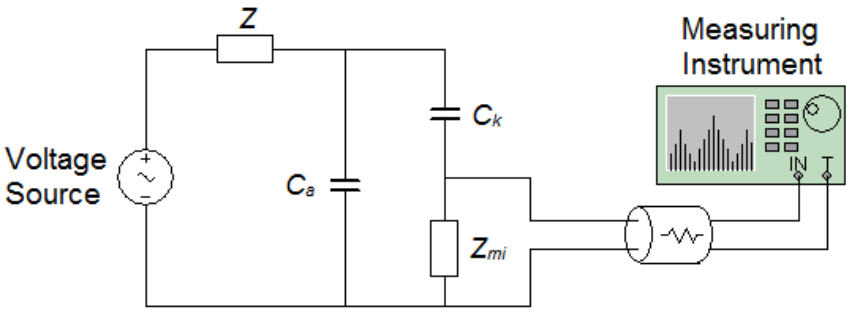

Figure 2.8: Basic PD Measurement Circuit [16]

PD measurement characteristics are dependent on a variety of factors which include type and location of defects, operating and test voltages, circuit operating conditions and type of insulation material [11]. Most electric PD measurement circuits consist of a number of basic components namely; the test object usually represented by a capacitor (C_a), a coupling capacitor (C_k), a measuring instrument and a high-voltage supply [16]. The measurement system should have a sufficiently low level of partial discharges and background noise at the specified test voltage, and if need be, an impedance or filter can be introduced to reduce noise. A basic PD measurement circuit is shown in Figure 2.8.

PD measurements are most commonly conducted using any of the three different AC voltage source types namely; sinusoidal continuous (20-300 Hz), very low frequency (VLF) (0.01-1.0 Hz) and damped AC (20-500 Hz). The results of PD testing for these different sources cannot be directly compared, as the PD characteristics have been shown to be different at different frequencies [11]. VLF testing is advantageous because of the power requirements being directly proportional to the test frequency, thereby minimising the size of the test source [23]. Thus VLF test sets may be up to 500 times smaller than a power frequency (50 Hz) test setup of comparable capacity. Furthermore, insulation ageing changes are more visible at VLF than at power frequency [11]. Therefore, VLF is increasingly becoming the test frequency of choice, and it is in this context, that this research work focuses on studying cable accessory PD under VLF test voltage.

2.3 Cable Accessory Defects

A number of different cable fault analysis studies have shown that a high percentage of cable faults result from accessory failures [7, 24]. According to Jiang et al. [7], the State Grid Electric Power Research Institute in China has found that as high as 70% of cable failures resulted from cable accessory faults. In a cable accessory failure analysis conducted by the National Electric Energy Testing Research and Applications Center (NEETRAC) of the USA, it was found that cable accessories accounted for nearly half of the cable failures of the utilities involved in the study [24]. The accessories which include joints, terminations and junctions, showed a steady increase in the percentage of total cable failures since the 1970s [24]. The leading cause of these cable accessory failures was poor workmanship with 49% of the total failures, while manufacturing problems and dielectric breakdown only accounted for 24% combined [24].

A joint or termination failure can be defined as when a burned path is formed through or along the insulation of the joint/termination by the flow of power or test current to ground or an another phase [25]. In general cable termination and joint failures originate from one or more of following causes: improper application, wrong material, inadequate design, wrong assembly, hostile environment, mechanical damage, thermal damage, cable/device interface problems, abnormal voltages or potentially damaging test voltages such as applying DC to an AC cable [25]. The major failure modes of cable accessories relating to poor workmanship, along with the resulting damage is given in Table 2.1 [2]. According to the cable fault analysis studies mentioned above, as well as the causes and consequences of a cable accessory failure, it can be seen that defects in power cables pose significant potential risk. Therefore, this work focuses on defects in power cable accessories.

2.4 PD Testing of Cable Accessory Defects

Power cables along with their accessories should be tested in the field prior to operation as part of an acceptance test, to ensure the cables are free of defects [11]. However, due to factors such as outsourcing, there are many cases especially in medium voltage systems, where the cable accessories are mounted on site by

Table 2.1: Major Failure Modes of Cable Accessories [2]

Failure Mode	**Resulting Damage**
Improper stress grading	Failure spot near the insulation screen or shield boundary
Inadequate distance between conductors and shield boundary	Failure of the insulation along the surface between the conductor lug and screen boundary
Semi conducting layer partly or completely missing over stress control cone	Failure of insulation
Cut in insulation at the boundary of the semi conducting layer	Puncture of insulation in the region near the termination screen
Inadequate jointing of conductor	Overheating of insulation around conductor joint
Floating or missing metallic shield	Degradation leading to failure of joint insulation
Improper protective covering of termination	Erosion and tracking on the insulation and termination surfaces
Incorrect sealing of joint	Deterioration of joint as a result of moisture ingress
Knife cuts and/or traces of semiconductor material on the surface of the cable insulation	Rapid degradation and failure of insulation
Overloading of the cable accessory	Change in colour and softening/charring of insulation over the conductor joint and near the lug

subcontractors rather than by the cable/accessory manufacturers [26]. As a result, poor workmanship due to a lack of installation knowledge and quality awareness, may lead to partial discharges and dielectric stressing. Therefore, suitable testing procedures are employed to discover evidence justifying the removal of joints/terminations in anticipation of an imminent failure.

Insulation condition assessment of power cables is an important area of research which has been investigated by researchers such as Gulski et al. [9], with regard to supporting utility asset management in decision processes about cable maintenance and replacement policy. In the condition assessment of cables, the basic PD quantities such as magnitude, inception/exception voltages and derived quantities such as PRPD patterns, form what is termed a PD fingerprint [9]. These fingerprints may be useful for making decisions regarding the insulation integrity of cable systems, although the dependence on factors such as cable type, age, service history, and accessories (location/type) need to be taken into consideration.

Extensive research has been conducted in the area of testing cable accessory failures, with work done on HV terminations and joints in [6, 7, 10] and similar work conducted at MV in [26–28]. A summary of the literature is given in Table 2.2. Although the PD magnitudes are in similar ranges, and resemblance may be drawn between different discharge patterns, it is difficult to directly compare and find correlation between results in the literature, due to the many factors involved. Therefore, continued research into the effect of these different factors, such as the test voltage source and the type of defect, may provide useful diagnostic information.

In terms of PD testing of cable accessory failures, particular focus has been placed on HV terminations and joints [6, 7, 10]. Ahmed et al. [6] found that PD most often occurred in the stress-relief assembly of the HV transmission cable terminations which were tested. The PD activity creates high frequency pulses which propagate alongside the cable conductor and ground connection of the terminations [6]. Rush [10] reported that corona inception/extinction voltages were used to characterize HV termination performance in terms of its connectors. Typically, connectors made with good overall quality control had inception/extinction values with small variance, while large variances indicated poor control of internal dimensions such as creep lengths, seals and geometries.

Table 2.2: PD Testing of Cable Accessories; A review of the literature

Researchers	Voltage Range & Type	Highlights of Findings			Comments
		Magnitude (pC)	PDIV (kV)	PDRP (°)	
Y. Jiang et al. [7]	110 kV at Power Frequency	20-100 (max)	-	Peaks at 90 & 270	Defects included insulation incision, semi-conductor layer tip & air-gap and metal particles on insulation.
K. Rethmeier et al. [26]	6.6 kV VLF (0.1 Hz) and Power Frequency	400-500 (max)	5-17	Peaks at 90 & 270	The PD diagnostic results at VLF (0.1 Hz) showed good comparability to those achieved at power frequency.
S. Tokunaga et al. [28]	6.6 kV at Power Frequency	650 (max)	-	Peaks on rising/ trailing edges of test voltage	The PD mechanism of degradation for the needle void defect is interpreted; whereby PD concentrates at the weak point (void), forming a pit and leading to tree initiation.
Y. Wang et al. [29]	10 kV Damped Oscillating Voltage	500-2000 (max) 100-700 (average)	-	Peaks at 30-70 & 220-250	Statistical maps of different defects significantly distinct & increasing severity of defect resulted in a magnitude difference of up to 10 times.
W. Wang et al. [27]	110 kV Damped Oscillating Voltage	-	12.2-56.4	-	Acoustic PD detection was used in this investigation, other non-electrical methods include visual/optic and chemical detection.

Connectors which failed during testing, experienced dielectric breakdown for the following reasons [10]:

- Irregular geometry of braid shields at the wire/braid shield interface leading to concentrated electric fields.
- Breakdown through an insulator wall to the electrode contact, as a result of sharp corners in the electrode geometry.
- Dielectric breakdown in the connector interface area between the mated plug/receptacles interfaces. This is indicative of a lack of dimensional control of mechanical interfaces resulting in a reduction of mating forces and thus compromising the seal.

The PD pattern characteristics of six artificial defects typically found in HV (110 kV) cable joint terminations, were studied by Jiang et al. [7]. The artificial defects were metal particles on XLPE insulation, insulation incision, semi-conductor layer tip, axial direction shift, semi-conductor layer air gap and a high potential tip on the conductor. Some of these defects are illustrated in Figure 1.1. A variety of discharge magnitude versus phase angle patterns (PDPRP) were observed for the different artificial defects, with the majority of the peaks occurring around 90° and 270°. The semi-conductor layer tip defect pattern was distinct from the rest with two clusters of PD maximum magnitudes around 80-100 pC occuring before 90°. The maximum magnitudes ranged from 20 pC for the insulation incision defect to as high as 100 pC for the semi-conductor layer tip defect.

In terms of MV cables, PD experimentation involving cable accessories has been studied in [26, 28, 29]. Wang et al. [29] studied partial discharges of four typical artificial defects in 10 kV XLPE cable accessories of varying severity. The PD activity of all four defects differed in number and quantity of discharge, while concentrating around 30°-70° and 220°-250° in the PRPD patterns. The maximum discharge quantities ranged between 500 pC and 2000 pC for the different defects, while the average quantities ranged between 100 pC and 700 pC. It was found that the statistical maps of the different defects showed significant difference and that increasing the severity of a defect such as doubling the dimensions of a semicon cusp or air-gap, resulted in a PD magnitude difference of up to ten fold [29].

A similar study by Rethmeier et al. [26] was conducted measuring PD of MV cable systems with artificial defects, focusing on inception voltages. The PD inception voltage was lowest for a short cable test sample missing a termination (∼5 kV) and highest for a needle artificial defect (∼17 kV), while a void under the stress cone of a termination resulted in an inception voltage of about 10 kV. Furthermore, the PRPD pattern of the void artificial defect showed four significant clusters symmetrical to the zero-line around the rising positive and trailing negative edges [26]. The discharges were again concentrated before 90° and 270° as seen in the study by Wang et al. [29], but closer to the patterns observed by Jiang et al. [7].

Tokunaga et al. [28] studied the PD characteristics until the failure/breakdown of 6.6 kV XLPE cable joints with needle void defects. Discharge patterns resembling those found by Wang et al. [29], with peaks of up to 650 pC occurring on the rising and trailing edges of the test voltage, were recorded. The mechanism of degradation for the needle void was interpreted as follows [28]: after a certain ageing time, PD occur and concentrate at the weak point (needle void defect). When PD concentrate at the weak point, the area of PD appearance decreases, resulting in the PD charge decreasing below a detectable level due to the electric field concentration caused by the weak point. Then a pit is formed as degradation caused by PD processes, until after a time whereby PD activity greatly increases leading to tree initiation [28]. An increase in residual charge left at the predeceasing half-cycle gives rise to a sudden increase in PD charge at the next half-cycle [28]. This abrupt increase in the PD magnitude leads to tree formation and eventual breakdown.

While damped oscillating test voltages were used in studies by Wang et al. [27] and Gulski et al. [9], power frequency (50/60 Hz) was the most commonly used test frequency investigated in the literature review [7, 10, 26, 28]. However, as highlighted in [26], lower test voltage frequencies such as VLF (0.1 Hz) are more commonly being used for field testing due to test system size and costs. According to the research of Rethmeier et al. [26], PD diagnostic results at 0.1 Hz and power frequency showed good comparability for cable accessory testing, confirming previous work done by Kalkner et al. [30].

Non-electrical methods of PD detection exist, including acoustic, visual/optic

and chemical detection [16]. An example of this is the study of the acoustic emissions of PD signals in 110 kV XLPE cable accessories with known defects by Wang et al. [27]. Four different insulation defects were investigated namely; cavity, protrusion, semi-conductor layer cusp/ tip and a floating piece of semi-conductor layer. Partial discharges were measured for an applied voltage of 12.2 kV for the protrusion defect, while applied voltages of between 46.4 kV and 56.4 kV resulted in PD activity for the remaining defects [27]. The frequency spectrums of all the PD emissions were largely concentrated between 100 and 300 kHz [27].

As can be seen from the reviewed literature section, a large volume of research has been conducted into the partial discharges of cable accessories with artificial defects for both MV and HV cables. From this previous work, PD fingerprints may be extrapolated in order to diagnose defects in the accessories of cable systems. However, due to these fingerprints being influenced by a wide range of variables and because different cables/accessories as well as their typical defects may be more relevant to certain industries/countries, continued research is imperative to expanding the knowledge database of PD in cable accessories.

Although a range of defect types have been investigated in the literature, the two most common types are semi-conductor layer contaminants and cavity/void defects in the cable insulation. As a result, this research focused on these two defect types. The PD testing was conducted at VLF (0.1 Hz) due to its increasing use in industry, thereby motivating the need for further research into the effect of different test frequencies on PDs when compared to traditional 50 Hz testing. According to the literature, the common method of experimental study of defects in cable accessories, involves creating artificial defects in cable samples, applying an appropriate voltage and measuring the resulting PDs. This is the method which was adopted for this research work and is presented in detail in the next chapter.

2.5 Summary

As this research work is motivated by improving cable fault diagnosis through the use of PD measurements, an understanding of electric fields in cables is necessary. Furthermore, the basic concepts of partial discharges and its testing methods are essential background knowledge. Lastly, a thorough analysis of PD cable testing

literature, gives a complete review of the platform of previous work. From all the aspects presented in this chapter, the basis of the experimental work can now be covered in detail. This background information and review of the literature allows for an explanation of the experimental methodology that will be used to investigate the PD diagnosis of defects in MV cable accessories.

Chapter 3

EXPERIMENTAL WORK METHODOLOGY

The experimental work methodology consisted of cable terminations sample preparation, followed by the implementation of a suitable testing protocol. This chapter details the preparation of the cable termination artificial defects, followed by the PD test setup and procedure, described in terms of the test circuit, test durations and data collection. Lastly, a brief outline of the measurement data analysis is covered.

3.1 Sample Preparation

The cables under test were 3 core 6.6/11 kV XLPE, 70 mm^2 copper conductor, with individual screening on each core. An illustration of the terminations used in this investigation is shown in Figure 3.1. This choice of MV cable was motivated by its common use in the South African mining industry. Furthermore, three-core cables allowed for test results to be compared for adjacent phases with the same configuration (defect) [11]. Properly prepared (defect free) terminations were first applied to both sides of two 20 m test cables. The healthy terminations were then

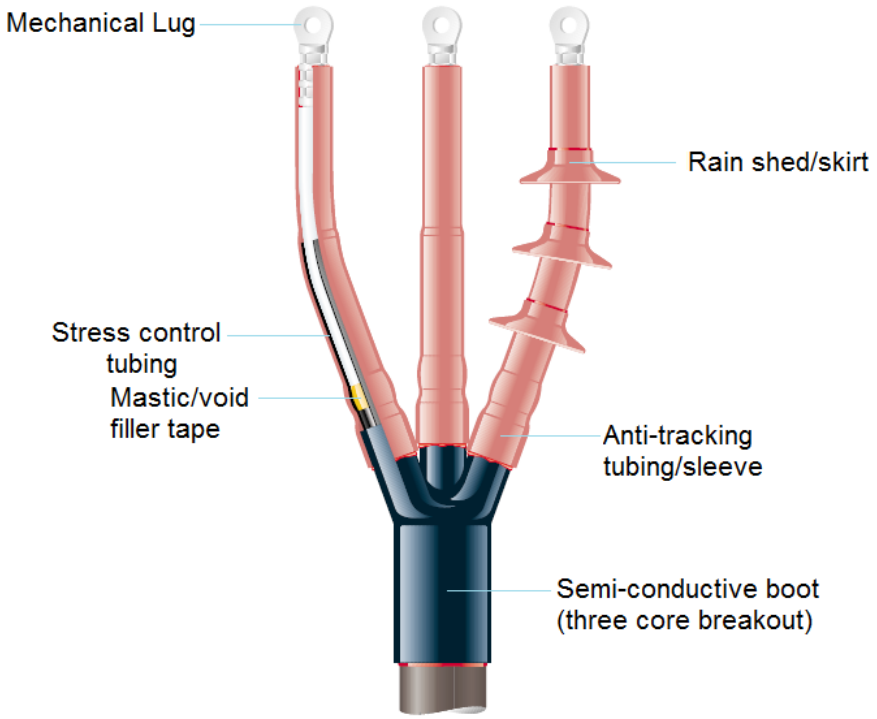

Figure 3.1: The Major Components of a Medium Voltage Heat-Shrinkable Three-Core Cable Termination System [31] reproduced with permission from © TE Connectivity Ltd

tested at 50 Hz and verified to have an acceptable PD level below 5 pC (at 1.7 U_0), according to South African and International standards [5]. Both cables were then cut in half into two 10 m lengths. Each of the four (10 m) cable lengths were then terminated with a different artificial defect. For each artificial defect, identical test samples were prepared on two of the cores to ensure verification and reproducibility of the results. The severity of the defect on the third core was increased in terms of its dimensions, in order to identify any trends. In each test sample, typical identical defects were created as explained in the following section.

3.1.1 Type of Defects

Cables' semi-conductor layers are designed to increase the effective radiating surface area of electrodes and to minimize the electrical stress caused by the transition of electric fields between materials with dissimilar dielectric constants [32].

Therefore, any abnormalities or defects introduced in and around the semi-conductive layer may result in excess electrical stresses beyond the design limits of the cable and the accessories. This research focused on defects in the semi-conducting layer and the XLPE insulation layer of the terminated cables being tested, namely; a semi-conductor layer feather (Figure 3.2), tram lines cut into the XLPE layer (Figure 3.3) and a ring cut in the XLPE insulation at the border of the semi-conductive layer (Figure 3.4). These defects were chosen due to their relevance in the industry, as being some of the most common causes for cable accessory failure. In terms of the artificial defects' dimensions, the following were used for each:

- Semi-conductor feather: Triangular canals with 10 mm base & perpendicular height (core 1&2) and 5 mm base & 25 mm perpendicular height (core 3).

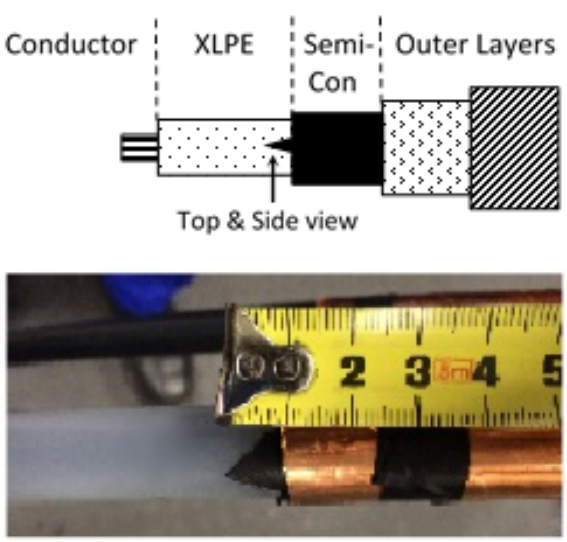

Figure 3.2: Semi-conductor Feather Defect

- XLPE tram line: 1 mm deep, 0.4 mm maximum thickness (cores 1&2) and 2 mm deep, 0.6 mm maximum thickness (core 3).

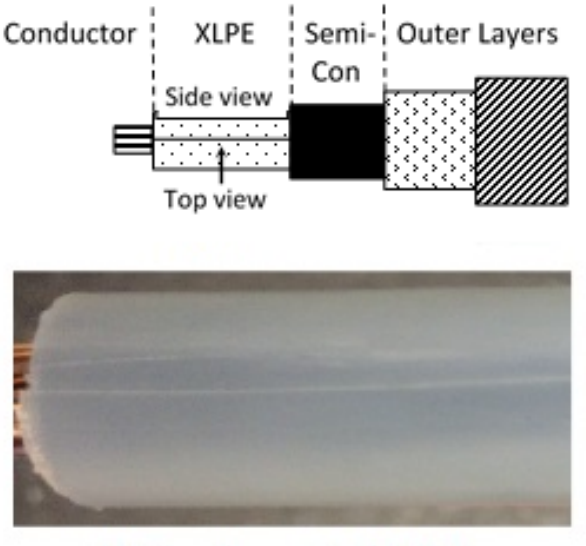

Figure 3.3: XLPE Tram Line Defect

- XLPE ring cut: 1 mm deep, 0.6 mm maximum thickness (cores 1&2) and 2 mm deep, 0.8 mm maximum thickness (core 3).

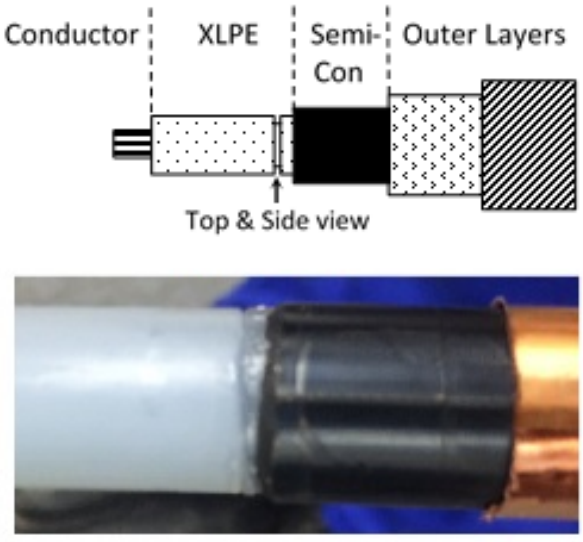

Figure 3.4: XLPE Ring Cut Defect

3.2 PD Measurement Experimental Setup and Procedure

3.2.1 Overvoltage and PD Testing

High voltage field testing is commonly conducted at VLF due to the portability of the test system [26, 33]. It is therefore necessary to understand PD characteristics at VLF of common defects in cable accessories, allowing for the results of this research to be used for comparative purposes in future field testing.

Since the key objective of this research was to characterise artificial defects which pass high voltage installation tests and yet have significant PD activity, a typical overvoltage (withstand) commissioning test was conducted during which PD activity was monitored.

The testing procedure was in accordance with the IEC 60270 (VLF PD testing), IEEE 400 (insulation testing of power cable systems) standards, SANS 1339 & 6284 and South African industry standards [5]. The test circuit is illustrated in Figure 3.5, with photos of the setup shown in Figures 3.6 and 3.7 .

According to IEEE 400.3 (Guide for Partial Discharge Testing of Shielded Power Cable Systems in a Field Environment), currently there is no specific standardised test protocol for online/off-line PD testing [34]. The standard does however recommend test voltages and durations, albeit only for power frequency. Typically, PD testing is restricted to 2.0 U_0, where U_0 is the phase-to-ground cable operating voltage, in order to accommodate for abnormal operating conditions which the cable may experience, such as an earth fault transient voltage of 1.7 U_0 [11]. However, new cables and accessories may be tested to a maximum of 3 U_0.

The test protocol used in this research work is presented in a flowchart format as given in Figure 3.8. The test procedure involved subjecting the cable to a VLF (0.1 Hz) sine wave at 1.7 U_0 for 30 min, which is the industry standard voltage withstand test according to Goodwin [5]. The applied voltage was then increased to 2.0 U_0 up until 3.0 U_0 in steps of 0.5 U_0 every ten minutes.

The IEEE 400.3 standard specifies a maximum test time of 15 min at power frequency to protect the cable from damage, while ensuring sufficient time for electrons to be available in cavities to initiate PD [34]. Once the PD magnitude

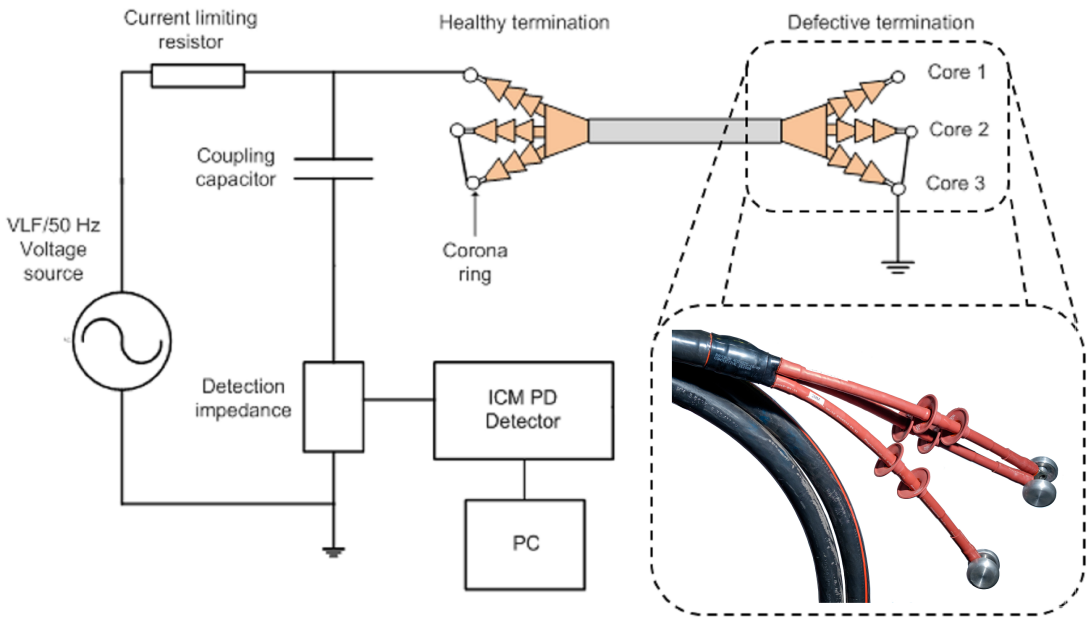

Figure 3.5: Test Setup for Cable Terminations

level exceeds that of the acceptable level of the cable (inception voltage), the data should be recorded for a maximum of 15 s to allow for accumulation of sufficient data. These test times are recommended for 50 Hz testing with a period of 0.02 s, therefore these values needed to be adapted for this research. For testing at VLF (0.1 Hz), which has a period of 10 s, and to ensure collection of sufficient test data, a data collection time of 10 min/60 cycles of the source voltage and a complete test time of 60 min were used. These values correspond to 1.2 s and 0.12 min at 50 Hz respectively, scaled according to the number of cycles.

During the testing, the values of relative humidity, temperature and air pressure were in the following ranges; 42-52%, 21-23°C and 98.5-101.6 kPa. The environmental conditions did not change significantly throughout the experiments, conducted in the controlled lab environment, and thus would have negligible effect on the results between tests. Other common practices for PD testing were followed, such as ensuring the surface of the external insulation of the test cable is clean and dry making sure that moisture or contamination do not cause additional PD activity [16].

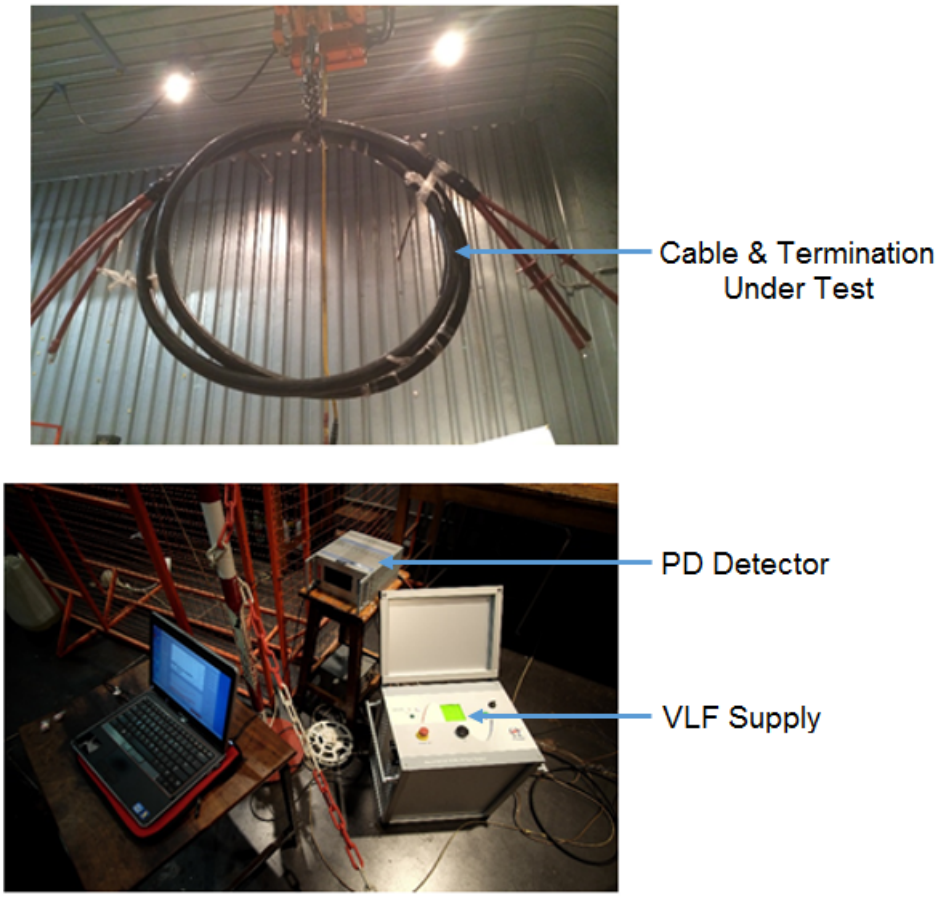

Figure 3.6: Photos of the Test Setup; Cable under test (top left) and VLF supply & PD Detector (bottom left)

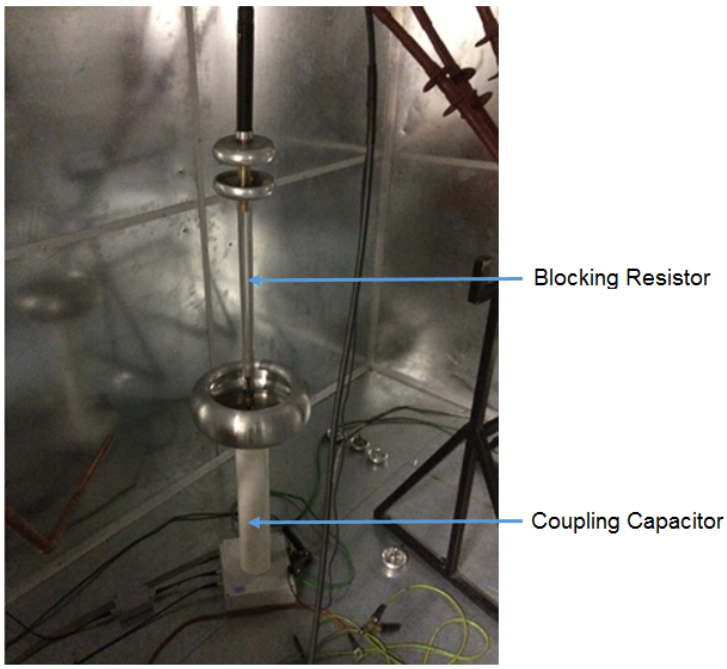

Figure 3.7: Photos of the Test Setup; Blocking Resistor & Coupling Capacitor

Following the completion of the overvoltage (withstand) test, an inception/extinction voltage test procedure was conducted for the defects that showed PD activity below 11 kV. The voltage was increased in steps of 0.5 kV up until 11 kV and then decreased in the same fashion, allowing for a minimum of three cycles at each voltage level. Inception voltage was defined as the voltage value that the apparent charge rose above the noise floor for three consecutive cycles. Similarly, extinction voltage was defined as the lowest voltage at which the maximum apparent charge was above the noise floor for three consecutive cycles.

The last PD test procedure was pattern acquisition to obtain PRPDPs for the different defects. The hold function of the PD instrument was employed to capture the charge magnitude and count at discrete phase angles over a test duration of ten minutes. Although a longer test duration is advantageous in producing a more clear pattern with a greater number of readings, ten minutes was decided upon in order to limit total testing time for each defect.

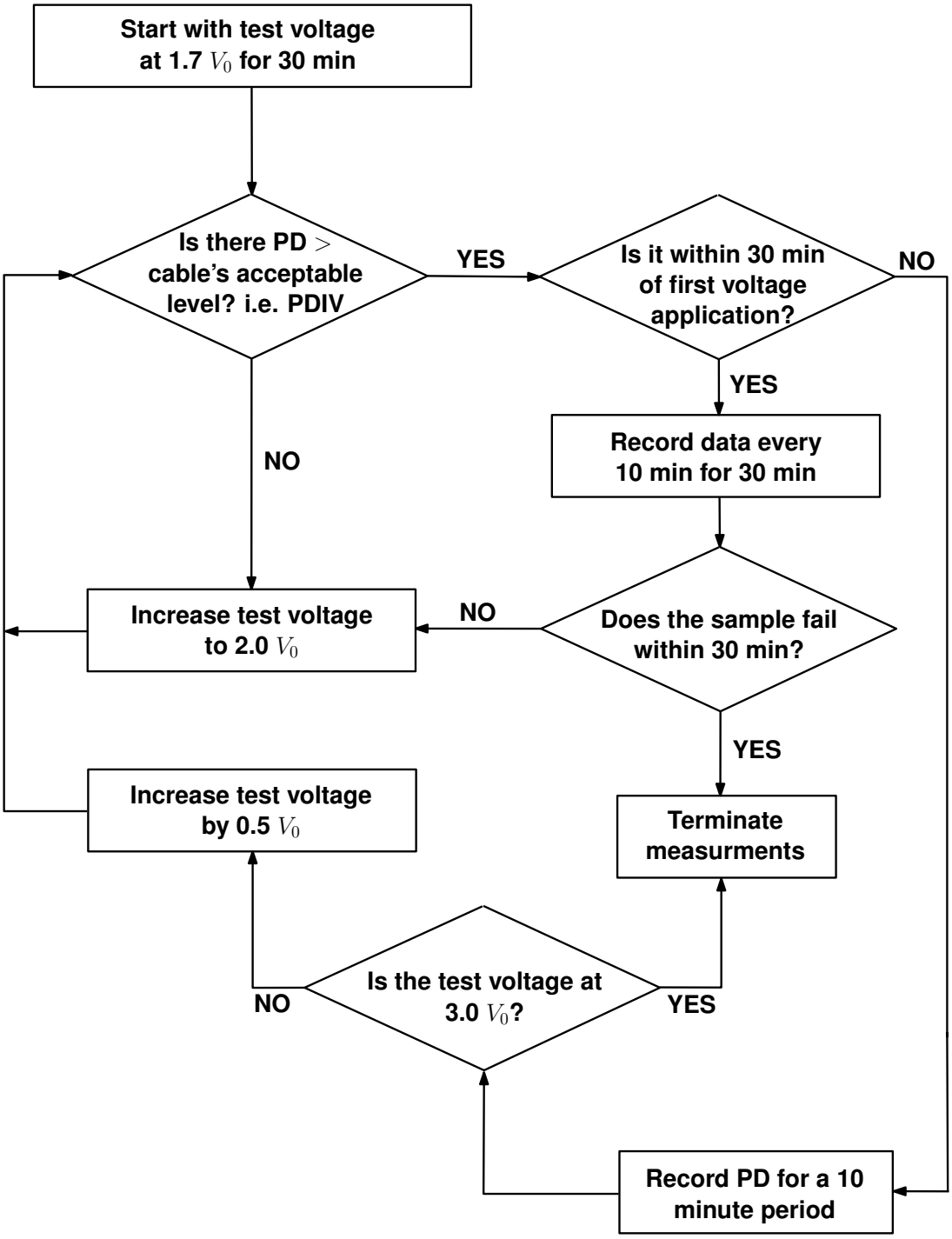

Figure 3.8: The Experimental PD Test Procedure

All the terminations with artificial defects passed the VLF overvoltage commissioning test in accordance with the IEEE 400.2 standard [35], SANS 1339 [36] and South African Industry standards [33], whereby a voltage of 1.7 U_0 & higher was applied for 60 minutes without failure.

The VLF PD parameters as well as the discharge patterns of the terminations at 11 kV_{RMS} (1.7 U_0), are presented in Appendix A. The maximum ($Qmax$) and mean (Qav) apparent charge are average values over the 30 min test duration, while the inception/extinction voltages were measured after the overvoltage test. It should be noted that the tests were conducted in a screened room and the noise floor was typically between 1 pC and 2 pC, which was deemed an acceptable variation between experiments.

3.2.2 Comparative PD Testing at 0.1 Hz and 50 Hz Test Voltages

In addition to the original scope of this research, the work was extended into characterizing and comparing the PD activity of the termination installation defects at 0.1 and 50 Hz test voltages. The results of this additional work form an important control to validate the experimental results of this study, with 50 Hz testing being a common and relatively well understood type of PD test. Details of this work may also be found in Appendix B.

In terms of experimental work methodology, the additional testing was conducted on the same cable/termination samples as used in the initial overvoltage testing. Similarly, an identical test setup (Figure 3.5) was used with the only modification being that of the voltage source for the 50 Hz testing. Two procedures were adopted to compare and contrast the PD activity under the different test frequencies, with a particular focus on discharge patterns. The first procedure involved recording PD data for both test frequencies for the same number of test voltage cycles. A test period of 10 s (500 cycles) was chosen for 50 Hz excitation to ensure significant data was captured while ensuring that the corresponding VLF test period of 5000 s (∼83 min) was practical. Conversely, the second test procedure involved recording PD data of both test frequencies for the same number of PD pulses (∼500 000). Both procedures were conducted using a test voltage of

1.7 U_0.

An inception/extinction voltage test procedure was also conducted for the defects showing significant PD activity below 1.7 U_0. The voltage was increased in a linear fashion for 50 Hz and in steps of 0.1 kV for VLF, up until 1.7 U_0, and then decreased in the same fashion, allowing for a minimum of three cycles at each voltage level. Inception voltage was defined as the voltage that the apparent charge rose above 10 pC for three consecutive cycles, with extinction voltage defined similarly as the voltage at which the apparent charge dropped below 10 pC.

3.3 PD Data Analysis Techniques

An important aspect of the research methodology is that of the data analysis and verification. There are a variety of different ways of PD characterisation, which were briefly discussed in Section 2.2. While the apparent PD charge magnitude and the inception/extinction voltages are quantities that were directly measured during testing, other important characteristics such as phase angle, repetition rates and phase resolved patterns were determined through post-processing. This test data processing was conducted using Visual Basic (VB) scripting to obtain the raw data from the Power Diagnostix ICM Compact™ PD instrument as well as for manipulation, after which Matlab® was used for final processing and graphic output. Furthermore, a statistical analysis of the results was conducted using VB scripting to further classify, understand and compare the data with similar investigations, such as those described in Section 3.1.1. The VB script files were obtained from the PD instrument's manufacturers (PDIX) and were modified according to the needs of this research, thus further details of the script files and their procedures are deemed outside the scope of this project.

3.4 Electric Field Simulations in the Cable Terminations

A number of simple finite element analysis 2D simulations were conducted using the FEMM software package. These simulations were aimed at investigating the inception electric field of each defect under ideal conditions, in order to compare and contrast the results of the physical testing. The terminations and defects were modelled as accurately as possible according to their known dimensions/properties, however, there were limitations on the results which are further discussed in Section 4.1.

Each artificial defect was simulated as a static magnetics problem, using the material properties as given in Table 3.1. Only the most aggravated defects (core three) of each of the terminations were simulated, as well as healthy terminations for comparative purposes. All the terminations were simulated at 11 kV_{RMS}/15.6 kV_P (1.7 U_0) and the electric field plot results are presented here, while the inception field strengths are presented in Section 4.1.6. The semi-conductor feather and tram line defects were simulated as planar problems, due to their geometries being unsuitable for axisymmetric simulation. Conversely, the ring cut defect was more accurately simulated as an axisymmetric problem. Due to possible singularities/abnormalities in the simulated electric field patterns occuring at material boundaries, only electric field strengths not closer than 0.01 mm to a boundary, were considered for the inception field strength and maximum electric field measurements.

Simulations were conducted at both 0.1 and 50 Hz, with comparative results between the frequencies being mixed. For the healthy and tram line planar models, no change was observed in the electric field distribution or magnitude between frequencies, therefore only one plot for each is presented. Conversely, for the healthy and ring cut axisymmetric models, as well as for the semi-conductor feather planar model, a difference in electric field plots were observed for the two frequencies. Therefore, plots at both 0.1 and 50 Hz are presented. The effect of frequency on the electric field simulations will be further discussed in Section 4.1.5.

The limitations of these simulated results should be noted as follows:

- All three defects were simulated as two-dimensional problems and therefore information pertaining to the three-dimensional electric field may be lost in the simulations.
- It is difficult to accurately estimate the geometry (dimensions) of possible air bubbles trapped on the tip of the semi-conductor layer.
- The radius of curvatures (sharpness) of the voids are approximated according to the known dimensions of the tram line & ring cuts.

Two different simulation configurations were investigated for healthy terminations using the same assumptions and conditions used for the defect simulations. For comparative purposes with the semi-conductor feather and tramline defects, the healthy termination was first simulated as a planar, cross section at the border of the semi-conductor layer, with a 1 mm depth. All the measurements (diameters) are either taken to be ideal from the cable data sheet or have been measured from the real test specimens (such as the heat shrinked products). The second simulation for healthy terminations was modelled as an axisymmetric problem along the z-axis (length of the termination), for comparison with the ring cut defect.

The PD inception field strength in the simulations was defined as the electric field strength corresponding to the breakdown voltage of air for each defect gap length. The breakdown voltages were calculated using the simplified expression for Paschen's law, Equation (3.1), which is taken from [14].

$$V_b = 6.72 * sqrt(pd) + 24.36(pd)\ kV \tag{3.1}$$

Where V_b represents the breakdown voltage, p is air pressure and d is the gap

Table 3.1: Electrical Properties of Materials used in Simulations

Material	**Electrical Conductivity** $[S/m]$	**Relative Permeability** $[\epsilon_r]$
Air	5.50×10^{-15} [37]	1
XLPE	1.00×10^{-14} [38]	2.5 [38]
Stress Control Tube	1.00×10^{-7} [39]	35 [39]
Stress Control Mastic	1.00×10^{-8} [39]	15 [39]

length. Equation (3.1) is valid for homogenous, uniform field gaps in air at 20°C. Although the coaxial field of a cable is non-uniform on a macroscopic level, the field surrounding the defects on a microscopic level can be assumed to be uniform. Furthermore, the temperature differential between the test conditions and the stated temperature of Equation (3.1), are assumed to be negligible.

The values calculated from Equation (3.1) (with p=100 kPa) are thus taken as the breakdown strength of air, whereby partial discharges are likely to occur. It should be noted that the exact breakdown strength of air is a complex calculation, dependent on a number of interrelated factors such as air pressure, humidity, temperature and electrode configuration, and therefore the values used in this project are an estimate. Furthermore, the same limitations of the electric field plots may have an effect on the accuracy of the simulated inception voltages.

3.5 Summary

Each component of the experimental work methodology was covered in detail, beginning with the cable termination sample preparation, followed by the PD measurement procedure, the PD data analysis and concluded with the electric field simulations in the cable terminations. Three types of artificial defects were prepared in the cable termination samples, which included a semi-conductor feather defect, an XLPE tram line and an XLPE ring cut. Two types of PD tests were carried out, namely; the overvoltage PD tests and the frequency comparative PD tests. Data analysis involved the collation and plotting of results through VB scripting and Matlab. Electric field simulations for each defect were conducted using the finite element software package, FEMM, for verification and comparison of the physical test results.

Chapter 4

RESULTS, ANALYSIS & DISCUSSION

This chapter presents all the experimental and simulation results, followed by the analysis, interpretation and discussion of each set of results.

4.1 Simulation Results: Electric Fields in the Terminations

4.1.1 Healthy Terminations Electric Field Distribution

The electric field plot of the planar healthy termination model is displayed in Figure 4.1, while electric field strength versus radial length for the model is plotted in Figure 4.2 along the line indicated by (x) in the first figure. Furthermore, the numerical (theoretical) electric field strength is plotted and is calculated according to Equation 2.1. As can be seen from the figure, both lines have a very similar decreasing gradient. However, the theoretical line is more smooth due to the limitations of the simulations, such as the solver precision of the finite element modelling.

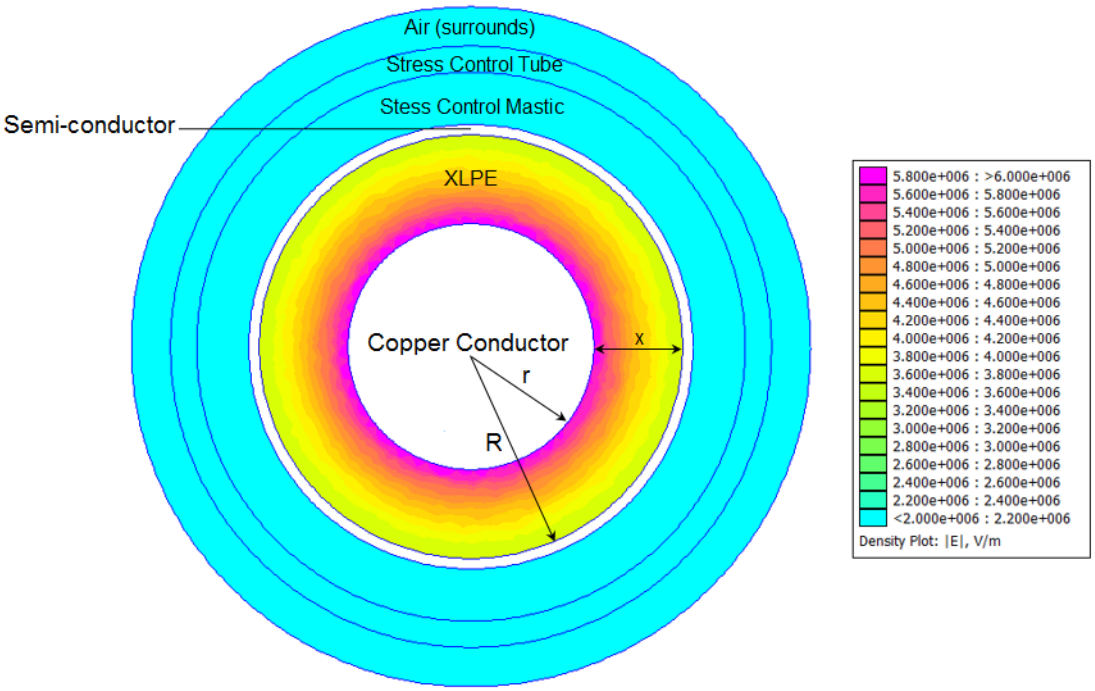

Figure 4.1: Electric Field Plot of a Planar Termination Model at 0.1/50 Hz

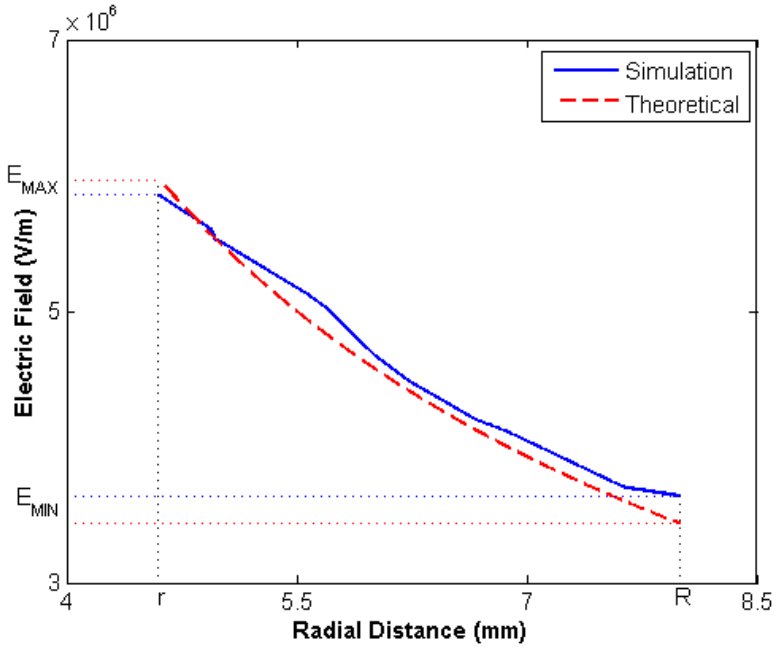

Figure 4.2: Electric Field Strength versus Radial Length Plot for Planar Model

The second healthy termination model, that of the axisymmetric configuration, is shown in Figure 4.3 with a similar electric field density plot. Typically, the dielectric strength of polymer insulating materials is greater than 10 kV/mm [20], however, the electric field stress should be kept well below this level to reduce ageing. As can be seen from the stress field enhancement around the semi-conductor (core screen)/insulation layer interface in Figure 2.5 when compared with a similar plot of a healthy termination model (Figure 4.3), the stress control products have successfully mitigated the critical region of high stress. The maximum electric field strength (at 0.1 Hz) has been reduced from 2.6×10^7 V/m to 0.45×10^7 V/m. The electric field strength has been successfully controlled through the use of stress control mastic tape and stress control tubing. More specifically, through the application of multi-layer conductor/insulator theory and the use of high permittivity (ϵ_r >15) linear stress control layers, the termination design effectively produces a less concentrated electric field distribution.

The simulated electric field plots of the healthy terminations (Figures 4.3 and 4.1) are as expected for the electric field distribution of a MV power cable. The electric field between the electrodes is distributed (relatively) evenly in the XLPE insulation, concentrating at the interface between the semi-conductive layer and the stress control products. Although relatively high electric field strength peak values are recorded for the healthy termination models (6×10^6 & 4.579×10^6 V/m), these values are well below the dielectric (breakdown) strength of XLPE, which is typically $> 20 \times 10^6$ V/m. Therefore, no partial discharges would be expected.

4.1.2 Semi-conductor Feather Defect Electric Field Distribution

The semi-conductor feather was simulated as a small, differential cross-section of the cable termination near the end of the feather's sharp point with a 1 mm planar depth. The cross-section of the feather was simulated as a rectangle with height equal to that of the semi-conductor thickness (0.4 mm) and a width of 1 mm. This configuration only involving the semi-conductor feather was first simulated. After initial analysis and comparison with test results, a modified

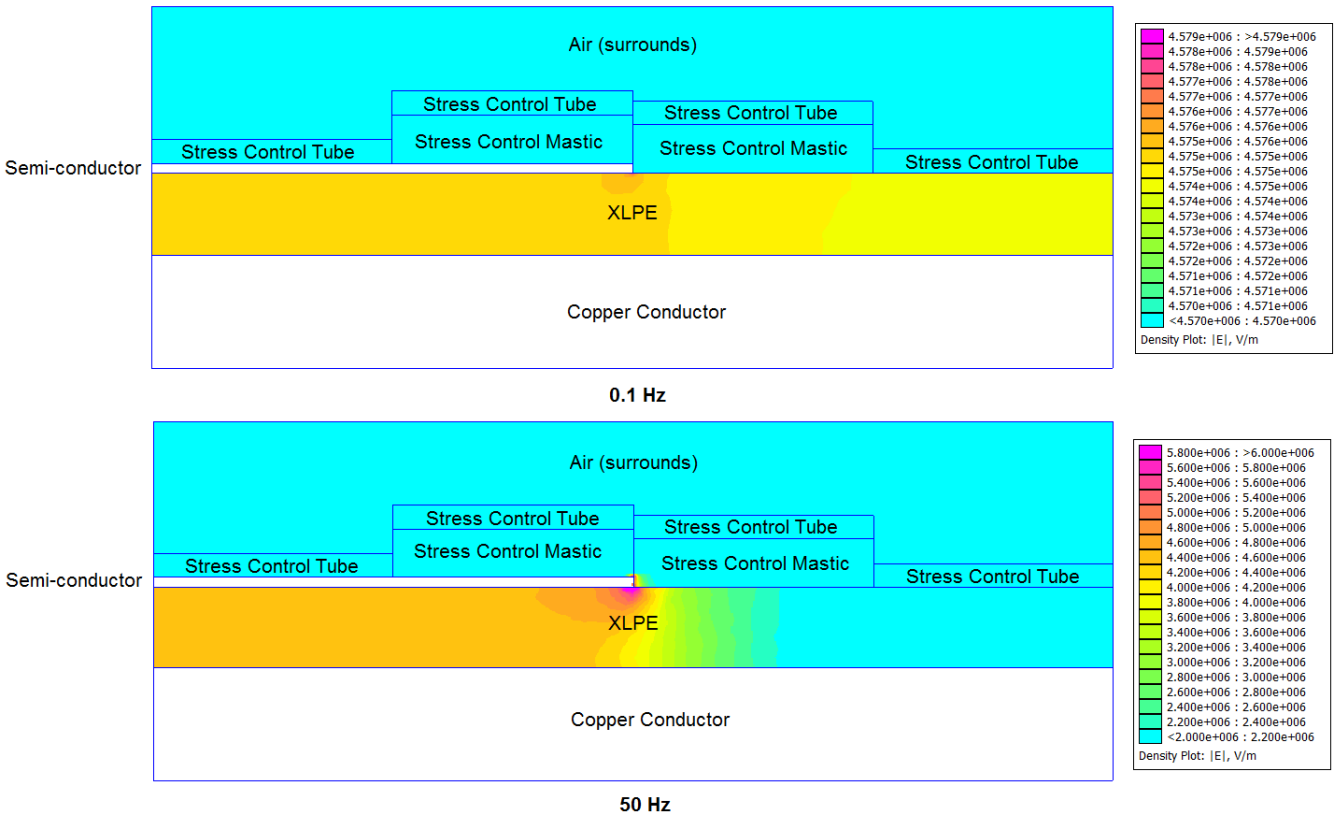

Figure 4.3: Electric Field Plot of an Axisymmetric Termination Model at 0.1 Hz (above) and 50 Hz (below)

configuration involving an air bubble was simulated, in order to explain and better approximate the real/physical implementation test results. The small air bubble trapped between the feather, stress control tube and the XLPE was simulated to model the effect of such an air pocket on the resultant electric field. The air bubble was simulated as a sector of a circle with a central angle of 90° and a radius of 0.25 mm. Although other air bubble configurations were simulated, such as different dimensions and shapes, similar results were obtained.

The electric field plot of the semi-conductor feather defect is shown in Figure 4.4 for 0.1 Hz and Figure 4.5 for 50 Hz. As can be seen from the figures, the electric field distribution in and around the semi-conductor feather/air bubble differs between test frequencies, with higher magnitudes at 50 Hz. In both cases, the electric field in the air bubble does concentrate at the interface with the semi-conductor feather and the XLPE insulation. This result is expected as the feather forms the return path electrode (earth) and therefore the electric field will be highest nearest to the other electrode (XLPE interface). The electric field strength magnitudes in the air bubble, at both frequencies, exceeds the breakdown strength of air (2.54×10^6 V/m) for the semi-conductor feather configuration as calculated using Equation (3.1). Therefore, partial discharges would be expected granted that the conditions for PD activity were fulfilled, such as the availability of initiating electrons.

4.1.3 Tram Line Defect Electric Field Distribution

The tram line defect was simulated according to the dimensions for the most aggravated defect (core 3). The tram line was simulated for the worst case scenario, i.e. at the edge of the semi-conductor layer. As with the semi-conductor feather, the tram line simulation had a 1 mm planar depth. The electric field plot of the tram line defect is shown in Figure 4.6. In comparison to the sharp concentration of the semicon feather's electric field, the (air) void of the XLPE tram line had a much more evenly distributed electric field. As mentioned previously, no change was observed in the electric field distribution or magnitude between frequencies.

With reference to the cross-sectional sketch in Figure 4.6, the radial variation of the electric field across the healthy and defective parts of the cable are plotted in

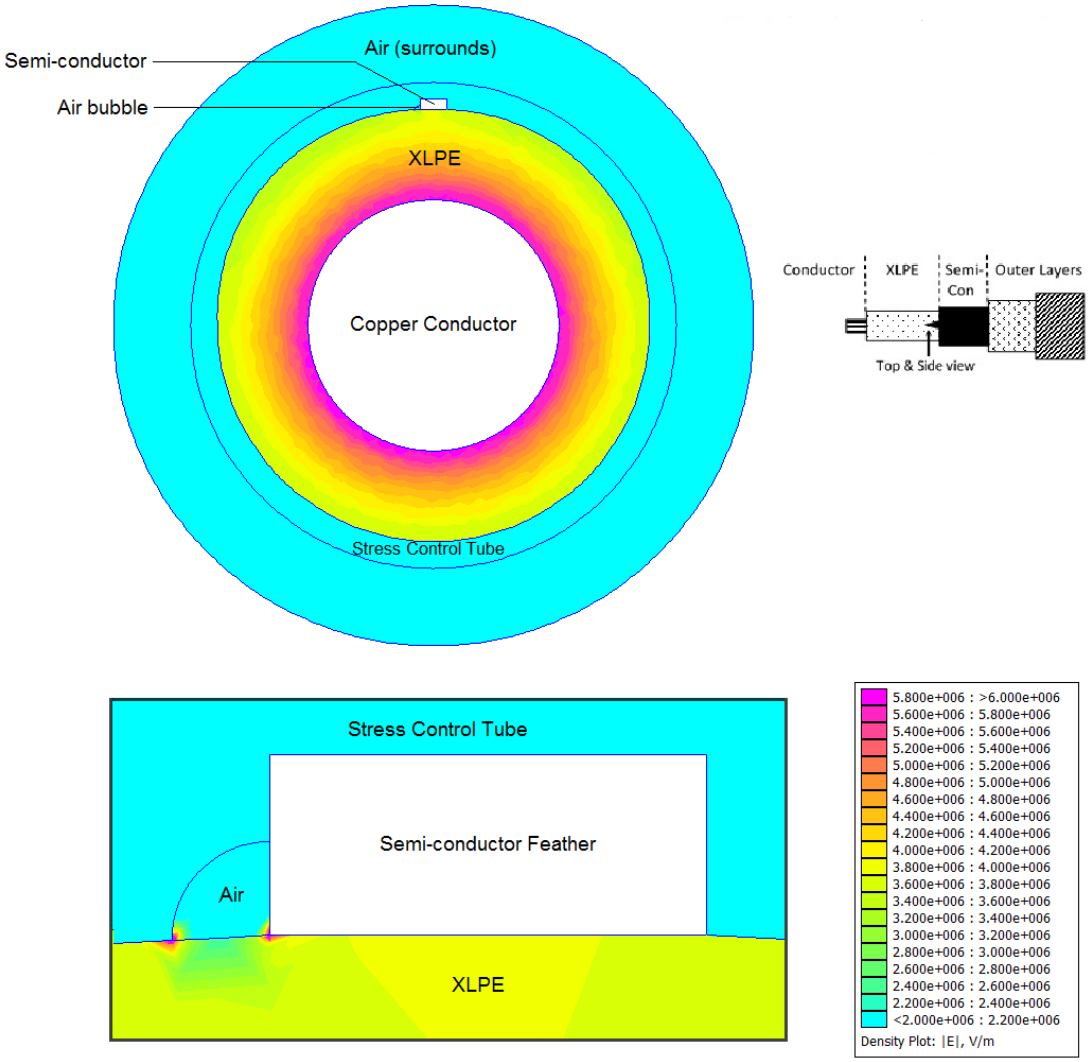

Figure 4.4: Electric Field Plot of the Semi-conductor Feather Defect at 0.1 Hz

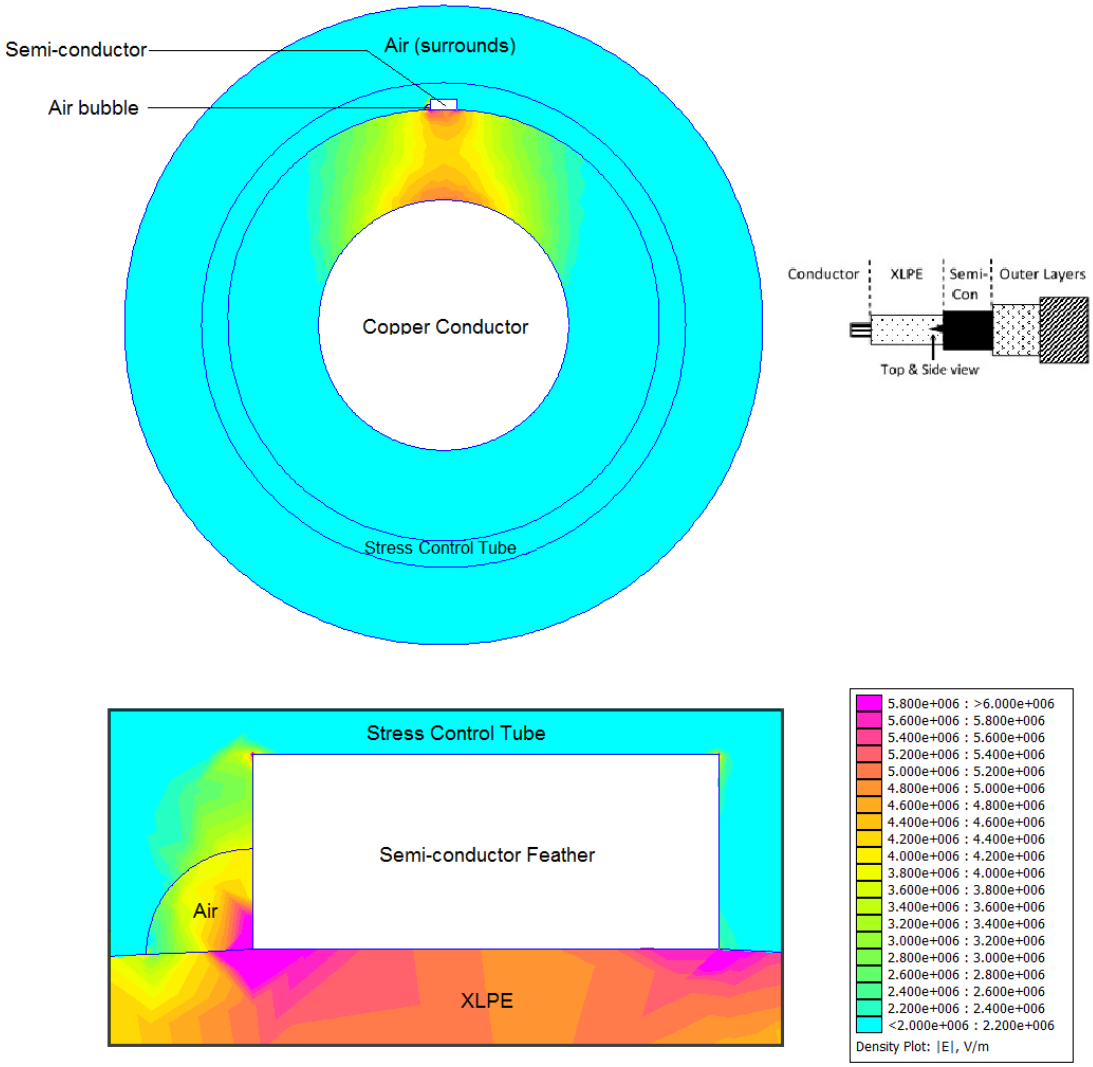

Figure 4.5: Electric Field Plot of the Semi-conductor Feather Defect at 50 Hz

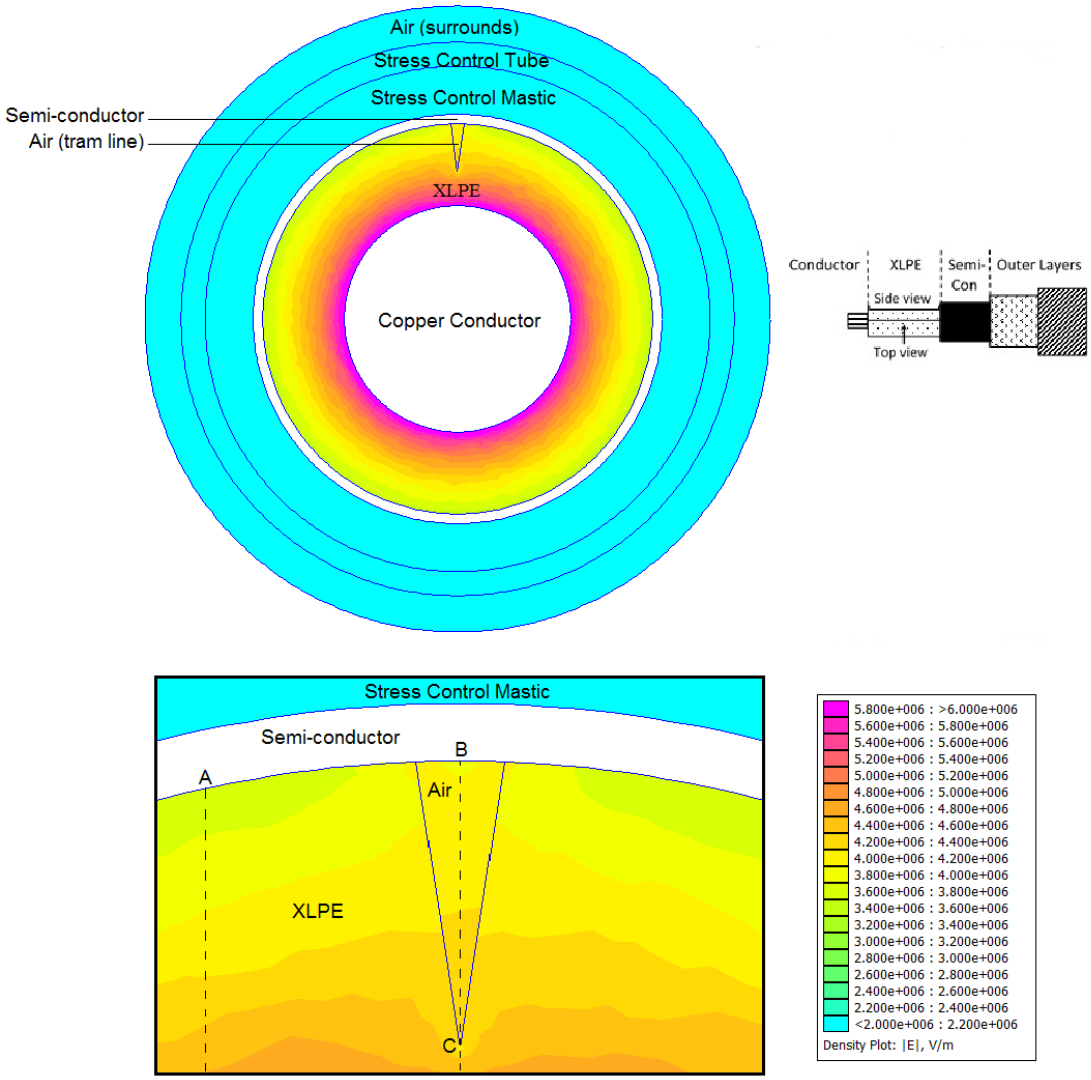

Figure 4.6: Electric Field Plot of the Tram Line Defect at 0.1/50 Hz

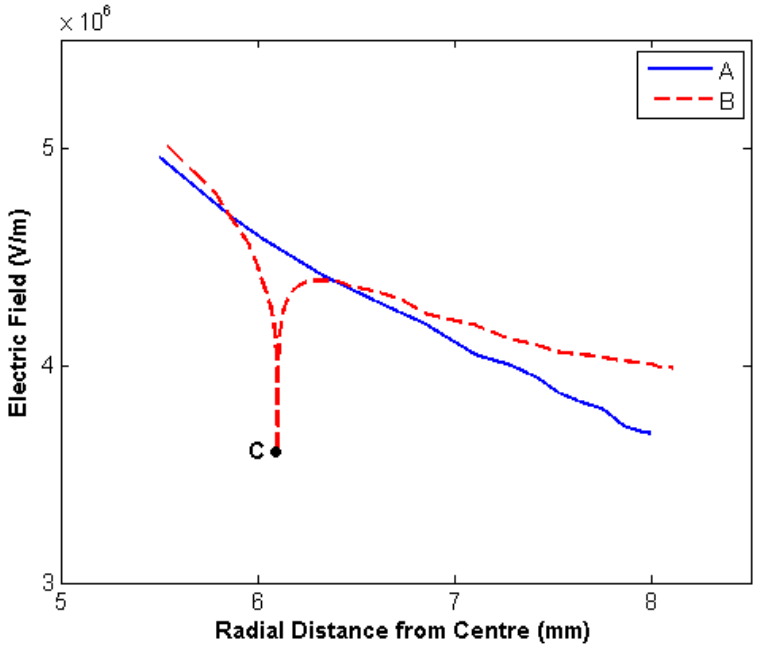

Figure 4.7: Electric Field Strength versus Radial Distance from the Centre of the Cable for the Tram Line

Figure 4.7. The electric field profiles along lines A & B of Figure 4.6, are plotted up until the semi-conductor layer interface. Point C is illustrated in both Figure 4.6 and Figure 4.7, to show the tram line boundary. The tram line runs from point C to the boundary of the stress control mastic at 8.1 mm. The profile along line A is similar to that of the healthy profile (Figure 4.2), while the tram line profile of line B has a notch at point C, before rising above line A in the tram line. The electric field strength magnitude throughout the tram line is greater than the breakdown strength of air for the tram line defect (2.48×10^6 V/m) and therefore PD activity could be expected.

4.1.4 Ring Cut Defect Electric Field Distribution

As with the tram line defect, the ring cut defect was simulated for the most aggravated defect (core 3). The ring cut defect was simulated as an axisymmetric problem along the z-axis (length of the termination). The electric field plots of the ring cut defect are shown in Figure 4.8 for 0.1 Hz and Figure 4.9 for 50 Hz.

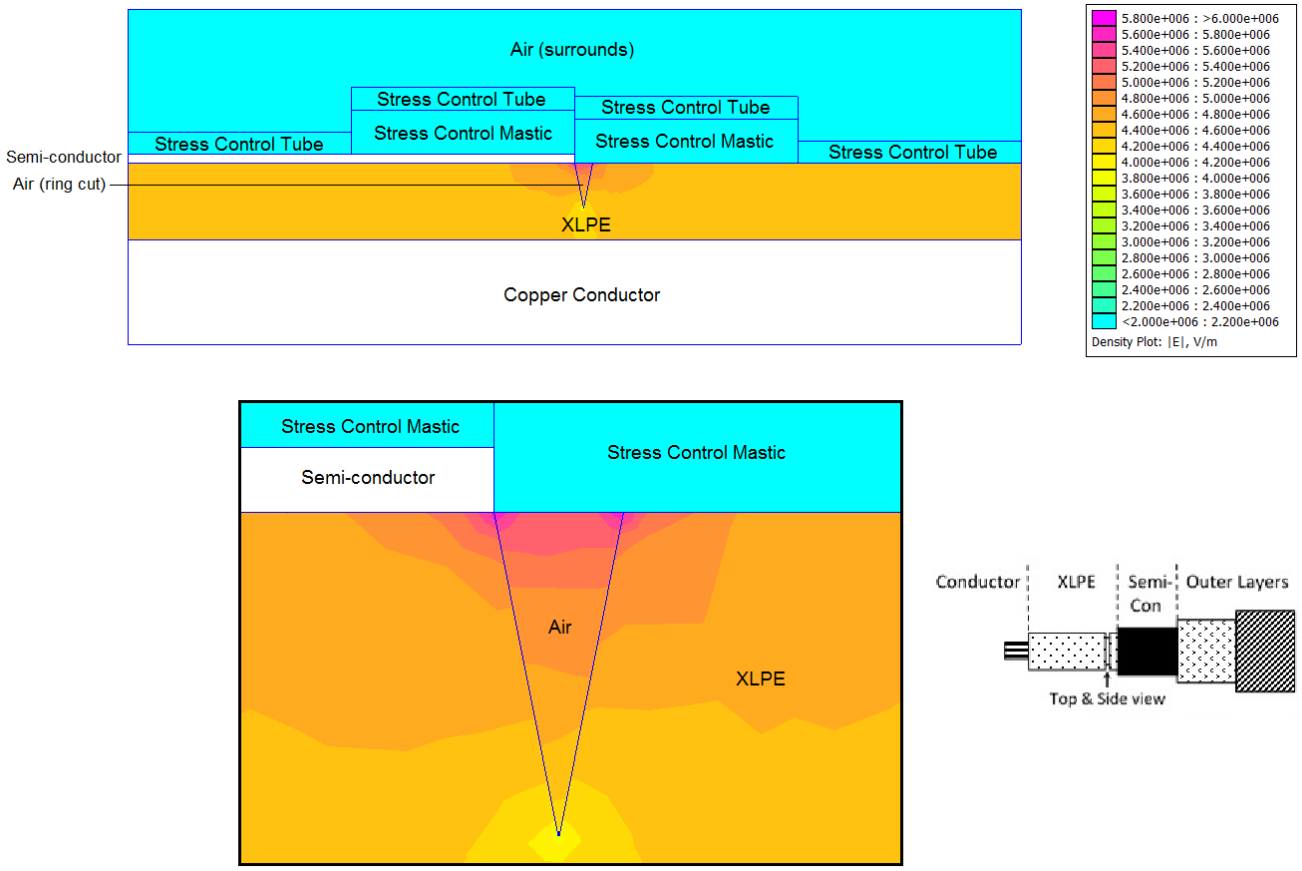

Figure 4.8: Electric Field Plot of the Ring Cut Defect at 0.1 Hz

The ring cut has both a distributed electric field in its void and sharp concentrations at the corners bordering the semi-conductor & stress control mastic layers. As with the semi-conductor feather, the electric field distribution in and around the ring cut, differs between test frequencies. Although a similar electric field gradient was observed in the ring cut between frequencies, magnitudes at 50 Hz were greater than at 0.1 Hz. As with the first two defects, the electric field strength magnitudes in the ring cuts, at both frequencies, exceed the breakdown strength of air for the ring cut (2.48×10^6 V/m).

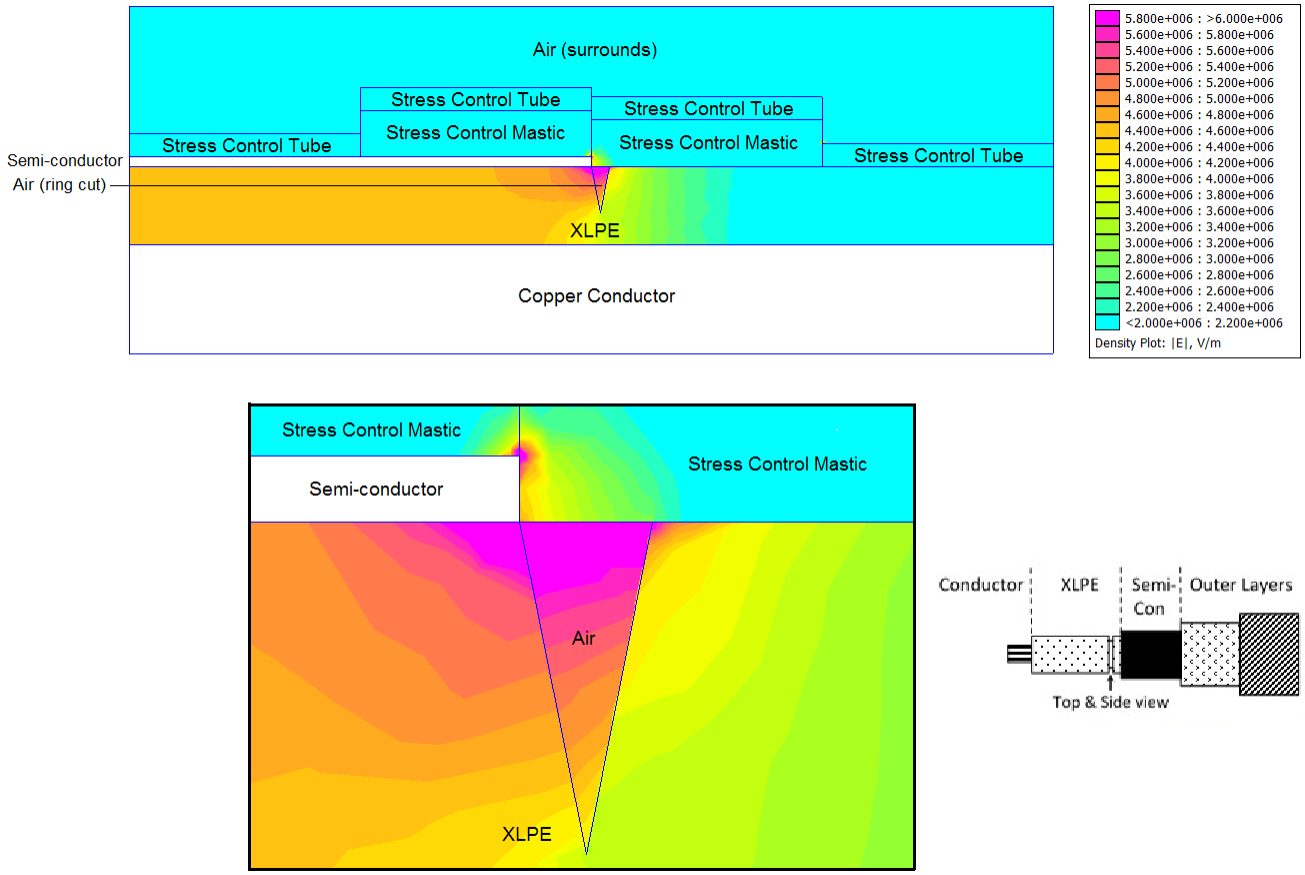

Figure 4.9: Electric Field Plot of the Ring Cut Defect at 50 Hz

Table 4.1: Maximum Simulated Electric Field Strength for the Defects at 50 and 0.1 Hz

Artificial Defect	Maximum Electric Field Strength (V/m)	
	50 Hz	0.1 Hz
Semicon Feather	10.0×10^6	4.9×10^6
Tram Line	4.4×10^6	4.4×10^6
Ring Cut	9.3×10^6	5.9×10^6

4.1.5 Effect of Frequency on Electric Field Simulations

For the healthy and tram line planar models, no change was observed in the electric field distribution or magnitude, between frequencies. Conversely, for the healthy and ring cut axisymmetric models, as well as for the semi-conductor feather planar model, a significant difference in the electric fields were observed between 0.1 Hz and 50 Hz. Therefore, in terms of simulations, test frequency had no effect on the models with a continuous semi-conductor layer (electrode) structure, i.e. the healthy planar and tram line models. However, due to the fact that the healthy, axisymmetric termination model experienced a change in electric field between frequencies, suggests that the planar models do not fully simulate the physical conditions of a termination. More specifically, the planar models do not simulate the core screen cut back (discontinuous semi-conductor layer). Therefore it is assumed that the electric field distributions of all terminations (healthy and with defects) are affected by frequency, according to the simulations.

As can be seen from the healthy termination electric field plot in Figure 4.3, frequency has an effect on the electric field, in terms of magnitude and distribution. The simulation at 0.1 Hz yields a maximum electric field strength of 0.46×10^7 V/m versus 1.34×10^7 V/m at 50 Hz. Similarly, for the semicon feather and ring cut defects, the maximum electric field strengths in the defects were smaller for 0.1 Hz than 50 Hz (Table 4.1).

This trend towards greater electric field strengths at 50 Hz than at 0.1 Hz confirms work done by Walker et al. [38], on simulating electric stress distribution in cable accessories at different test frequencies. The electrical stress of some of the cable accessory layers (XLPE, insulation) were higher (relatively) at the

supply voltage for 50 Hz when compared to 0.1 Hz sinusoidal. Furthermore, the electrical stress distribution in cable joints was found to be influenced by the test voltage frequency, according to simulations done in [38]. It was found that phase shifts of the electric stresses of the joint layers occur relative to the supply, for sinusoidal test frequencies of less than 10 Hz, while above this value no phase shifts occur. This phenomenon is the result of cable accessories being made up of multiple layers, each having a varying response to different frequencies in terms of electrical stressing, according to the permittivities and volume resistivities of the materials. Typically, at higher frequency voltages (such as 50 Hz), the voltage and electrical stress distribution is a function of the permittivity of the materials, whereas at lower frequencies closer to DC, the voltage and stress distribution is a function of the volume resistivity of the materials [38]. Therefore, as frequency is decreased to 0.1 Hz, charge distribution is dependent on both the permittivity and conductivity of the materials, and interfacial/space charge polarization may have a larger effect at VLF than at 50 Hz. Physical testing supporting this phenomenon may be found in [40], whereby low frequency electric fields stressed the resistance of a cable's insulation, while the effect of the cable's capacitance dominated at higher frequencies. The cable's tanδ readings, which are a measure of resistive power loss, were an order of magnitude higher at VLF than at 50 Hz [40]. The direct result of these phase shifts in electrical stress due to supply frequency, may be an accompanying phase shift in PD activity between patterns recorded at 50 Hz and 0.1 Hz.

4.1.6 Simulated PD Inception Electric Field Strength

The VLF and 50 Hz simulated and measured inception voltages of the most aggravated defects (core three) of each of the terminations are presented in Table 4.2.

Table 4.2: Simulated versus Measured Inception Voltages of the Artificial Defects at 50 and 0.1 Hz

Defect	PDIV (kV_{RMS})			
	50 Hz		0.1 Hz	
	Measured	Simulated	Measured	Simulated
Semicon Feather	8.8	2.8	8.5	5.8
Tram Line	8.2	6.4	7.1	6.4
Ring Cut	9.1	3.0	3.9	4.7

In a similar fashion to the electric field plots, the simulated inception voltages of the artificial defects agreed well with the measured test results, according to Table 4.2. Although the same limitations of the electric field plots may have an effect on the accuracy of the simulated inception voltages. In comparing the measured and simulated PDIV values, it may be seen that the 0.1 Hz results show greater agreement. Simulated inception voltages decreased with increasing frequency (except for the tram line), as a result of the simulated inception voltages largely being a inverse function of electric field strength. Conversely, measured PDIVs increased for increasing frequency, and thus were higher for 50 Hz than at 0.1 Hz. Therefore, inception voltage is dependent on factors over and above the electric field strength necessary for PD inception. This concept will be further explored in Section 4.2.3.

The difference between simulation and experimental results may be decreased by improving the simulation modelling. Much effort was made to ensure the accuracy of the physical experimental results such as following the relevant standards for PD testing and adhering to good scientific principles, such as reproducibility. Therefore, improvement in the agreement between simulation and experimental results, would largely involve increasing the accuracy of the simulations. A number of improvements could involve:

- Improving the geometrical modelling of the cable terminations, in particular, moving from 2D planar models to full 3D models.
- Dynamic electric field modelling rather than static modelling. This would

better represent the electric field stressing of AC frequency voltages.

- Different solver algorithms and increased solver precision of the modelling package could be used.
- Important partial discharge characteristics/parameters such as statistical time delay could be incorporated into the model.

4.2 Experimental Results: Frequency Comparative PD Test Results

The frequency comparative PD test results for the different artificial defects, under both 0.1 Hz and 50 Hz excitation, are given in Table 4.3. The results presented include average (taken over each test duration) and maximum apparent discharge magnitudes, PDIV, PDEV and repetition rates for the same number of pulses test protocol. Similar values, typically within a variation of 10%, were recorded for same number of cycles tests. The cables were subjected to minimal stress for the shortest possible time to avoid the effects of ageing. However, the 0.1 Hz (cycles) testing of the 25 mm semi-conductor feather (core 3) was not completed before the effects of ageing were seen in the form of complete PD extinction at 11 kV. It is postulated that the sharp point of the semi-conductive feather responsible for the PD activity may have burnt out.

4.2.1 PD Magnitude as a Function of Defect Type & Test Voltage Frequency

Semi-conductor Feather Defect

The semi-conductor feather defects on cores 1 & 2 of test specimen 1, gave average (Qav) and maximum ($Qmax$) apparent discharge values only slightly above the average noise floor. As expected, the more severe defect on the third core gave significantly bigger PDs, well above the noise floor. This is the result of the PD levels of the semi-conductor feather defects being largely dependent on the length and sharpness of the feather. The length of the feather has an influence due to the

Table 4.3: PD Characteristics of the Terminations tested at 50 and 0.1 Hz

Measured Quantities	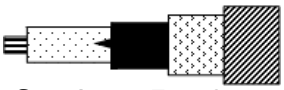 Semicon Feather		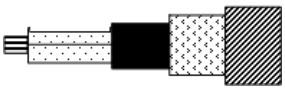 Tram Line		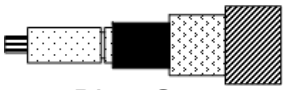 Ring Cut	
	10 mm	25 mm	1 mm	2 mm	1 mm	2 mm
0.1 Hz						
Qmax (pC)	11	171	21	346	747	1223
Qav (pC)	5	69	8	139	300	491
Repetition rate (pulses/s)	971	924	978	894	817	910
50 Hz						
Qmax (pC)	5	397	17.8	722	2042	2972
Qav (pC)	2	160	7	290	1071	1648
Repetition rate (pulses/s)	9758	4838	9527	3785	8435	3490

stress control mastic tape being applied over the XLPE layer typically for 10 mm for this cable type and rating. Therefore, any feathers with a length of 10 mm or less may be masked by the mastic tape. The sharpness of the feather also has an impact on the PD activity of the defect, as it results in a more intensified electric field at that point compared to the rest of the semi-conductive layer.

Tram Line Defect

The 1 mm deep tram line defects of test specimen 2 (cores 1 & 2) generated relatively small PD in comparison to the deeper 2 mm tram line of core 3. At 1.7 U_0, all the tram line defects generated PD magnitudes greater than the acceptable level of 5 pC, in accordance with the IEC 60502-2 standard. The relatively small PD values from the 1 mm tram lines may be the consequence of the mastic tape filling up part of the tram line, as well as due to the heat shrink products (stress control tubing and anti-tracking heat shrink) contracting the XLPE insulation upon heating. Therefore, the significantly bigger PD magnitudes of the 2 mm tram line would be the result of the covering layers being unable to fill up the deeper and wider void.

Ring Cut Defect

All of the ring cut defects generated significant PD magnitude values, with the 1 mm deep cuts of test specimen 3 (cores 1 & 2) having similar magnitude values, thereby showing good reproducibility. The ring cut defects showed a much higher PD magnitude than the tram line & feather defects and the possible reasons for this are as follows:

- The ring cut voids had a much larger cross-sectional area between the electrodes, as can be seen in Figure 4.17.
- The entire ring cut voids are in close vicinity to the semi-conductor layer, while in the case of the tram lines, only a short length of the void is near the semi-conductor layer (region of high electric field strength).
- The covering heat shrink products would have little to no effect in contracting the ring cut voids.

Test Voltage Frequency dependency of PD Magnitudes

According to Table 4.3, the average and maximum PD magnitudes showed a trend of significantly larger discharge magnitudes at 50 Hz than at 0.1 Hz, for magnitudes greater than $\sim$20 pC. This trend holds for all the defects generating significant discharges, including the third cores for both the semi-conductor feather and tram line defects, as well for all three cores of the ring cut defect. The factor between the corresponding PD magnitudes (>20 pC) at 50 Hz and 0.1 Hz is typically between 2-3. This trend confirms the work by Voigt & Mohaupt [41] and Irani et al. [40], where comparable differences between the PD magnitudes measured at 50 and 0.1 Hz, were found. Furthermore, research into the breakdown voltage of cables with contaminants [42], has found that the VLF (0.1 Hz) test voltage needed to be between 2-3 times that of the 50 Hz voltage in order to achieve breakdown within a comparable time.

The partial discharge magnitude distribution histograms in Figure 4.10 confirm the second trend, namely that at power frequency, PD magnitudes are generally bigger in terms of average and maximum PD magnitude, than at VLF. The PD magnitude distribution histograms are for the same number of pulses recorded

for power frequency and VLF excitation voltages. Similar plots are obtained for the same number of cycles measurements. As can be seen from Figure 4.10, for the higher discharge magnitudes (>20 pC), the number of discharges at 50 Hz is far greater than at 0.1 Hz, thereby resulting in greater average PD magnitude. Furthermore, the tail of the histograms which effectively represent the maximum PD magnitudes, extend further for 50 Hz than for 0.1 Hz.

This observed behaviour of partial discharge magnitude as a function of the excitation voltage frequency can be explained in terms of the influence of the following parameters on the discharge process:

i seed electron statistical availability time lag,

ii gap overvoltage (overstress),

iii rate of increase of the electric field.

Two well known conditions necessary for the initiation of a discharge avalanche in a gas medium (partial discharge) are; an electric field equal or greater than a critical threshold value (E_{inc}) and the availability of a seed electron. Furthermore, the seed electron should be in a favourable position to initiate self-sustaining ionization avalanches. The background electric field (E_0) in a discharge gap will increase as the voltage across the electrodes increases, until it reaches E_{inc}. If a seed electron is available, a partial discharge should occur. However, if a seed electron does not become available, the background electric field will continue to increase beyond E_{inc} at a rate proportional to the supply voltage frequency. If and when the seed electron becomes available, E_0 will have exceeded E_{inc} by Δ E_0 (gap overstress). The resultant ionisation avalanches will thus occur under the influence of a higher electric field ($E_{total} = E_{inc}+\Delta\ E_0$) than E_{inc}. The bigger the gap overstress E_0, the bigger the resultant PD magnitude. This concept of gap overstress phenomenon resulting from the delayed availability of a seed electron is illustrated in Figure 4.11.

In void discharges such as the tram line and ring cut defects, the majority of seed electrons are availed through surface emission mechanisms [43]. The rate of rise of the background electric field is proportional to the supply voltage frequency. As a result, there is a higher probability that a discharge occurs at higher

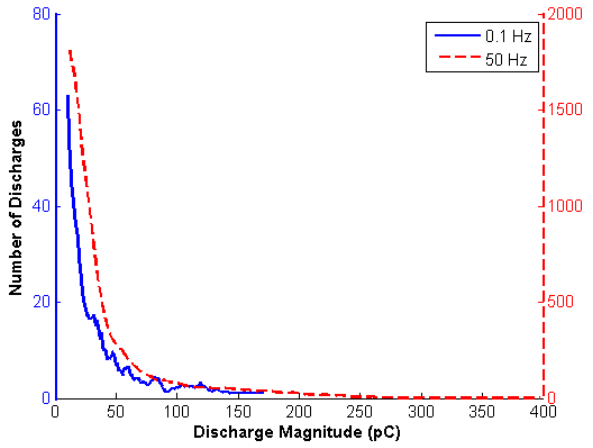

(a) Semicon feather

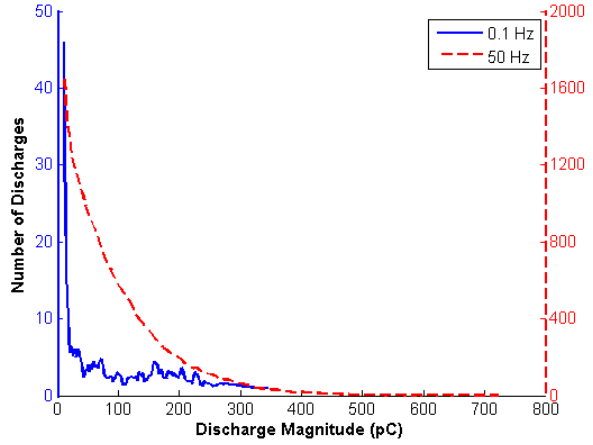

(b) Tramline

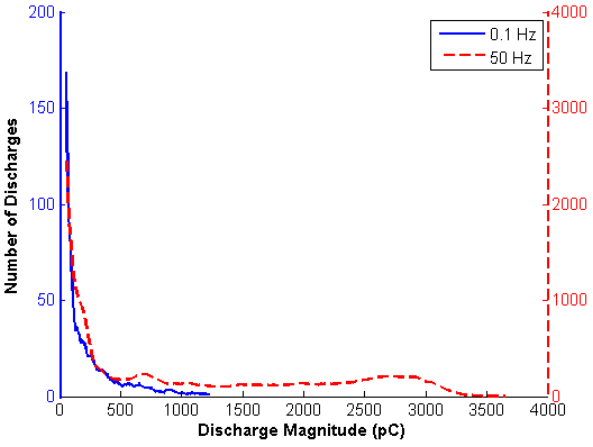

(c) Ring-cut

Figure 4.10: Partial Discharge Magnitude Distribution Histograms; (a) Semicon Feather, (b) Tram Line and (c) Ring Cut

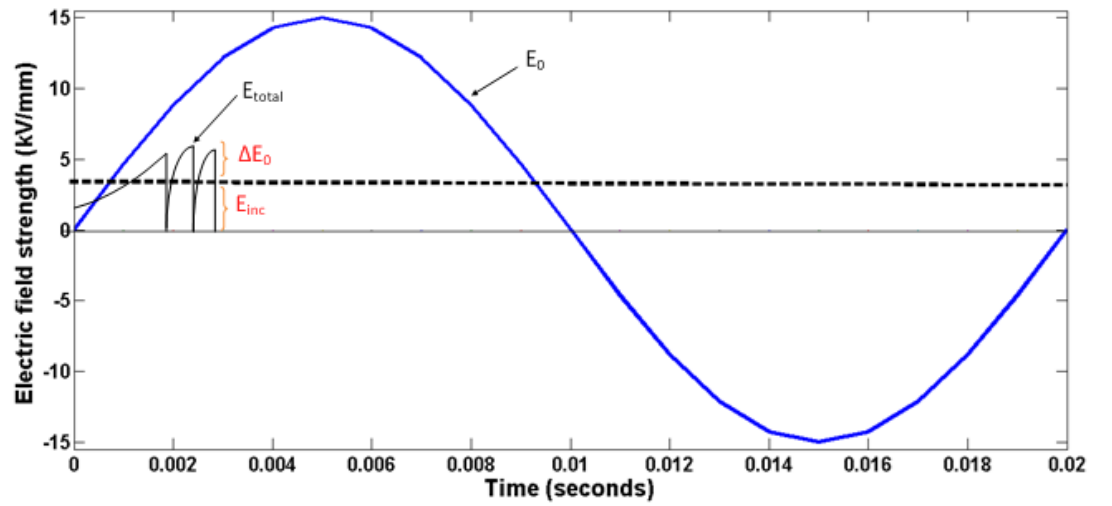

Figure 4.11: Gap Overstress Phenomenon due to Delayed Availability of Seed Electron to Initiate PD

gap overstress ($\Delta\ E_0$) for power frequency than at VLF, as is the case in this work. Other researchers such as Bodega et al. [44], Forssen et al. [45], Miller et al. [46] and Wester et al. [47] have reported similar results. These findings suggest that the acceptable partial discharge limits outlined in various standards/guidelines need to be evaluated and stated for corresponding frequency ranges of the excitation voltage, rather than having a single limit for all frequencies, as is the case traditionally.

4.2.2 PD Magnitude as a Function of Supply Voltage Magnitude

The apparent charge versus test voltage graph of Figure 4.12 shows a steady increase in charge magnitude for increasing test voltage for the semi-conductor feather defect, with no such increase for the other two types of defects. The same trend was observed for the maximum apparent charge and the number of PDs per cycle. Similar results to those of the semi-conductor feather defect were found by Illias et al. [48], specifically for surface discharges. However, for the void-type discharges generated by the tram line and ring cut defects, there was constant apparent charge (average & maximum) for increasing test voltage. This result is

characteristic of void discharges, whereby a step increase of charge versus voltage is expected at inception voltage, after which charge magnitudes plateau [49]. It is suggested that the observed manner in which PD magnitudes respond to an increase in test voltage is a distinguishing criterion for different defects.

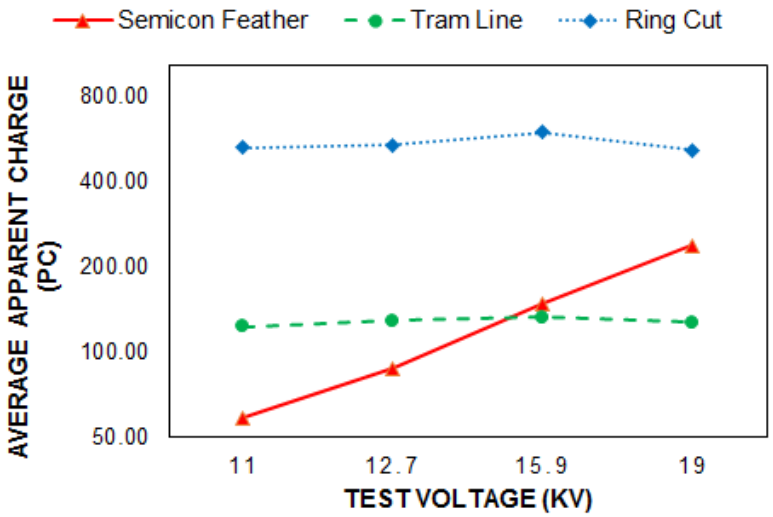

Figure 4.12: Average Apparent Charge versus Test Voltage for Different Defect Types

4.2.3 PD Inception/Extinction Voltage as a Function of Defect Type & Test Voltage Frequency

Defect Type

The inception and extinction voltages (Tables 4.2 and 4.4) did not provide any unique or distinct trends across the different defects. However, for the same defect type but of different severity, it was found that there is a relationship between the PD magnitudes and the inception/extinction voltage. A defect generating relatively big PD magnitudes, had a corresponding relatively low inception and extinction voltage. Therefore, the conclusion that may be drawn from these results, is that the value of the inception/extinction voltage gives an indication of the resulting PD magnitudes and thus the severity of the defect.

Table 4.4: Measured PD Inception/Extinction Voltages of the Terminations tested at 50 and 0.1 Hz

Measured Quantities	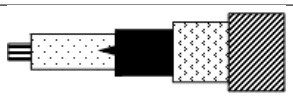 Semicon Feather		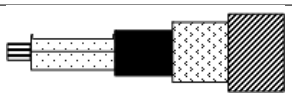 Tram Line		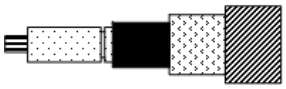 Ring Cut	
	10 mm	25 mm	1 mm	2 mm	1 mm	2 mm
0.1 Hz						
PDIV (kVrms)	-	8.5	9.2	7.1	4.0	3.9
PDEV (kVrms)	-	8.5	8.8	7.0	3.9	3.8
50 Hz						
PDIV (kV_{RMS})	-	8.8	11.0	8.2	6.7	9.2
PDEV (kV_{RMS})	-	8.7	11.0	8.0	6.4	8.9

Test Voltage Frequency

The literature regarding PD inception/extinction voltages at 50 and 0.1 Hz for cable testing, is typically inconclusive about any overriding trends, with no significant difference of PDIV/PDEV noted between the frequencies [40, 41, 50].

In the present work, it was found that the inception/extinction results for the semi-conductor defect (core 3) showed a good correlation between 50 and 0.1 Hz. Conversely, the tram line and ring cut defects showed a substantial difference between the test frequencies. In particular, the 0.1 Hz inception/extinction voltages were about half of the corresponding 50 Hz values, for the ring cut defects. It is postulated that the delayed availability of a seed electron, as outlined in Section 4.2.1, may also result in bigger PDIV at power frequency than at VLF. The delayed availability of a seed electron, also known as statistical time lag or inception time delay (Δt_{inc}), may be one of the major contributing factors to the significant variation in inception/extinction voltages between test frequencies. This phenomenon has been studied by Gross et al. [51], where it was found that despite an internal electric field greater than that of the inception field, no seed electron may be available to trigger the partial discharge electron avalanche. The PD event will only occur when a free electron that is being accelerated in the electric field strongly enough, is available [51]. Therefore, it follows that PD inception will only occur when the voltage & electric field strength across the cavity are greater than

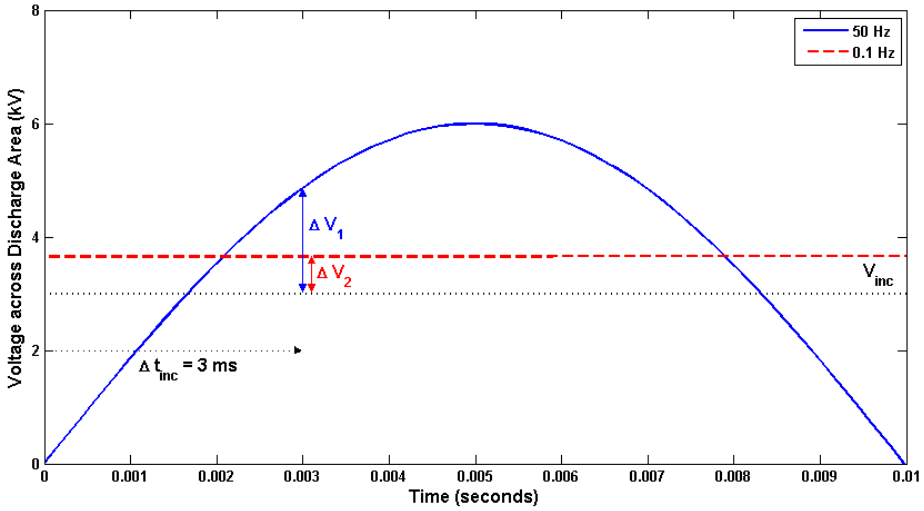

Figure 4.13: The Influence of Statistical Time Lag on Partial Discharge Inception for Varying Voltage Test Frequencies

the corresponding inception values, for a time longer than the statistical time lag (Δt_{inc}).

Assuming a typical statistical time lag in the range of tens of milliseconds for XLPE, which is a reasonable assumption according to Forssen et al. [52] and Gross et al. [51], it follows that PD inception is more likely to occur at a lower voltage for 0.1 Hz than at 50 Hz. At 50 Hz, the voltage across the discharge area can reach and exceed the intrinsic PD inception voltage (V_{inc}) before a seed electron is available to initiate discharge. The actual discharge thus occurs at a point, where the voltage across the discharge gap exceeds V_{inc} by ΔV (gap overvoltage). The intensity of the discharge channel ionic avalanche processes and therefore the corresponding PD magnitude is directly proportional to the gap overvoltage, as discussed in Section 4.2.1. At VLF the rate of the rise of voltage is 500 times slower than at 50 Hz, therefore, ΔV_2 and the effective PDIV (V_{inc}+ΔV_2) is much smaller than ΔV_1 and the corresponding PDIV (V_{inc}+ΔV_1) for the 50 Hz case. This concept is shown in Figure 4.13, with the voltage-time graph displaying the effect that statistical time lag may have on the inception of different voltage test frequencies.

This concept of a delayed seed electron resulting in a gap overvoltage and larger inception voltage for power frequency compared to VLF, is further reflected in the inception field strength simulation results (Section 4.1.6). For VLF, there was a relatively good agreement between the measured and simulated results, indicating that PD inception at 0.1 Hz is largely dependent on the intrinsic voltage & electric field strength inception values. This would be expected, as the lengthy period of 10 s ($\gg \Delta t_{inc}$) results in the statistical time delay having minimal effect on inception. Conversely, at power frequency, the much shorter period of 20 ms means that the statistical time lag will result in inception delay and an overvoltage. The nature of the inception field strength simulations do not account for this delay/overvoltage and therefore there is a much larger disparity between the measured and simulated results.

Other factors which may influence PD inception/extinction voltages, includes the presence of electronegative gases in the void, which can have an effect on the statistical time-lag of the first PD according to Kim et al. [53]. In [53], it was found that a decrease in oxygen and the resulting production of electronegative molecules (CO_2 and H_2O) may influence the inception time/time lag of PD activity, due to the capture/attachment of free electrons by oxygen and electronegative molecules. Therefore, future work expanding upon the work done in [53], needs to be conducted into the effect of test frequency on the inception time/time lag of PD due to molecular changes.

4.2.4 PD Phase Resolved Pattern Variations as a Function of Defect Type and Frequency

The theory used in interpreting the phase resolved patterns obtained in this work, is presented first. The obtained phase resolved PD patterns of each defect are then presented and discussed in their respective sections.

The observed PDPRP features of the different artificial defects can be explained using the space charge dynamics in the discharge area according to Neimeyer's model for partial discharges [43], [54]. The three electric fields interacting in the discharge give a resultant electric field, that when big enough initiates a discharge, as illustrated in Figure 4.14.

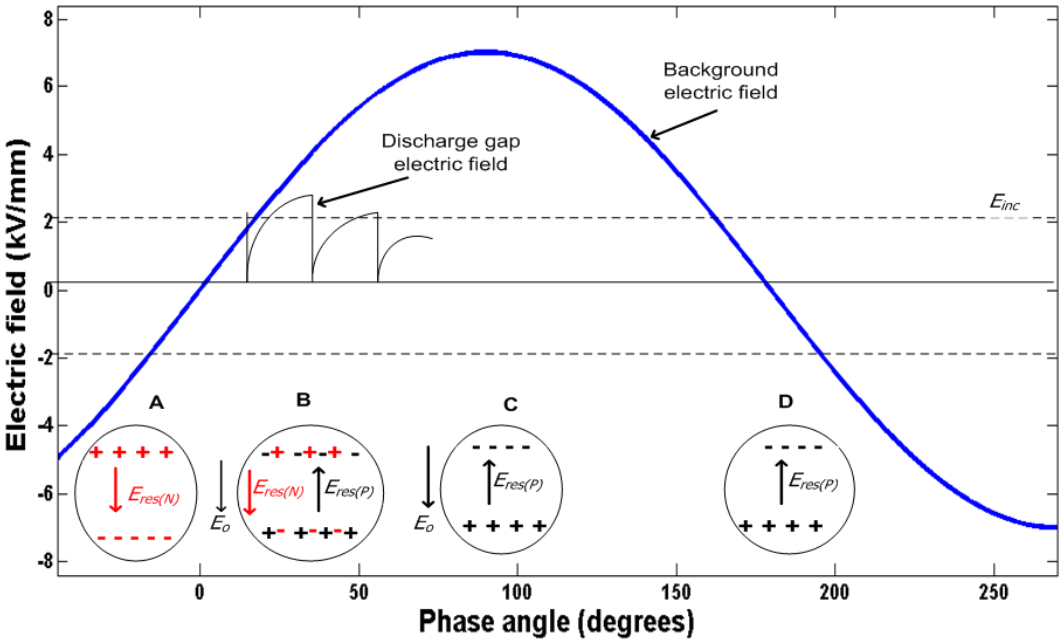

Figure 4.14: Space Charge Dynamics in a Partial Discharge Event

The effect of the excitation voltage frequency, the interaction of the various electric fields in the discharge gap and the resultant shaping effect on the PRPDP is illustrated schematically in Figure 4.14, with corresponding explanations in Table 4.5.

Table 4.5: The Interaction of Various Electric Fields in the Discharge Area as a Function of the Phase Position and the Resultant Effect on PDs

(A): Zero crossing PDs on transition from the negative to positive half cycle	**(B): Early positive half cycle PDs**	**(C): Late positive half cycle PD**	**(D): Zero crossing PDs on transition from the positive to negative half cycle**
• E_{total}=$E_{res(N)}$ • If $E_{total} \geq E_{inc}$ and a seed electron is available, PD will occur. • PD can occur at the zero crossing, in the absence of the background electric field, due to the residual charge electric field.	• E_{total}=$E_{res(N)}$+E_0-$E_{res(P)}$ • If $E_{total} \geq E_{inc}$ and a seed electron is available, PD will occur. • The additive superposition of $E_{res(N)}$ and E_0 intensifies the resultant stress in the discharge area. • If the statistical time delay (Δt_{inc}) of the seed electron does not change, the resultant PDs are relatively bigger than in the previous events, thereby forming the 'rabbit ear' part of the "rabbit ear" profile resultant PRPDP.	• E_{total}=E_0-$E_{res(P)}$ • The space charges from the negative half cycle have completely depleted. • If $E_{total} \geq E_{inc}$ and a seed electron is available, PD will occur. • The absence of $E_{res(N)}$ and the reduced rate of increase of E_0 diminishes the resultant stress in the discharge area relative to previous events. • If the statistical time delay (Δt_{inc}) of the seed electron does not change, the resultant PDs are relatively smaller than in the previous events, thereby forming the 'body' part of the "rabbit ear" profile resultant PRPDP.	• E_{total}=$E_{res(P)}$ • If $E_{total} \geq E_{inc}$ and a seed electron is available, PD will occur. • The sequence of PD events repeat but with the corresponding electric fields polarity being opposite to those in the positive half cycle.

The sequence of events A,B,C and D in Figure 4.14 and the corresponding descriptions in Table 4.5 use symbols defined as follows:

- $E_{res(P)}$ and $E_{res(N)}$ are the space charge deposited on the insulation surface of the discharge area by previous discharge events in the positive and negative half cycles respectively.
- E_0 is the background electric field in the discharge area due to the voltage across the test object.
- E_{total} is the vector sum of all the electric fields present in the discharge area, thereby forming the resultant electric field.

If the resultant electric field (E_{total}) becomes equal or bigger than the PD inception stress, E_{inc}, a discharge will occur provided a seed electron is available to initiate the electron avalanches. $E_{res(P)}$ and $E_{res(N)}$ may be termed the crossover residual electric field, responsible for stress enhancement in the discharge area giving rise to the "rabbit ear" shape of certain PRPDPs and PDs about the zero-crossings. The crossover residual electric field is a function of how much residual charge is retained on the insulation surface of the discharge area, which in turn is a function of the defect geometry and the discharge surface conductivity. The extent of the "rabbit ear" profile is thus dependent on the defect geometry and the ageing effects of the PD on the discharge area [53].

The PRPDPs for core number three of the tram line and ring cut defects are displayed in Figure 4.16 and Figure 4.18 for the cycles test, with these patterns being more pronounced than those of the pulses test. The PRPDP for the pulses test of core three of the semi-conductor feather defect is presented in Figure 4.15, for comparative purposes. It is observed that each type of defect has a distinct PDPRP. For each defect, the discharge patterns show a good visual correlation between the patterns at power frequency and at VLF, notwithstanding differences in PD magnitude ranges and population ranges of the PD.

Semi-conductor Feather Defect

The PRPDP of the third core of the semi-conductor feather (Figure 4.15) has a resemblance to that of a corona discharge, with the maximum discharges occurring

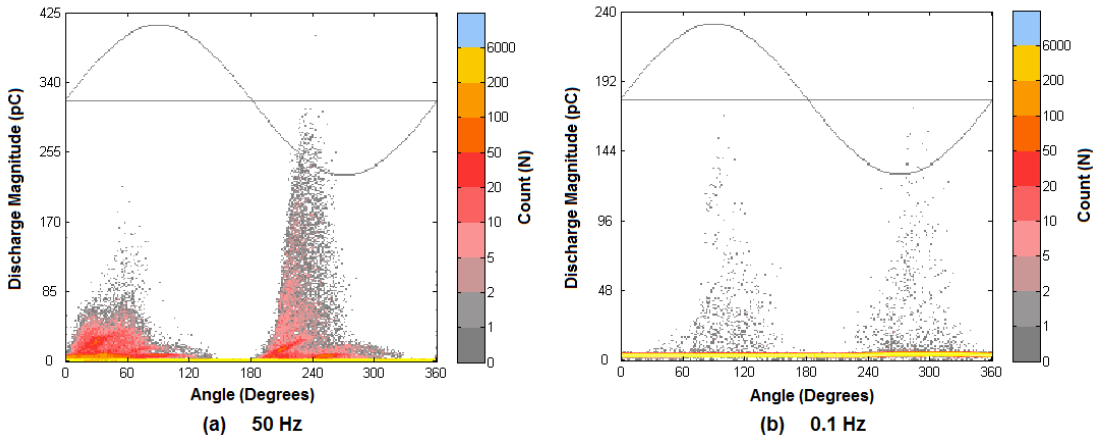

Figure 4.15: Semi-conductor Feather PD Patterns at 50 Hz and 0.1 Hz for the Pulses Test

near the peaks and troughs of the supply voltage (90° & 270°), particularly for the 0.1 Hz pattern. The occupied phase positions are the widest between 0-150° and 180-330°. The pattern may be differentiated from that of corona in air by the absence of Trichel pulses, which are characteristic of corona.

The semicon feather has a geometry which is less favourable to the trapping of residual charge compared to the tram line and ring cut defects, both of which are essentially cavity defects. Therefore, resulting PD pulses, unlike corona [18], are significantly displaced from the zero crossings and moreover do not have "rabbit ear-like" features.

The PD of the semi-conductor feather defect is essentially surface discharges along the insulation surface adjacent to the semi-conductive tip. The PD pattern is consistent with patterns found by Illias et al. [48], for a surface discharge between a pin electrode at HV separated from an earth electrode by XLPE, as well as by Jiang et al. [7], for metal/semi-conductive particles left on the XLPE of a HV cable joint.

The partial discharges of the semi-conductor defect occur when the electric field at the surface of the electrode (feather point) exceeds the breakdown strength of the air trapped between the stress control tube/mastic tape and the sharp point. The result of this, is the ionisation of the air near the sharp point [48]. The tangential electric field on the insulation surface reaches a high enough level to

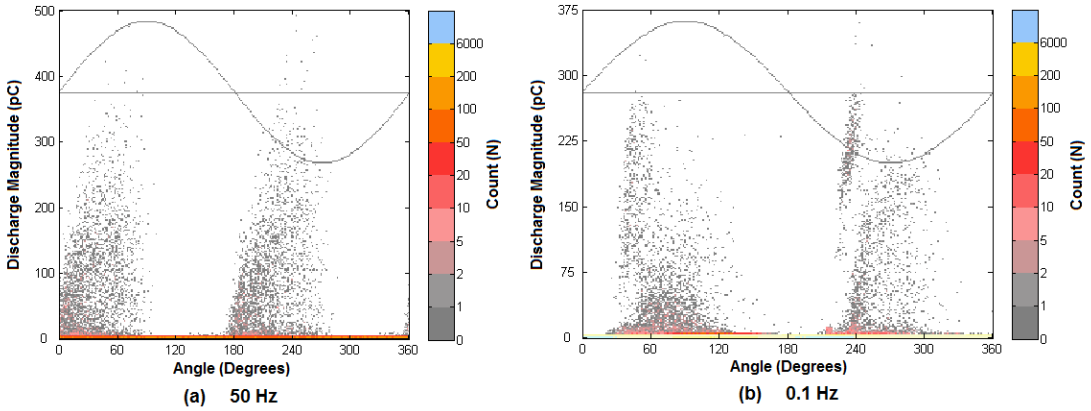

Figure 4.16: Tram Line PD Patterns at 50 Hz and 0.1 Hz for the Cycles Test

initiate PDs along the material's surface. If the applied voltage is increased, the number of electron ionisations increases and the electron avalanches can extend further along the material surface [48], therefore giving bigger PD as presented earlier in Figure 4.12.

Tram Line Defect

The PRPDP of the 2 mm tram line (Figure 4.16) displays PD activity on the rising edges of the source voltage waveform, with bigger magnitudes occurring just before the test voltage peaks and troughs. The phase positions of the tram line PDs are largely between 0 and 70° for the positive half cycle, and between 180 and 270° for the negative half cycle. Unlike the semi-conductor feather, the tram line is a cavity defect and consequently is more favourable to retaining crossover residual charge. As a result, the tram line PRPDP is displaced towards the zero crossings of the test voltage, forming a "rabbit ear" profile.

The tram line discharge pattern is indicative of a narrow cavity according to Gulski et al. [18], with a wide distribution of PD about the discharge peaks, which occur just before 90° and 270°. A narrow cavity is defined as a void in which the dimension of the cavity perpendicular to the electrodes (height) is much larger than that of the dimension parallel to the electrodes (width). This is illustrated in a cross-sectional view of the tram line in Figure 4.17.

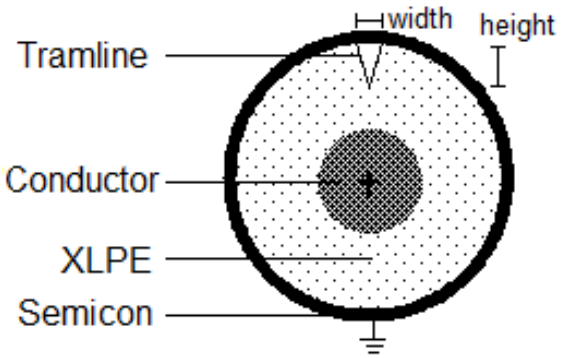

Figure 4.17: Cross-section of the Tram Line

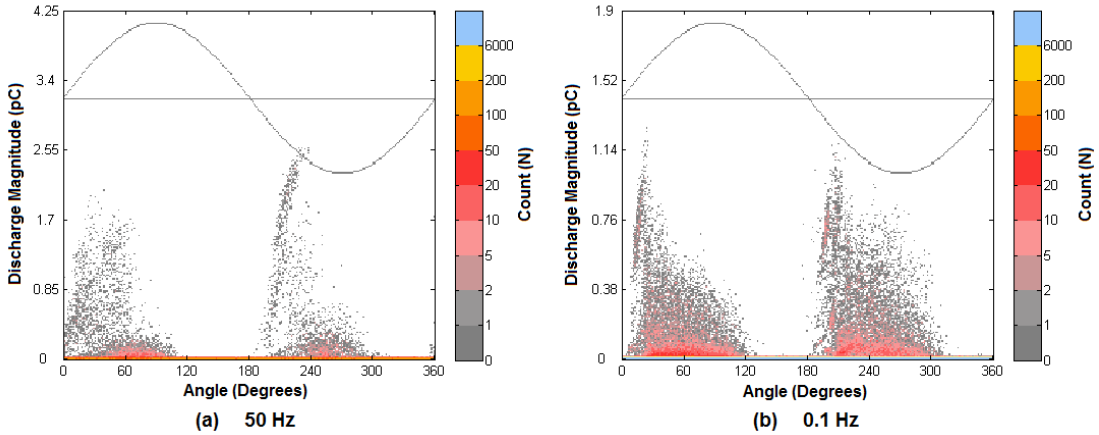

Figure 4.18: Ring Cut PD Patterns at 50 Hz and 0.1 Hz for the Pulses Test

Ring Cut Defect

The ring cut defects are more favourable to retaining crossover residual charge than the tram line and semicon feather defects, for similar reasons to those outlined in Section 4.2.1. As a result, the PRPDP of the 2 mm ring cut (Figure 4.18) gives a more enhanced "rabbit ear" feature than the other two defects, with an increased tapering off of PD magnitude from the peak discharge. The ring cut pattern has a wider distribution than the tram line, with PD pulses occupying the phase regions 0 to 120° and 180 to 300°, in the positive and negative half cycles respectively.

The ring cut discharge pattern is characteristic of a flat cavity, as investigated by Gulski et al. [18]. A flat cavity is the opposite of a narrow cavity with its

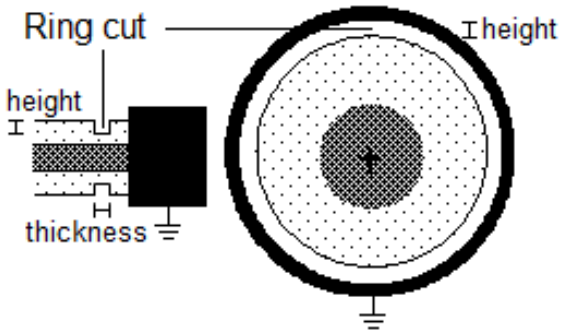

Figure 4.19: Cross-section of the Ring Cut

width being much larger than its height. In the case of a ring cut, the width of the void is much greater than the depth/height of the cut, as shown in Figure 4.19. The resulting discharge pattern is one that has sudden peaks on the rising edges of the test voltage near the zero-crossings. After these discharge peaks, the PD pattern tapers off to a minimum following the voltage source peaks/troughs. The first (large) partial discharge event is a streamer-like discharge, which is related to a higher overvoltage due to electronegative gases according to Kim et al. [53], after which the discharge magnitudes decrease as the gases are consumed.

Test Voltage Frequency Effect on PD Phase Resolved Patterns

In terms of discharge patterns, there was a good correlation between the PRPDPs recorded at 50 Hz and 0.1 Hz, for all three defects, for both the cycles and pulses tests. For the same number of cycles test, typically 3 to 5 million pulses were recorded at 0.1 Hz, whereas 30-100 thousand pulses were recorded at 50 Hz. Despite a much larger number of recorded pulses for the 0.1 Hz cycles test when compared to the 50 Hz test, the patterns appear similar in terms of the higher magnitude discharges (Figures 4.16 and 4.18). This result implies that at 0.1 Hz, the percentage of higher magnitude discharges was much less than at 50 Hz and thus more discharges of lower magnitudes were measured at 0.1 Hz. This trend is even more evident in the tests involving the same number of recorded pulses, which saw a typical test time of about 60 s at 50 Hz and 600 s at 0.1 Hz. Despite the same number of recorded pulses, the PRPDPs at 50 Hz appear more popu-

lated for higher magnitude pulses than at 0.1 Hz, as can be seen in Figure 4.15. This trend of more recorded (smaller magnitude) pulses at lower test frequencies as discussed in Section 4.2.1, has also been reported by Pepper [55], for a needle defect in XLPE cables.

4.2.5 Positive & Negative half-cycle PRPDP

For all three defects, the number and magnitude of the discharges occurring in the negative applied voltage cycle were slightly higher than in the positive cycle (on average). This trend is difficult to observe on the cumulative PRPDPs, but is more prevalent on the instantaneous discharge-time graphs, such as in Figure 4.20. This result may be attributed to the defects being located in closer vicinity to the semi-conductive layer at earth potential (negative electrode). At the moment of discharge, the nature of the material functioning as the cathode (electron supplier) influences the relative magnitude of the resultant PD. An insulating surface is a better supplier of electrons. Therefore if a defect is bounded by insulation on one side and a conducting material on the other, in the half cycle where the insulation acts as the cathode and the conducting surface is the anode, larger PDs occur [56].

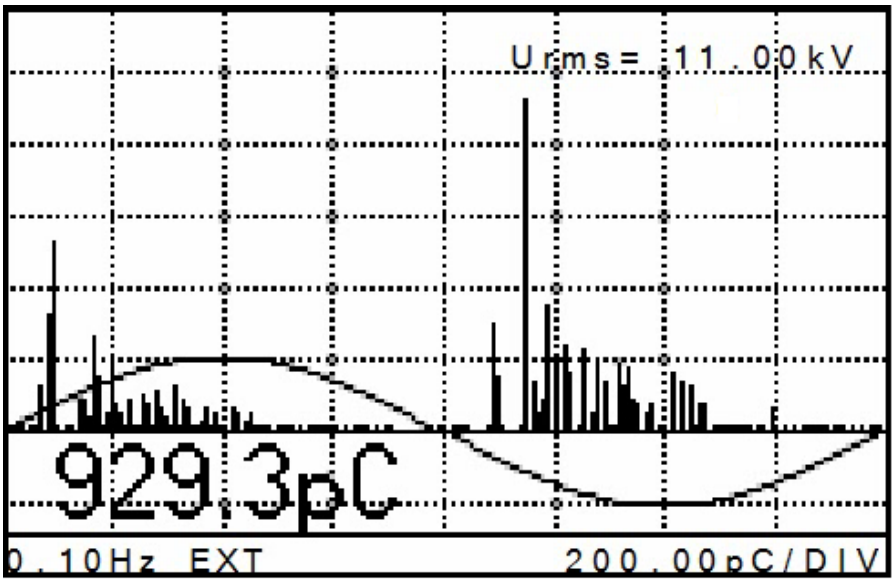

Figure 4.20: Average Apparent Charge versus Phase Graph of a Ring Cut at 11 kV

4.3 Summary of the Experimental Findings

The partial discharge activity of three different types of defects in MV power cable terminations was characterised, using VLF and power frequency testing. The defects investigated were semi-conductor feathers, tram lines cut into the XLPE insulation and ring cut in the XLPE. The cable termination defects were subjected to a typical overvoltage commissioning test, during and after which the PD performance of the terminations was measured at 0.1 and 50 Hz test voltages. These results were then compared and verified against the results of similar studies. The important findings which can be drawn from this work are as follows:

- All the defects passed the industry pressure (overvoltage) test, despite most of the terminations recording significant PD magnitudes.
- The PD magnitude values measured at power frequency were up to 3 times greater than the corresponding values at VLF. This disparity is the direct result of the (seed electron) statistical time lag and the rate of increase of the electric field resulting in a larger gap overvoltage at 50 Hz than at 0.1 Hz.
- The PD magnitudes of the semi-conductor feather defect surface discharges increased with voltage, while no such trend was evident for the void discharges (tram line/ring cut defects).
- The 50 Hz inception/extinction voltages of the defects were approximately double those of the corresponding 0.1 Hz voltages, for the ring cut defect. The tram line defects also had lower inception/extinction voltages at 0.1 Hz, while the semi-conductor feather defect had similar values for both test frequencies. As with the PD magnitudes, the differences in inception/extinction voltages between test frequencies, is the consequence of gap overvoltage/stress.
- Each typical defect gave distinct phase-resolved-patterns that are essentially invariant whether the test voltage is at 0.1 or 50 Hz.
- The discharge pattern of semi-conductor feather defect resembled that of a corona-like, surface defect, which was the result of an intensified electric field at the sharp point of the feather.

- The PRPDP and geometry of the tram line cut into the XLPE insulation is consistent with that of a narrow cavity.
- The distinct "rabbit ear" profile discharge pattern of the XLPE ring cut showed resemblance to that of a flat cavity. This pattern is the result of molecular changes and electronegative gases in the void and the influence of residual charge.

Chapter 5

CONCLUSION & RECOMMENDATIONS FOR FUTURE WORK

This research aimed to investigate answers to the following research questions:

- Are there any specific characteristics in the partial discharge measurements that uniquely distinguish different defects in MV cable terminations tested at VLF HV?
- How do the characteristics in MV XLPE cable termination defects compare and contrast at VLF & power frequency excitation voltages?

The results of this research work show that it is possible to use VLF PD testing as a suitable means to distinctly characterise common defects in MV cable terminations. The answers to the research questions and the key conclusions of this research work are as follows:

- A heat shrink MV cable termination may pass typical high potential commissioning tests and yet manifest significant PD activity, due to an underlying defect.
- The PD magnitudes of the defects were typically bigger at power frequency than at VLF, while the PD inception voltages were consistently lower at VLF.

- The PD magnitudes of the void defects, namely the tram line and ring cut defects, were found to be relatively constant with increasing applied voltage, while the surface discharges of the semi-conductor feather defect were found to increase in magnitude.

- The phase-resolved-patterns of the defects were each shown to be different, with the tram line and ring cut having distinct "rabbit ear" profiles and the semi-conductor feather exhibiting a corona-like, surface discharge pattern.

- The unique relationship between cable defects and their corresponding partial discharge characteristics suggests possibilities of automatic defect recognition using PD classification techniques.

More work may be necessary to investigate the influence of environmental conditions and ageing on partial discharge characteristics. Therefore two important extensions of this work could involve investigating the influence of temperature variations and extended periods of stressing on the PD performance of artificial cable defects. In terms of an investigation into ageing, the work could either take the form of investigating the breakdown performance of the terminations or partial discharge monitoring over time. An interesting combination of these two options could involve stressing the cable at higher frequencies (>400 Hz) in order to replicate the effects of ageing until breakdown occurs, while taking PD measurements at set time intervals. Furthermore, different PD test frequencies could be used such as 0.1 and 50 Hz, in order to further expand upon the comparative work done in this research. The results of this future work could provide valuable information for online condition monitoring, such as the long term effects of PD on different defects and the suitability of PD test frequencies for predicting breakdowns.

REFERENCES

[1] Mining IQ. "Mining in South Africa.", 2014. URL http://www.projectsiq.co.za/mining-in-south-africa.htm. [Last Accessed Jan. 6, 2016].

[2] K. Meena, B. Rao, T. Thirumurthy, and G. Raja. "Failure analysis of Medium Voltage Cable accessories during qualification tests." In *2012 IEEE 10th International Conference on the Properties and Applications of Dielectric Materials (ICPADM)*, pp. 1–4. Bangalore, India, July 2012.

[3] Angus Fynes-Clinton. Personal Communication, Sept. 2014.

[4] P. Cichecki, R. Jongen, E. Gulski, J. Smit, B. Quak, F. Petzold, and F. Vries. "Statistical approach in power cables diagnostic data analysis." *IEEE Transactions on Dielectrics and Electrical Insulation*, vol. 15, no. 6, pp. 1559–1569, Dec. 2008.

[5] R. Goodwin. *A Handy Guide to the Safe Over-Voltage Pressure Testing and Diagnostic Monitoring of Cable Installations*. H.V. Test, Johannesburg, South Africa, Sept. 2010.

[6] N. Ahmed, O. Morel, and N. Srinivas. "Partial discharge measurement in transmission-class cable terminations." In *1999 IEEE Transmission and Distribution Conference*, vol. 1, pp. 2–7. New Orleans, USA, Apr. 1999.

[7] Y. Jiang, H. Min, J. Luo, Y. Li, X. Jiang, R. Xia, and W. Li. "Partial Discharge Pattern Characteristic of HV Cable Joints with Typical Artificial Defect." In *2010 Asia-Pacific Power and Energy Engineering Conference (APPEEC)*, pp. 1–4. Chengdu, China, Mar. 2010.

[8] T. Neier, A. Gerstner, and M. Jenny. "Identification of joints affected by water ingress in complex hybrid MV cable networks: 2 Field examples of combined VLF withstand testing, with Tan Delta (TD) and Partial Discharge(PD) diagnostics." In *2012 International Conference on Condition Monitoring and Diagnosis (CMD)*, pp. 1018–1022. Bali, Indonesia, Sept. 2012.

[9] E. Gulski, J. Smit, P. Seitz, B. Quak, F. Petzold, and F. de Vries. "Novel Solutions in On-site Diagnosis for Distribution Power Cables." In *XVth International Symposium on High Voltage Engineering*. Ljubljana, Slovenia, Aug. 2007.

[10] J. Rush. "Partial discharge testing and AC characterization of HV connectors and terminations." In *2010 IEEE International Conference on Power Modulator and High Voltage (IPMHVC)*, pp. 521–525. Atlanta, USA, May 2010.

[11] "IEEE Std 400-2012: Guide for Field Testing and Evaluation of the Insulation of Shielded Power Cable Systems Rated 5 kV and Above." *IEEE Std 400-2012*, pp. 1–54, June 2012.

[12] Aberdare Cables. "Vultex XLPE Medium Voltage Electric Cable - 6,6kV-33kV." Brochure. URL http://www.aberdare.co.za/sites/default/aberdare_cables/files/brochures/427/brochures_427.pdf. [Last Accessed Jan. 6, 2016].

[13] R. Arora and W. Mosch. *High Voltage and Electrical Insulation Engineering*. IEEE Press Series on Power Engineering. Wiley, 2011.

[14] J. K. E. Kuffel, W. S. Zaengl. *High Voltage Engineering Fundamentals Second Edition*. Oxford, United Kingdom: Butterworth-Heineman, 2000.

[15] D. Cornish. *Characterising Electrical Trees in Nanocomposite Epoxy-resin using Partial Discharge Detection Methods*. Master's thesis, University of the Witwatersrand, 2014.

[16] "IEC Std 60270: High Voltage Test Techniques - Partial Discharge Measurements." *IEC Std 60270*, pp. 1–44, 2000.

[17] G. Stone. "Partial discharge diagnostics and electrical equipment insulation condition assessment." *IEEE Transactions on Dielectrics and Electrical Insulation*, vol. 12, no. 5, pp. 891–904, Oct. 2005.

[18] E. Gulski and F. Kreuger. "Computer-aided recognition of discharge sources." *IEEE Transactions on Electrical Insulation*, vol. 27, no. 1, pp. 82–92, Feb. 1992.

[19] F. H. Kreuger. *Discharge Detection in High Voltage Equipment*. London, United Kingdom: Temple Press Books Ltd, 1964.

[20] P. O'Hallaran. Personal Communication, Jan. 2013.

[21] R. Strobl, W. Haverkamp, G. Malin, and F. Fitzgerald. "Evolution of stress control systems in medium voltage cable accessories." In *2001 IEEE/PES Transmission and Distribution Conference and Exposition*, vol. 2, pp. 843–848. Atlanta, USA, 2001.

[22] R. Bartnikas. "Partial discharges. Their mechanism, detection and measurement." *IEEE Transactions on Dielectrics and Electrical Insulation*, vol. 9, no. 5, pp. 763–808, Oct. 2002.

[23] B. Rao and K. Mallikarjunappa. "Assessment of water logged cables by very low frequency tan delta testing technique." In *2012 IEEE 10th International Conference on the Properties and Applications of Dielectric Materials (ICPADM)*, pp. 1–4. Bangalore, India, July 2012.

[24] M. I. Qureshi, A. Al-Arainy, and N. H. Malik. "Effect of Accelerated Laboratory Aging on Selected Electrical Properties of Medium-voltage Heat Shrink Cable Joints." *Electric Power Components and Systems*, vol. 42, no. 5, pp. 496–506, 2014.

[25] IEEE Insulated Conductors Committee. "Analysis Of Joint Termination Failures On Extruded Dielectric Cables." *IEEE Transactions on Power Apparatus and Systems*, vol. PAS-103, no. 12, pp. 3464–3469, Dec. 1984.

[26] K. Rethmeier, P. Mohaupt, V. Bergmann, W. Kalkner, and G. Voigt. "New Studies on PD Measurements on MV Cable Systems at 50Hz and Sinusoidal 0.1 Hz (VLF) Test Voltage." In *19th International Conference on Electricity Distribution*. Vienna, Austria, May 2007.

[27] W. Wang, X. Cheng, C. Liu, Z. Yang, H. Huang, and Q. Xue. "Study on the frequency spectrums of acoustic emission PD signals in XLPE cable accessories." In *CMD 2008 International Conference on Condition Monitoring and Diagnosis*, pp. 1246–1249. Beijing, China, Apr. 2008.

[28] S. Tokunaga, T. Tsurusaki, Y. Arief, S. Ohtsuka, T. Mizuno, and M. Hikita. "Partial discharge characteristics till breakdown for XLPE cable joint with an artificial defect." In *Proceedings of the 7th International Conference on Properties and Applications of Dielectric Materials, 2003*, vol. 3, pp. 1206–1209. Nagoya, Japan, June 2003.

[29] Y. Wang, Y. Wang, C. Wang, and H. Xu. "The partial discharge characteristic of typical XLPE cable insulation defects under damped oscillating voltage." In *2014 IEEE Electrical Insulation Conference (EIC)*, pp. 290–293. Philadelphia, USA, June 2014.

[30] W. Kalkner, D. Pepper, and K. Rethmeier. "PD-Testing of Service Aged Joints in XLPE-insulated Medium Voltage Cables at Test Voltages with Variable Shape and Frequency." In *13th International Symposium on High Voltage Engineering*. Delft, Netherlands, 2003.

[31] Tyco Electronics. "Heat-Shrinkable Termination System for Cables up to 36 kV." Brochure, 1984. URL http://www.te.com/content/dam/te-com/documents/energy/global/productdocuments/energy-cable-accessories-epp1984-eng.pdf. [Last Accessed Jan. 6, 2016].

[32] W. Thue. *Electrical Power Cable Engineering*. Boca Raton, USA: CRC Press, 2001.

[33] M. Roets. *Cable Jointing and Termination Course (Medium Voltage)*. H.V. Test, Johannesburg, South Africa, Aug. 2014.

[34] "IEEE Std 400.3-2006: Guide for Partial Discharge Testing of Shielded Power Cable Systems in a Field Environment." *IEEE Std 400.3-2006*, pp. 1–44, Feb. 2007.

[35] "IEEE Std 400.2-2013: Guide for Field Testing of Shielded Power Cable Systems Using Very Low Frequency (VLF)(less than 1 Hz)." *IEEE Std 400.2-2013*, pp. 1–60, June 2013.

[36] "SANS 1339:2010: Electric cables Cross-linked polyethylene (XLPE) insulated cables for rated voltages 3,8/6,6 kV to 19/33 kV." *SANS 1339:2010*, pp. 1–55, 2015.

[37] S. D. Pawar, P. Murugavel, and D. M. Lal. "Effect of relative humidity and sea level pressure on electrical conductivity of air over Indian Ocean." *Journal of Geophysical Research: Atmospheres*, vol. 114, no. D2, 2009.

[38] J. Walker and A. Wolmarans. "Electrical stress distribution in cable accessories when testing at different frequencies." In *2010 International Conference on High Voltage Engineering and Application (ICHVE)*, pp. 152–155. New Orleans, USA, Oct. 2010.

[39] K. Väkeväinen. *The effect of material properties to electric field distribution in medium voltage medium voltage underground cable accessories*. Ph.D. thesis, Arcada University of Applied Sciences, Helsinki, Finland, 2010.

[40] Y. Irani, A. Lapthorn, and P. Bodger. "A Comparison of VLF and 50 Hz Field Testing of Medium Voltage Cables." In *EEA Conference & Exhibition*. Auckland, New Zealand, 2003.

[41] P. Voigt, G; Mohaupt. "Partial Discharge Measurements on Service Aged Medium Voltage Cables at Different Frequencies." In *Jicable*. Paris, France, 2003.

[42] F. Mauseth, E. Ildstad, M. Selsjord, and R. Hegerberg. "Quality Control of Extruded HVDC Cables: Low Frequency Endurance Testing of Model Cables with Contaminants." In *2010 International Conference on High Voltage Engineering and Application (ICHVE)*. New Orleans, USA, 2010.

[43] L. Niemeyer. "A generalized approach to partial discharge modeling." *IEEE Transactions on Dielectrics and Electrical Insulation*, vol. 2, no. 4, pp. 510–528, Aug. 1995.

[44] R. Bodega, P. Morshuis, M. Lazzaroni, and F. Wester. "PD recurrence in cavities at different energizing methods." *IEEE Transactions on Instrumentation and Measurement*, vol. 53, no. 2, pp. 251–258, Apr. 2004.

[45] C. Forssen and H. Edin. "Partial discharges in a cavity at variable applied frequency part 1: measurements." *IEEE Transactions on Dielectrics and Electrical Insulation*, vol. 15, no. 6, pp. 1601–1609, Dec. 2008.

[46] R. Miller and I. Black. "Partial Discharge Measurements over the Frequency Range 0.1 Hz to 50 Hz." *IEEE Transactions on Electrical Insulation*, vol. EI-12, no. 3, pp. 224–233, June 1977.

[47] F. Wester, E. Gulski, and J. Smit. "Detection of Partial Discharges at Different AC Voltage Stresses in Power Cables." *IEEE Electrical Insulation Magazine*, vol. 23, no. 4, pp. 28–43, July 2007.

[48] H. Illias, T. S. Yuan, A. Bakar, H. Mokhlis, G. Chen, and P. Lewin. "Partial discharge patterns in high voltage insulation." In *2012 IEEE International Conference on Power and Energy (PECon)*, pp. 750–755. Kota Kinabalu, Malaysia, Dec. 2012.

[49] F. Kreuger. *Partial discharge detection in high-voltage equipment*. Oxford, United Kingdom: Butterworths, 1989.

[50] K. Rethmeier, P. Mohaupt, P. Bergmann, W. Kalkner, and G. Voigt. "New Studies on PD Measurements on MV Cable System at 50 Hz and Sinusoidal 0.1 Hz (VLF) Test Voltage." In *19th International Conference on Electricity Distribution*. Vienna, Austria, 2007.

[51] D. W. Gross and M. Soller. "On-site Partial Discharge Testing of Distribution Class Cables using VLF and Power Frequency Excitation." In *Jicable*. Paris, France, 2007.

[52] C. Forssen and H. Edin. "Modelling of a discharging cavity in a dielectric material exposed to high electric fields." In *The COMSOL Multiphysics User's Conference*, pp. 1–6. Stockholm, Sweden, 2005.

[53] C.-S. Kim, T. Kondo, and T. Mizutani. "Change in PD pattern with aging." *IEEE Transactions on Dielectrics and Electrical Insulation*, vol. 11, no. 1, pp. 13–18, Feb. 2004.

[54] F. Gutfleisch and L. Niemeyer. "Measurement and simulation of PD in epoxy voids." *IEEE Transactions on Dielectrics and Electrical Insulation*, vol. 2, no. 5, pp. 729–743, Oct. 1995.

[55] D. Pepper. "PD-measurements on typical defects on XLPE-insulated cables at variable frequencies." In *10th Symposium on High Voltage Engineering*. Montreal, Canada, 1997.

[56] G. Paoletti and A. Golubev. "Partial discharge theory and applications to electrical systems." In *Record of 1999 Annual Pulp and Paper Industry Technical Conference*, pp. 124–138. Seattle, WA, USA, June 1999.

Appendix A

ISH 2015 PUBLICATION

A paper covering the base research needed to complete this research report, entitled "Partial Discharge Patterns of Typical Installation Defects in MV Power Cable Terminations", is presented in this appendix. The paper was published in the proceedings of the 19th International Symposium on High Voltage Engineering 2015.

The 19th International Symposium on High Voltage Engineering, Pilsen, Czech Republic, August, 23 – 28, 2015

Partial Discharge Patterns of Typical Installation Defects in MV Power Cable Terminations

D.A. Fynes-Clinton [1*], D.R. Cornish[1] and C. Nyamupangedengu[1]
[1]School of Electrical and Information Engineering, University of the Witwatersrand, Johannesburg, South Africa
*Email: daniel.fynes-clinton@students.wits.ac.za

Abstract: The partial discharge patterns of three typical defects in MV cable terminations were characterised. The defects included a semi-conductor feather, a tram line in the cross-linked polyethylene insulation and a ring cut in the cross-linked polyethylene. Terminations were prepared with these artificial defects and subjected to a standard overvoltage test, during which partial discharge activity was monitored. All the defects passed the voltage test, despite some showing significant discharges. The semi-conductor feather defect exhibited partial discharge behaviour resembling a corona-like discharge. The tram line defect had a discharge pattern consistent with that of a narrow cavity, and the ring cut showed a flat cavity partial discharge pattern. Partial discharge magnitudes of the semi-conductor feather were found to increase with increasing applied voltage, consistent with surface discharge behaviour. In contrast, the tram line and ring cut defects showed constant discharge magnitudes with increasing voltage, thereby verifying the two defects as void discharges. The results showed that common installation defects in MV cable terminations can be characterised using partial discharge measurements.

1 INTRODUCTION

The mining industry in South Africa is one of the biggest in the world, accounting for a large percentage of the gross domestic product (GDP) annually. As a result, there is a large demand for medium voltage (MV) equipment such as motors, transformers, circuit breakers and cables. A consequence of this, is the demand for a reliable power network supported by its cable system. Cross-linked polyethylene (XLPE) cables are typically employed in South African mining operations due to their superior electrical and thermal characteristics [1].

A number of independent cable failure analysis studies have shown that a high percentage of cable failures result from accessory faults [2, 3]. According to the State Grid Electric Power Research Institute in China, as high as 70% of cable failures resulted from cable accessory faults [2]. In a cable accessory fault analysis conducted by the National Electric Energy Testing Research and Applications Center (NEETRAC) of the USA, it was found that cable accessories account for nearly half of the cable failures of the utilities involved in the study [3]. The accessories, which included joints, terminations and junctions, have shown a steady increase in the percentage of total cable failures since the 1970s [3]. The leading cause of these cable accessory faults was poor workmanship with 49% of the total failures, while manufacturing problems and dielectric breakdown only accounted for 24% combined [3].

Power cables along with their accessories should be tested in the field after installation prior to operation as part of an acceptance test, to ensure the cables are free of defects [4]. However, due to factors such as outsourcing, many cable accessories are installed on site by subcontractors rather than by the cable/accessory manufacturers [5]. As a result, poor workmanship due to a lack of installation knowledge and quality awareness, may lead to partial discharges (PD) and dielectric stressing. Therefore, suitable testing procedures are developed to discover evidence justifying the removal of joints/terminations in anticipation of an imminent failure.

While joints and terminations are both important cable accessories, terminations are used more frequently as they are required for all connections to equipment, whereas joints are only used for very long cable sections or damaged cables. Therefore, this paper focuses on XLPE MV terminations. Common defects on MV XLPE cable terminations in a South African context include:

- Semi-conductor layer not removed properly leaving a feather, or removed with a rasp.
- Stress relief tube damaged or cut.
- Mastic tape incorrectly applied or not applied at all.
- XLPE layer cut into, either as a ring cut or tramline, when removing the semi-conductor layer.

This study is aimed at improving the quality control of MV cable terminations, with particular focus on South African mining operations.

PD diagnosis is now a widely accepted method of characterising the condition of electrical insulation. In the literature on PD diagnosis of MV cable accessories, PD magnitudes are in similar ranges across various studies, and resemblance may be drawn between different discharge patterns. It is difficult, however, due to the many factors involved, such as the test voltage and the type of defect, to directly compare and find correlation between results in the literature. Therefore,

continued research into the effect of these different factors may provide useful diagnostic information. While damped oscillating test voltages were used in [6] and [7], power frequency (50/60 Hz) has been the most commonly used test frequency investigated in the literature [2, 5, 8]. However, as highlighted in [5], lower test voltage frequencies such as very low frequency (VLF) (at 0.1 Hz) are more commonly being used for field testing due to test system size and costs. In [5], PD diagnostic results at 0.1 Hz and power frequency showed good comparability for cable accessory testing.

This paper presents test results of an experimental investigation into PD characteristics of typical installation defects in MV cable terminations at VLF (0.1Hz) test voltage.

2 EXPERIMENTAL WORK METHODOLOGY

2.1 Experimental Setup and Procedure

Since the key objective of this research was to characterise artificial defects which pass high voltage installation tests and yet have significant PD activity, a typical overvoltage (withstand) commissioning test was conducted during which PD activity was monitored.

The testing procedure followed the IEC 60270 (VLF PD testing) and IEEE 400 (insulation testing of power cable systems) standards as much as possible. The test circuit is illustrated in Figure 1. According to IEEE 400.3, currently there is no specific standardised test protocol for online/off-line PD testing [9]. The standard does however recommend test voltages and durations, albeit only for power frequency. Typically, PD testing is restricted to 2.0 U_0, where U_0 is the cable operating voltage, in order to accommodate for abnormal operating conditions which the cable may experience, such as an earth fault transient voltage of 1.7 U_0 [4]. However, new cables and accessories may be tested to a maximum of 3 U_0. Therefore, the test procedure involved subjecting the cable to a VLF (0.1 Hz) sine wave at 1.7 U_0 for 30 min, which is the industry standard voltage withstand test according to [1]. The applied voltage was then increased to 2.0 U_0 up until 3.0 U_0 in steps of 0.5 U_0 every ten minutes. The IEEE 400.3 standard specifies a maximum test time of 15 min at power frequency to protect the cable from damage, while ensuring sufficient time for electrons to be available in cavities to initiate PD [9]. However, once the PD magnitude level exceeds that of the acceptable level of the cable (inception voltage), the data should be collected for a maximum of 15 s, while allowing for a record of sufficient data. This procedure was adapted for this research due to the fact that testing was conducted at VLF (0.1 Hz), which has a period of 10 s. Therefore, to ensure collection of sufficient test data, a data collection time of 10 min/60 cycles of the source voltage was used.

An inception/extinction voltage test procedure was conducted for the defects showing PD activity below

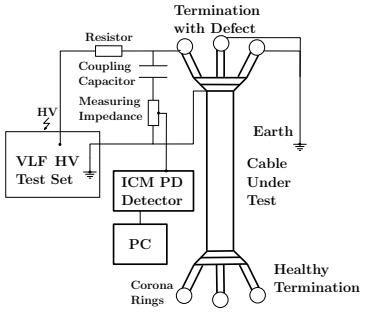

Figure 1: Test Setup for Cable Terminations

11 kV. The voltage was increased in steps of 0.5 kV up until 11 kV and then decreased in the same fashion, allowing for a minimum of three cycles at each voltage level. Inception voltage was defined as the voltage value that the apparent charge rose above the noise floor for three consecutive cycles. Similarly, extinction voltage was defined as the lowest voltage at which the maximum apparent charge was above the noise floor for three consecutive cycles.

2.2 Sample Preparation

The cables under test were 3 core 6.6/11 kV XLPE, 70 mm^2 copper conductors, with individual screening on each core. This choice of MV cable was motivated by its extensive use in the South African mining industry. Furthermore, three-core cables allowed for test results to be compared for adjacent phases with the same configuration (defect) [4]. Properly prepared (defect free) terminations were applied to both sides of two 20 m test cables. The healthy terminations were tested at 50 Hz and verified to have an acceptable PD level below 5 pC at 1.7 U_0, according to South African and International standards [1]. The cables were then cut in half into two 10 m lengths. Each cable length was then terminated with a different artificial defect. For each artificial defect, identical test samples were prepared on two of the cores to ensure verification and reproducibility of the results. The severity of the defect on the third core was increased in order to identify any trends.

2.2.1 Type of Defects

The semi-conductive insulative layers of cables are designed to increase the effective radiating surface area of electrodes and to minimize the electrical stress caused by the transition of electric fields between materials with significantly different dielectric constants [8]. Therefore, any abnormalities or defects introduced in and around the semi-conductive layer may result in excess electrical stresses for which the cable and accessories are not designed. This research focused on defects in the semi-conductive and the XLPE insulation

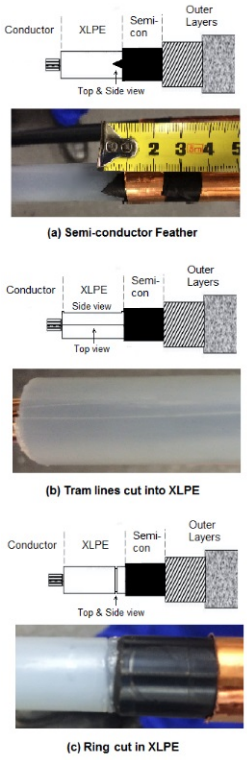

Figure 2: Artificial Termination Defects with Illustrations Adapted from [6]

layers of the terminated cables being tested, namely; a semi-conductor layer feather (Figure 2a), tram lines cut into the XLPE layer (Figure 2b) and a ring cut in the XLPE insulation at the border of the semi-conductive layer (Figure 2c). These defects were chosen due to their relevance in industry, as being some of the most common causes for cable accessory failure. In terms of the artificial defects' dimensions, the following were used for each:

- Semi-conductor feather: Triangular canals with 10 mm base & perpendicular height (core 1&2) and 5 mm base & 25 mm perpendicular height (core 3)
- XLPE tram line: 1 mm deep, 0.4 mm maximum thickness (cores 1&2) and 2 mm deep, 0.6 mm maximum thickness (core 3)
- XLPE ring cut: 1 mm deep, 0.6 mm maximum thickness (cores 1&2) and 2 mm deep, 0.8 mm maximum thickness (core 3)

3 RESULTS AND ANALYSIS

3.1 Results

All the terminations with artificial defects passed the overvoltage commissioning test. The PD characteristics of the terminations at 11 kV (1.7 U_0) are presented in Table 1. The maximum (Qmax) and mean (Qav) apparent charge are averaged values over the 30 min test duration, while the inception/extinction voltages were measured after the overvoltage test. It should be noted that the tests were conducted in a screened room and the noise floor was typically between 1pC and 2pC, which was deemed an acceptable variation between experiments.
The phase resolved PD patterns (PRPDP) of core three of each of the terminations are presented in Figure 3, with their patterns being more pronounced due to their aggravated defects.

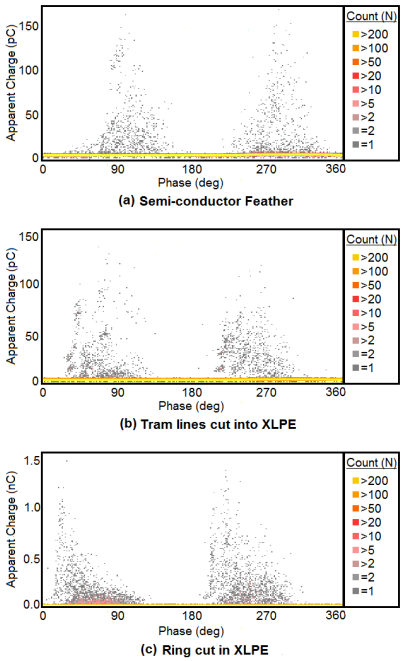

Figure 3: PD Patterns of the Terminations Defects at 11kV

3.2 Results Analysis and Discussion

3.2.1 Semi-conductor Feather Defect
Test specimen 1 with the semi-conductor feather termination (on cores 1 & 2) gave Qav and Qmax values

Table 1: PD Characteristics of the Terminations tested at 11 kV

	Test Specimen 1			Test Specimen 2			Test Specimen 3		
Measured	Semi-conductor Feather			XLPE Tram line			XLPE Ring cut		
Quantities:	Core 1	Core 2	Core 3	Core 1	Core 2	Core 3	Core 1	Core 2	Core 3
Qmax (pC)	6.0	6.5	65.4	18.3	16.5	183.4	408.7	437.2	690.1
Qav (pC)	3.5	3.8	52.9	11.5	11.1	139.7	375.6	371.7	551.6
Inception (kV)	-	-	8.5	10.5	11.0	5.5	4.5	4.5	4.0
Extinction (kV)	-	-	8.5	10.5	11.0	5.0	4.0	4.5	4.0

hardly above the average noise floor. However, the third core with a longer semi-conductor feather defect gave significantly bigger PDs well above the noise floor. This is due to the PD levels of the semi-conductor feather defects being largely determined by the sharpness and length of the feather. The sharpness of the feather results in a more intensified electric field at that point compared to the rest of the semi-conductive layer. The length of the feather also has an influence due to the stress control mastic tape being applied over the XLPE layer typically for 10 mm for this cable type and rating. Therefore, any feathers with a length of less than 10 mm may be masked by the mastic tape.

When the electric field at the surface of the electrode (feather point) exceeds the breakdown strength of the air trapped between the stress control tube/mastic tape and the sharp point, ionisation of the air near the sharp point occurs [10]. The tangential field on the insulation surface reaches a high enough level to initiate PDs along the material's surface. If the applied voltage is increased, the number of electron ionisations increases and electron avalanche can extend further along the material surface [10].

The PRPDP of core 3 of the semi-conductor feather (Figure 3b) resembles that of a corona discharge, with the discharges occurring around the peaks and troughs of the supply voltage (90° & 270°). However, the defect pattern may be differentiated from that of corona discharge in air by the absence of Trichel pulses, which are characteristic of corona. The PD behaviour of the defect is fundamentally that of a surface discharge along the insulation surface adjacent to the semi-conductive tip. The pattern is consistent with patterns found in [10], for a surface discharge between a pin electrode at HV separated from an earth electrode by XLPE, as well as in [2] for metal/semi-conductor particles left on the XLPE of a HV cable joint.

3.2.2 Tram Line Defect

The 1 mm deep tram line defects in test specimen 2 (cores 1 and 2) generated relatively small PD activity compared to the deeper 2 mm tram line in core 3. At 1.7 U_0, all the tram line defects gave PDs of magnitude greater than the 5pC acceptable levels in accordance with the IEC 60502-2 standard. For the 1 mm tram lines, the relatively small PD may be the consequence

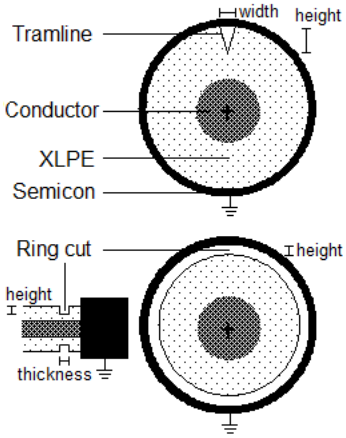

Figure 4: Cross-sections of the Cable Voids

of the mastic tape filling up part of the tram line, as well as due to the stress control tubing and the anti-tracking heat shrink contracting the XLPE insulation upon heating. The significantly bigger PD magnitudes for the 2 mm tramline would therefore be the result of the covering layers not being able to fill the deeper and wider void.

The PRPDP of the 2 mm tramline (Figure 3c) shows PD activity on the rising edges of the applied voltage, with bigger magnitudes just before the test voltage peaks and troughs. This pattern is characteristic of a narrow cavity according to Gulski et al. [11], with a wide distribution of PD about the discharge peaks which occur just before 90° and 270°. A narrow cavity is a void in which the dimension of the cavity perpendicular to the electrodes (height) is much larger than that of the dimension parallel to the electrodes (width). This is illustrated in Figure 4 for both the tram line and ring cut voids in a cross-sectional view.

3.2.3 Ring Cut Defect

The 1 mm deep ring cuts of test specimen 3 (cores 1 and 2) generated similar PD magnitude values, thereby

showing good reproducibility. The ring cut defects showed a much higher PD magnitude than the tram line defects. This is due to the following reasons:

- Ring cut voids had a much larger cross-sectional area between the electrodes, as can be seen in Figure 4.
- The entire ring cut void is in close vicinity to the semi-conductor layer, while in the case of the tram lines, only a short length of the void is near the semi-conductor layer (region of high electric field strength).
- The covering heat shrink products would have little to no effect in contracting the ring cut void.

The PRPDP of the ring cut in (Figure 3c) shows close resemblance to the pattern of a flat cavity investigated in [11]. A flat cavity is the opposite of a narrow cavity with its width being much larger than its height. In the case of a ring cut, the width of the void (dimension parallel to the electrodes) is the circumference of the cable which is much greater than the depth/height (perpendicular to the electrodes) of the cut, as illustrated by Figure 4. The resulting pattern is that of sudden peaks on the rising edges of the voltage source near the zero-crossings. Following these peaks, the PD pattern tapers off to almost zero after the voltage peaks/troughs. The first (large) PD is a streamer-like discharge, which is related to a higher overvoltage due to electronegative gases according to [12], after which the PDs then slowly decrease since the gases are consumed. The PRPDP has a rabbit ear profile [12] and may also be explained by a strong influence of residual charge deposited on the cavity walls. The geometry of the ring cuts make it easier for residual charge to be trapped after each PD event, which in turn affects the magnitude of the subsequent pulse.

3.2.4 PD Inception/Extinction Voltage

The inception and extinction voltages did not provide any unique or distinct trends across the different defects, however, for the same defect type but of different severity, there is a relationship between the PD magnitudes and the inception/extinction voltage. A defect that would give a relatively big PD magnitude had a corresponding relatively low inception/extinction voltage. Therefore, the value of the inception/extinction voltage gives an indication of how big the resulting PDs would be and thus the severity of the defect.

3.2.5 PD Magnitude vs Supply Voltage Magnitude

The apparent charge versus test voltage graph of Figure 5 shows a steady increase in the Qav for increasing test voltage for the semi-conductor feather defect, with insignificant change for the other two types of defects. The same trend was observed for the Qmax and the number of PDs per cycle. For the semi-conductor feather, similar results were found in [10], but for surface discharges. However, for the tram line and ring cut defects, both of which are void-type discharges, there

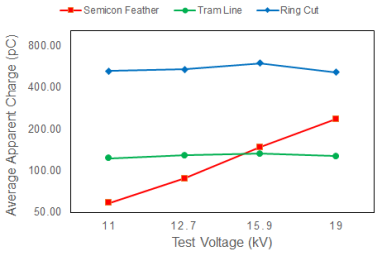

Figure 5: Average Apparent Charge versus Test Voltage

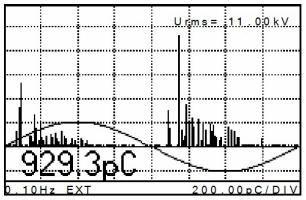

Figure 6: Apparent Charge versus Phase Graph of the Ring Cut at 11kV

was constant apparent charge (average and maximum) for increasing voltage. This outcome is indicative of void discharges, whereby a step increase of charge versus voltage will be observed at the inception voltage, after which the graph plateaus [13].

It can be suggested that the observed manner in which PD magnitudes respond to an increase in test voltage can be used as a distinguishing criterion for different defects.

3.2.6 Positive & Negative half-cycle PRPDP

On average for all three defects, the number and magnitude of the PDs occurring in the negative applied voltage cycle were slightly higher than in the positive cycle. Although difficult to observe on the discharge patterns, this trend is more prevalent in the instantaneous PD charge versus time graphs, such as in Figure 6. This may be attributed to the defects being located closer to the negative electrode, which in this case is the semi-conductive layer at earth potential. As a result, more electrons are readily available from this electrode under negative applied voltage and thus electron avalanches are more easily developed [10]. In the case of a void defect being located in the middle of the XLPE insulation, a symmetrical PRPDP between the positive and negative cycles of the applied voltage would be expected [10]. Furthermore, if the surface discharge was due to a defect on the positive electrode, this should result in a pattern with a higher number of discharges during the positive voltage cycle.

4 CONCLUSION

The partial discharge patterns of three different types of defects in MV cable terminations were investigated, namely; a semi-conductor feather, a tram line in the XLPE insulation and a ring cut in the XLPE. The research was conducted to investigate the PD activity of cable termination defects at VLF which pass typical industry pressure testing, as well as to verify and compare the results of similar studies conducted at other test frequencies. The key findings can be summarised as follows:

1. All the defects passed the overvoltage commissioning test despite showing significant PD.
2. The semi-conductor feather defect showed a corona-like, surface discharge which was the result of the electric field concentrating at the sharp point of the feather.
3. The geometry and discharge pattern of the tram line in the XLPE insulation resembled that of a narrow cavity.
4. The ring cut was confirmed to have a flat cavity discharge pattern with a rabbit ear profile, as a possible result of electronegative gases in the void and/or the influence of residual charge.
5. PD magnitudes of the semi-conductor feather defects (surface discharge) increased with test voltage, while remaining constant for the void discharges, i.e. the tram line/ring cut defects.

The results of this study shows that it is possible to use PD to distinctly characterise common defects in MV cable terminations.

ACKNOWLEDGMENTS

The authors would like to thank Powertech System Integrators and Aberdare Cables for their contribution to this work, in terms of training, donations of terminations and cables, as well as technical support throughout this research. Furthermore, the authors would like to thank B&W Instrumentation and Electrical and RWW Engineering for their donation of cables.

REFERENCES

[1] R. Goodwin, *A Handy Guide to the Safe Over-Voltage Pressure Testing and Diagnostic Monitoring of Cable Installations*, H.V. Test, September 2010.

[2] Y. Jiang, H. Min, J. Luo, Y. Li, X. Jiang, R. Xia, and W. Li, "Partial Discharge Pattern Characteristic of HV Cable Joints with Typical Artificial Defect," in *Power and Energy Engineering Conference (APPEEC), 2010 Asia-Pacific*, March 2010, pp. 1–4.

[3] M. I. Qureshi, A. Al-Arainy, and N. H. Malik, "Effect of Accelerated Laboratory Aging on Selected Electrical Properties of Medium-voltage Heat Shrink Cable Joints," *Electric Power Components and Systems*, vol. 42, no. 5, pp. 496–506, 2014.

[4] "IEEE Guide for Field Testing and Evaluation of the Insulation of Shielded Power Cable Systems Rated 5 kV and Above," *IEEE Std 400-2012 (Revision of IEEE Std 400-2001)*, pp. 1–54, June 2012.

[5] K. Rethmeier, P. Mohaupt, V. Bergmann, W. Kalkner, and G. Voigt, "New Studies on PD Measurements on MV Cable Systems at 50Hz and Sinusoidal 0.1 Hz (VLF) Test Voltage," in *19th International Conference on Electricity Distribution*, May 2007.

[6] W. Wang, X. Cheng, C. Liu, Z. Yang, H. Huang, and Q. Xue, "Study on the frequency spectrums of acoustic emission PD signals in XLPE cable accessories," in *Condition Monitoring and Diagnosis, 2008. CMD 2008. International Conference on*, April 2008, pp. 1246–1249.

[7] E. Gulski, J. Smit, P. Seitz, B. Quak, F. Petzold, and F. de Vries, "Novel Solutions in On-site Diagnosis for Distribution Power Cables," in *XVth International Symposium on High Voltage Engineering*, August 2007.

[8] J. Rush, "Partial discharge testing and AC characterization of HV connectors and terminations," in *Power Modulator and High Voltage Conference (IPMHVC), 2010 IEEE International*, May 2010, pp. 521–525.

[9] "IEEE Guide for Partial Discharge Testing of Shielded Power Cable Systems in a Field Environment," *IEEE Std 400.3-2006*, pp. 1–44, Feb 2007.

[10] H. Illias, T. S. Yuan, A. Bakar, H. Mokhlis, G. Chen, and P. Lewin, "Partial discharge patterns in high voltage insulation," in *Power and Energy (PECon), 2012 IEEE International Conference on*, Dec 2012, pp. 750–755.

[11] E. Gulski and F. Kreuger, "Computer-aided recognition of discharge sources," *Electrical Insulation, IEEE Transactions on*, vol. 27, no. 1, pp. 82–92, Feb 1992.

[12] C.-S. Kim, T. Kondo, and T. Mizutani, "Change in PD pattern with aging," *Dielectrics and Electrical Insulation, IEEE Transactions on*, vol. 11, no. 1, pp. 13–18, Feb 2004.

[13] F. Kreuger, *Partial discharge detection in high-voltage equipment*. Butterworths, 1989.

Appendix B

IEEE Electrical Insulation Magazine Paper

A paper covering the additional research work, entitled "PD Characterisation of XLPE MV Power Cable Termination Defects at VLF (0.1 Hz) and Power Frequency Test Voltages", is presented in this appendix. The paper has been accepted to be published in the July/August 2016 issue of the IEEE Electrical Insulation Magazine.

PD Characterisation of XLPE MV Power Cable Termination Defects at VLF (0.1Hz) and Power Frequency Test Voltages

Key words: partial discharges, XLPE cable termination, VLF, PDPRP, supply voltage frequency

Daniel Fynes-Clinton, Cuthbert Nyamupangedengu
University of the Witwatersrand, Johannesburg
School of Electrical and Information Engineering
Private Bag, 3
Wits 2050
Johannesburg, South Africa

PDPRP of typical installation defects in MV XLPE power cable terminations are similar at VLF and power frequency voltages and yet distinct for each defect type. Apparent PD magnitude and PDIV parameters are generally bigger at power frequency than at VLF.

Introduction

Most power cable faults begin as defects in the cable accessories; terminations, joints and junctions. Poor workmanship is a common cause of the accessory faults [1], [2]. A contributing problem is that power cable accessories are sometimes conveniently assembled manually on site by subcontractors rather than by the cable/accessory manufacturers thereby increasing the risk on compromising quality.

A common practice in checking the quality of a cable system after installation is conducting Hipot (high voltage withstand) tests in accordance with the applicable standards. It is however now known that some faulty cable accessories can easily pass the after-installation Hipot tests and yet would eventually fail well before the anticipated end of life. Hipot commissioning tests should therefore be complemented by other diagnostic tests such as partial discharge (PD) measurements [1], [3].

Partial discharges (PD) in power cable accessories

Since most of power cable accessory installation defects produce partial discharges when a voltage is applied, PD diagnosis has become a useful integral part of power cable installations commissioning tests. PD tests can be used to determine whether or not a cable accessory has been properly installed. The after-installation PD measurements are also useful benchmarks for PD trending in the subsequent condition-based maintenance of the cable system. In PD diagnosis technology, it is known that many typical insulation defects can be recognized through the corresponding PD 'signatures' or 'fingerprints'. In 1968, Cigré published a brochure of typical insulation defects and the corresponding typical PD signal characteristics [4]. Subsequently through significant contributions by researchers such as Gulski [5], the concept of automatic PD pattern recognition is now an inherent feature in PD diagnosis technology. Since in principle each type of PD source gives a unique PD fingerprint, researchers are interested in correlating typical cable accessory defects with the corresponding PD signatures. Such knowledge enables more accurate diagnosis and prognosis of newly installed cable systems. In that regard, the present paper contributes knowledge focusing on typical installation defects in XLPE medium voltage (MV) power cable terminations that were comparatively tested using power frequency and Very Low Frequency (VLF) excitation voltages.

Types of excitation voltages used in equipment diagnosis - a cursory state of the art review

In order to detect and measure partial discharges in power cable accessories as part of cable systems commissioning tests, an excitation voltage has to be applied. The challenge with power cable systems is that at power frequency, due to the relatively high capacitance of the power cable, the test voltage source has to be capable of supplying high cable charging current. Consequently power cable test sets become costly, heavy and physically big for viable field test applications. In mitigation, alternative cable test voltage sources have been devised such as the VLF [6], tuned series resonant [7] and the Oscillating Voltage Wave also known as the Damped ac Voltage (DAC) [8]. Since offline cable tests are now often conducted at non-power frequency voltages, a major interest among various researchers has been on how partial discharges generated at non-power frequency voltage compare and contrast with those at normal operational power frequency voltage; below are highlights of the key findings in that regard.

In the 70s, contributions by Miller and Black [9], [10] concluded that the behavior of PD in response to the test voltage frequency variations was a function of temperature. Furthermore for air-filled cavities encapsulated in epoxy, the most probable PD magnitude was found to be independent of the test voltage frequency at room temperature (20°C). At a higher temperature (27°C) however, the most probable PD magnitude decreased with decrease in test voltage frequency. The behavior was explained in terms of how the electric field strength in the discharge area becomes more dependent on the material conductivity at lower frequencies. With increase in insulation conductivity at higher temperature, the relative electric field strength in the cavity decreases giving rise to the observed smaller PD pulses. In all cases investigated in [9], the PDIV was generally not responsive to changes in the test voltage frequency.

Subsequent to Miller and Black's work, it has become increasingly necessary to search for more comprehensive understanding of the relationships between the test voltage frequency and diagnostic parameters of insulation [11]. Other researchers have reported that cavity PD magnitudes in cast polyester at VLF were either smaller or equal compared to those at 50 Hz [12], [13]. They also reported that there was a threshold frequency beyond which the discharge magnitudes decreased with increase in frequency. Such findings to some extent correlate with Miller's work. In addition to PD magnitude, other PD parameters such as PD phase-resolved-patterns (PDPRP), PDIV and PD repetition rate are usually also investigated with respect to how they respond to variations in the test voltage frequency.

Another notable contribution is by Forssén and Edin [14]. Among other findings, they concluded that the average PD magnitude decreased with decrease in frequency of the supply voltage but only for the voltage magnitudes slightly above the PDIV. For higher voltages, the PD magnitudes were independent of the test voltage frequency.

While in most of the literature, there are some close correlations in trends between PD characteristics and variations in the test voltage frequency, findings by Cavallin and Montanari [15] are somewhat contrary. They reported that PD magnitudes in air-filled cavities encapsulated in epoxy resin decreased with increase in the test voltage frequency as the frequency was varied from 0.1 Hz to 300 Hz. It is therefore evident that there is not yet consensus on the understanding of how partial discharges behave across different test voltage frequencies for the same defect type and material. It is also noted that despite variations in the experimental findings, many researchers tend to use, Niemeyer's phenomenological model of partial discharge mechanisms in the interpretation of PD measurements [16], [17].

The present work was conceived and conducted to search for incremental knowledge on PD characterization of common installation defects in MV XLPE power cable heat shrink terminations using VLF in comparison with power frequency test voltage. The obtained measurement results are analysed and discussed using Niemeyer's model on PD mechanisms [16[, [17].

Experimental methods

Test specimen preparation

The cable test specimens comprised of 10 lengths of 3-core 70 mm^2 6,6/11 kV XLPE insulated copper conductor with individual screening on each core as shown in Figure 1. Such cable types are extensively used in electrical distribution networks such as power utilities and the mining industry in South Africa.

In making the test specimens, properly prepared (defect free) terminations were installed on both ends of a 20 m long cable. The cable was then subjected to high voltage withstand and partial discharge tests in accordance with the IEEE 400-3 2006 guideline [6] and the IEC 60270 standard [18]. A properly terminated power cable is supposed to withstand 1,7 U_0 voltage for 15 minutes and the PD apparent charge magnitude not to exceed 5 pC [6]. The properly terminated cable would then be cut into two equal pieces of 10 m each with one end properly terminated. The other end would be stripped and terminated but with specific identical defects deliberately introduced in each of the three cores. The procedure was repeated to make a total of 3 lengths of 3-core cable test specimens each with one set of 3 similar defects. On each test specimen, 2 cores had identical defects and this was to check on measurement repeatability. On the third core a similar defect (same geometry) was created but with bigger dimensions to check on the effect of increased severity.

Power cable termination defects that are attributed to poor workmanship include knife cuts into the insulation (ring-cut and tramlines) and semiconducting material protrusions (semicon feather) as depicted and described in Table 1 [19].

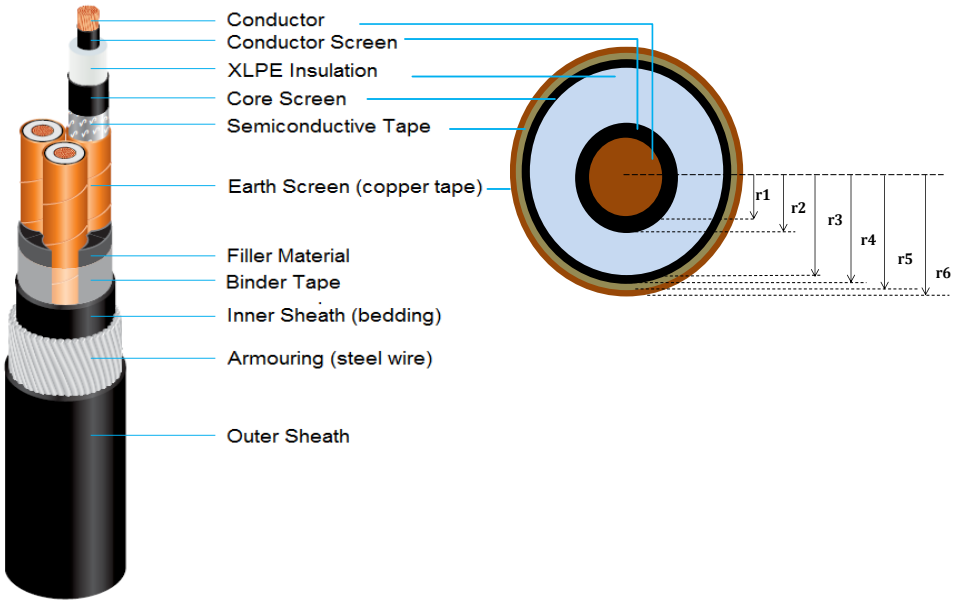

Figure 1. The 3 core 6,6/11 kV XLPE cable used in the experimental investigation where r_1=4.85 mm , r_2=5.45 mm , r_3=8.85 mm , r_4=9.45 mm , r_5=9.55 mm and r_6 =9.65 mm (courtesy of Aberdare Cables™);

Table 1. The artificial defects created in the cable terminations [18]

Ring-cut	*Tramline*	*Semicon feather*
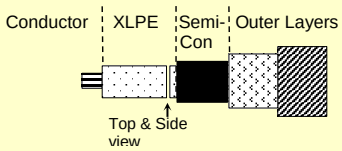	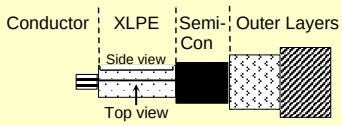	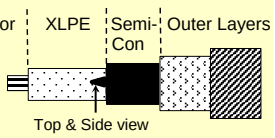
• When stripping off the outer semiconducting layer, the knife edge can cut into the insulation thereby forming a canal along the boundary of the semicon and the insulation. • Geometry: v-shaped air-filled canal • Dimensions: ➢ 1 mm deep, 0,6 mm maximum width (on cores 1 and 2). ➢ 2 mm deep and 0,8 mm maximum width (on core 3).	• While stripping off the outer semiconducting layer, the stripping tool (knife) can rip into the XLPE creating a canal running longitudinal to the exposed insulation surface and ends on the edge of the outer semiconducting layer. • Geometry: v-shaped air filled canal • Dimensions: ➢ 1 mm deep and 0,4 mm maximum thickness (on core 1 and 2). ➢ 2 mm deep and 0,6 mm maximum thickness (on core 3).	• The edges of the outer semiconducting layer are rugged with feather-like protrusions of the outer semiconducting layer. • Geometry: Triangular shape with tip protruding onto the insulation surface. • Dimensions: ➢ 10 mm base and 12,5 mm perpendicular height (on cores 1 and 2). ➢ 5 mm base and 25 mm perpendicular height (on core 3).

Setup and test procedure

In order to measure and record the PD parameters (PDIV, PD apparent charge magnitude and PDPRP) for each defect at VLF and power frequency test voltages, the IEC 60270 [18] PD detection setup was used as depicted in Figure 2.

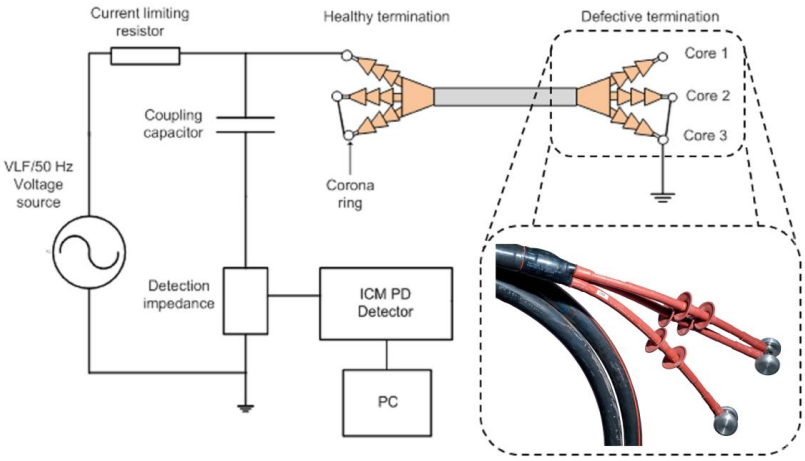

Figure 2. PD measurement setup for various defects in 3-core XLPE power cable terminations

The PD measurements were conducted in a shielded laboratory environment where the noise levels were typically below 1 pC for the 50 Hz tests and 2 to 4 pC for the 0,1 Hz tests. Calibration was done as

specified in the IEC60270 standard [18]. Corona rings were attached onto the conductor end of each core in order to prevent corona inception at the maximum voltage used. For each test specimen, one core was tested at a time while the other two were short circuited and connected to ground on both ends of the cable as shown in Figure 2. The voltage was gradually increased in steps of 0,1 kV up to 11,22 kV_{rms} (1,7 U_0) where it would be held constant for a preset duration while recording the PD data. In order to make meaningful comparisons across the PD data at different excitation voltage frequencies, the corresponding voltage application durations were chosen such that the same number of PD pulses (500 000) would be recorded at 0,1 Hz and at 50 Hz voltages. The test periods were therefore typically about 60 seconds at 50 Hz excitation and 600 seconds (10 min) at 0,1 Hz excitation. Fixing the number of PD pulses also ensured that the specimens were exposed to the same degree of PD-induced ageing and thereby eliminating differences that could arise due to ageing. A second test protocol was also conducted where PD measurements were taken for the same number of voltage cycles; 500 cycles at 50 Hz and 5000 s (~83 min) at 0.1 Hz.

The VLF voltage source was a 60 kV HVA60™ set to give a sinusoidal 0,1 Hz voltage. The PD measurement instrument used was the Power Diagnostix ICMcompact™ linked to a computer. PD quantities; PDPRP, PD apparent charge magnitude and PDIV were recorded for each specimen excited at VLF and power frequency. The PDIV was noted as the voltage at which the apparent charge rose above 5 pC, a level significantly above the noise floor, for three consecutive cycles.

Results and discussion

The average apparent charge PD magnitudes (averaged over the test duration) and PDIV test results for the different artificial defects in the power cable terminations under both 50 Hz and 0,1 Hz test voltages are presented in Table 2. The values are for the same number of pulses test protocol. Similar values, typically within variation 10%, were recorded for same number of cycles tests.

Table 2. The measured PD quantities of the termination defects at 0,1 Hz and 50 Hz test voltages

Defect type		Defect severity	Test voltage frequency (Hz)	PDIV (kV)	Average PD magnitude (pC) at 11,2 kV
Ring-cut	Core 1	1 mm deep	50	7	1071
			0,1	4	300
	Core 2		50	8	688
			0,1	4	284
	Core 3	2 mm deep	50	9	1647
			0,1	4	491
Tramline	Core1	1 mm deep	50	11	7
			0,1	9	8
	Core 2		50	No PD detected above the noise level	
			0,1	11	7
	Core 3	2 mm deep	50	8	290
			0,1	7	139
Semicon feather	Core 1	10 mm long	50	No PD detected above the noise level	
			0,1		
	Core 2		50		
			0,1		
	Core 3	25 mm long	50	9	160

			0,1	9	69

PD inception Voltage (PDIV) and PD magnitude

With reference to Table 2, for the ring-cut and tramline termination defects, generally the PDIV at power frequency are about twice higher than that at VLF. The average PD magnitudes at power frequency are about double those at VLF for all the defects. Partial discharge magnitude distribution histograms in Figure 3 confirm that at power frequency, PD magnitudes are generally bigger than at VLF. The PD magnitude distribution histograms are for the same number of pulses recorded at power frequency and at VLF excitation voltages. The same trends are obtained for the same number of cycles.

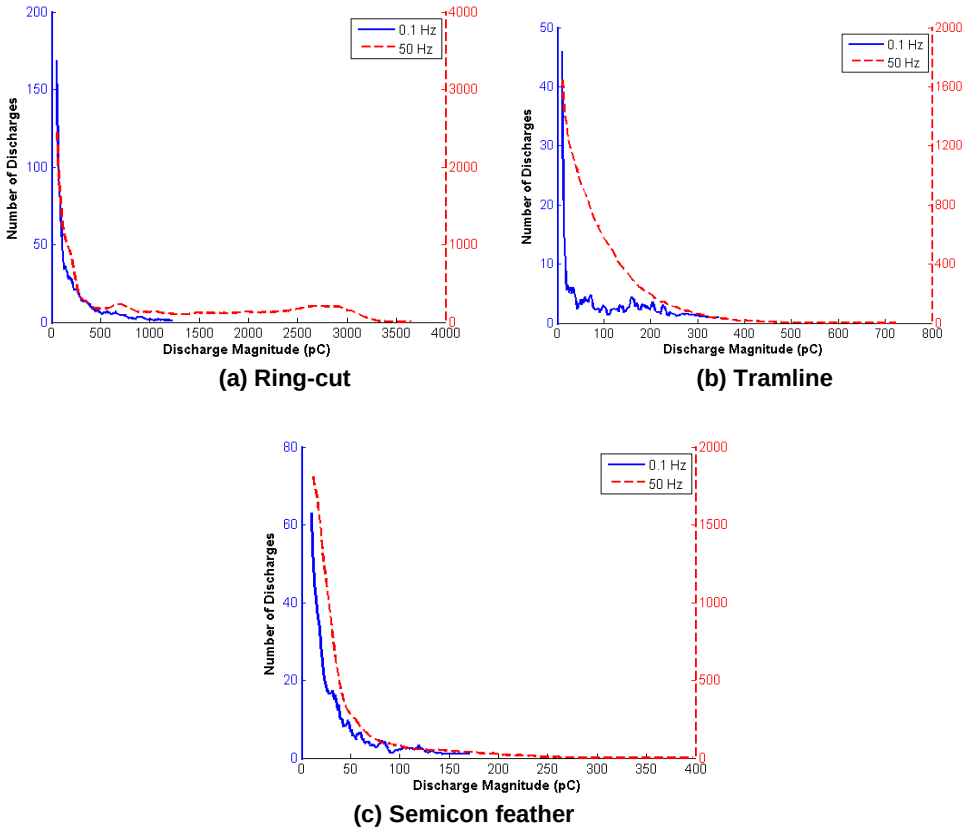

Figure 3. Partial discharge magnitude distribution histograms for the artificial defects in heat shrink MV XLPE power cable terminations; (a) ring-cut, (b) tramline and (c) semicon feather

The observed behavior of PD magnitude and PDIV as a function of the excitation voltage frequency can be explained in terms of the influence of the following parameters on the discharge process; seed electron statistical availability time lag, gap overvoltage (gap overstress) and the rate of increase of the electric field. The well-known conditions for initiation of a discharge avalanche in a gas medium are that the electric field

should be at least equal to a critical threshold value, E_{inc}, and that a seed electron is available at a favourable position to initiate self-sustaining ionization avalanches. As the voltage on the electrodes increases, the corresponding background electric field (E_0) in the discharge gap increases to E_{inc}. If the seed electron does not become available, the background electric field continues to increase beyond E_{inc} at a rate proportional to the frequency of the supply voltage. By the time the seed electron becomes available, E_0 could have exceeded E_{inc} by ΔE_0 (gap overstress) such that the resultant ionisation avalanches occur under the influence of a higher electric field ($E_{inc}+ \Delta E_0$) than E_{inc} as illustrated in Figure 4. The bigger the gap overstress ΔE_0, the bigger the corresponding PDIV and PD magnitude.

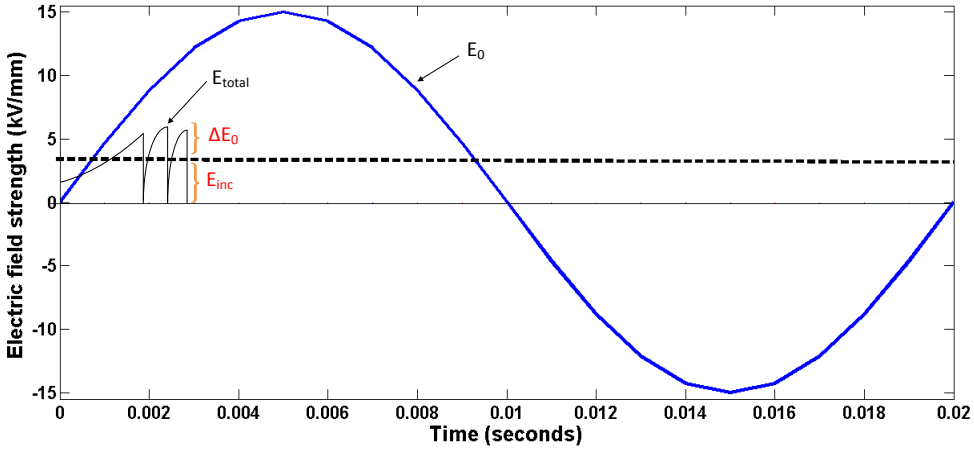

Figure 4. An illustration of the gap overstress phenomenon due to delayed availability of seed electron to initiate PD resulting in increased PD magnitude and PDIV

In cavity discharges such as the ring-cut and tramline defects in the cable terminations investigated in the present work, seed electrons are availed mainly through surface emission mechanisms [16]. Where the rate of rise of the background electric field is relatively high such as at power frequency, the probability that a discharge occurs at relatively high gap overstress, ΔE_0, is higher than at VLF and this translates into bigger PDIV and PD magnitudes as presented in Table 1. Similar results have been reported by other researchers [9], [12]-[14]. These findings suggest that the acceptable PD magnitude limits given in various standards and guidelines should be stated within the context of the corresponding frequency ranges of the excitation voltage.

PD Phase-Resolved-Patterns (PDPRP)

Typical PD phase-resolved-patterns (PDPRP) for the ring-cut, tramline and semicon feather artificial defects in XLPE heat shrink terminations at power frequency and VLF test voltages recorded for the same number of cycles are shown in Figure 5. It is observed that each type of defect has distinct PDPRP. Furthermore for each defect type the PDPRP are the same at power frequency and at VLF although the PD magnitude ranges are different. The PD pulse phase positions are a function of the defect type but independent from the frequency of the supply voltage. The PDPRP presented in Figure 5 also confirm that in all the cases the PD magnitudes are generally bigger at power frequency than at VLF.

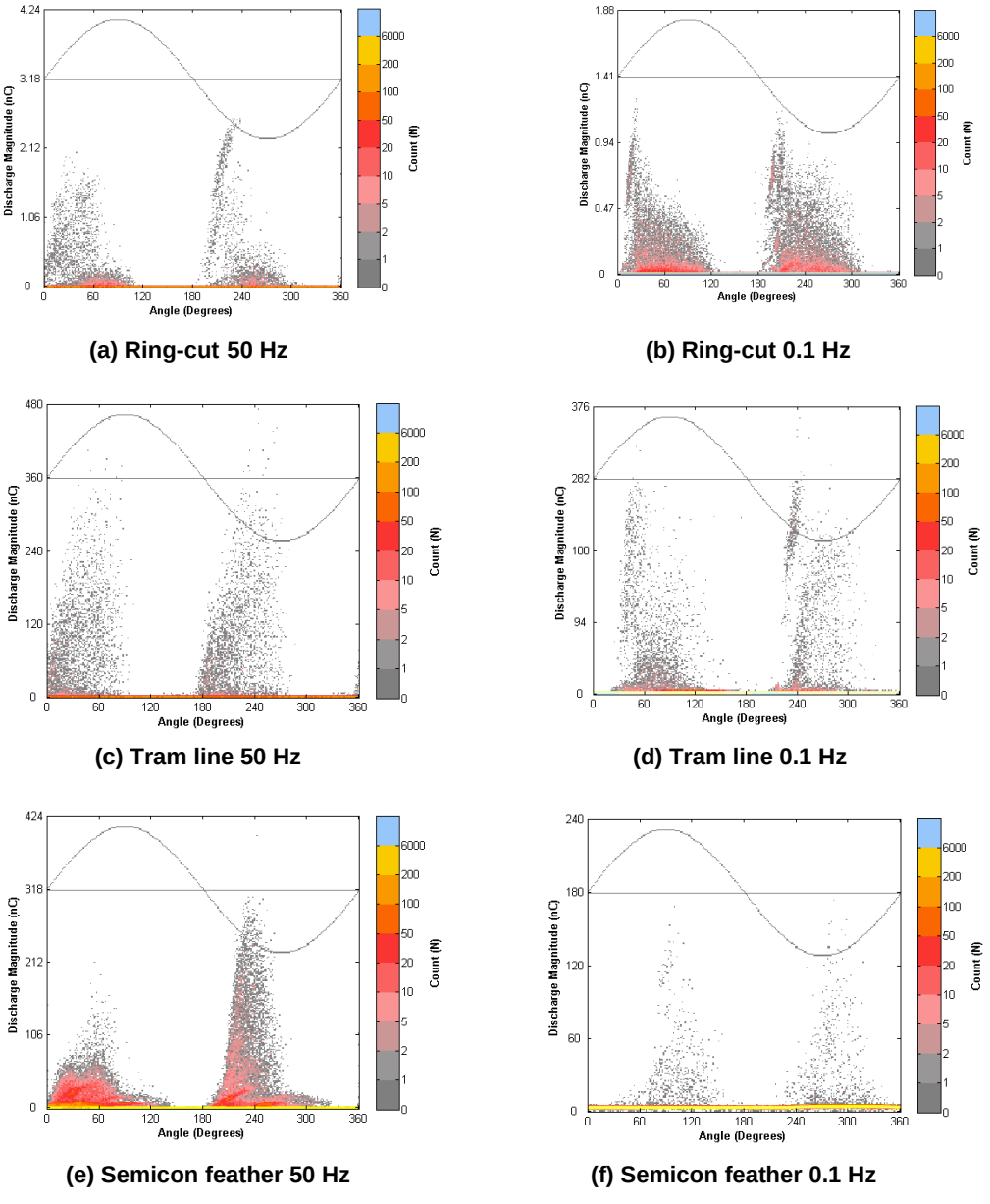

(a) Ring-cut 50 Hz

(b) Ring-cut 0.1 Hz

(c) Tram line 50 Hz

(d) Tram line 0.1 Hz

(e) Semicon feather 50 Hz

(f) Semicon feather 0.1 Hz

Figure 5. PD phase-resolved-patterns of ring-cut; (a) at 50 Hz and (b) at 0.1 Hz, tramline; (c) at 50 Hz and (d) 0.1 Hz and semicon feather; (e) 50 Hz and (f) at 0,1 Hz. power cable heat shrink terminations.

Ring-cut defects give patterns where the PD pulses occupy phase regions 0 to 120^0 in the positive half cycle and 180^0 to 300^0 in the negative half cycle and are characterized by distinct 'rabbit ear like' features. The tramline PDPRP are different from those of the ring-cuts in that the rabbit ears are less prominent and more importantly that the occupied phase regions are narrower than those of ring-cuts, that is, 0 to 70^0 and 180^0 to 270^0 in the positive and negative half cycles respectively. The semicon feather PDPRPs are more distinctly different from both the ring-cut and tramline defects. The occupied phase positions are the widest; 0 to 150^0 and 180^0 to 330^0. The distribution patterns are also close to normal Gaussian distribution. The negative half cycle PDs are more distinctly bigger than those in the positive half cycle in comparison to those of ring and tramline defects.

The observed PDPRP features of the ring-cut, tramline and semicon feather artificial defects in the cable terminations can be explained using the space charge dynamics in the discharge area based on Neimeyer's model [16], [17]. As illustrated in Figure 6, there are three electric fields interacting in the discharge area to give a resultant electric field that when big enough initiates a discharge. How the excitation voltage frequency influences the interaction of the various electric fields in the discharge gap and resultant shaping effect on the PDPRP is illustrated schematically in Figure 6 with corresponding explanations in Table 3.

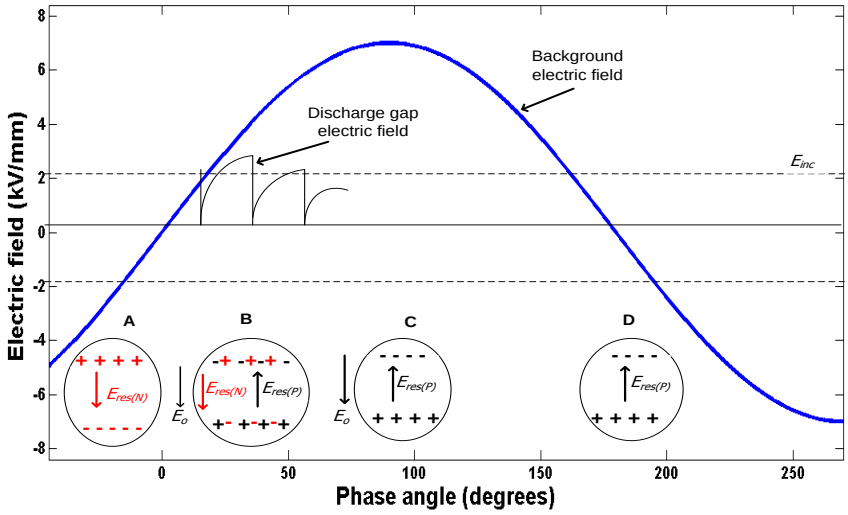

Figure 6. Space charge dynamics in a PD explaining the cause of rabbit ear like feature in the phase-resolved-patterns in ring-cut and tramline defects of MV XLPE power cable terminations [16], [17].

Table 3. The interaction of various electric fields in the discharge gap as a function of the phase position and the resultant effect on the PD

(A): Zero crossing PDs on transition from the negative to positive half cycle	**(B):** Early positive half cycle PDs	**(C):** Late Positive half cycle PDs	**(D):** Zero crossing PDs on transition from the positive to negative half cycle
• $E_{total} = E_{res(N)}$ • If $E_{total} \geq E_{inc}$ and seed electron is available, then PD occurs. • It is notable that PD can occur at zero crossing in the absence of the background electric field but due to the residual charge electric field.	• $E_{total} = E_{res(N)} + E_0 - E_{res(P)}$ • If $E_{total} \geq E_{inc}$ and seed electron is available, then PD occurs. • The additive superposition of $E_{res(N)}$ and E_0 enhances the resultant stress in the discharge gap. • If the statistical time delay t_s of the seed electron does not change, the resultant PD are relatively bigger than in the previous events thereby forming the 'Rabbit ear' part of the rabbit-shaped PDPRP.	• $E_{total} = E_0 - E_{res(P)}$; the space charges from the negative half cycle have completely depleted. • If $E_{total} \geq E_{inc}$ and seed electron is available, then PD occurs. • The absence of $E_{res(N)}$ and reduced rate of increase of E_0 weakens the resultant stress in the discharge gap relative to previous events. • If the statistical time delay t_s of the seed electron does not change, the resultant PDs are relatively smaller than in the previous events thereby forming the 'body' part of the rabbit shaped PDPRP.	• $E_{total} = E_{res(P)}$ • If $E_{total} \geq E_{inc}$ and seed electron is available, then PD occurs. • The sequence of PD events repeat but with the corresponding electric fields polarity being opposite those in the positive half cycle.

The sequence of events labelled A, B, C and D in Figure 6 and corresponding descriptions in Table 3 use symbols defined as follows: $E_{res(N)}$ and $E_{res(P)}$ are the space charge deposited on the insulation surface of the discharge gap by discharge events in the negative and positive half cycles respectively. E_0 is the background electric field in the discharge defect due to the voltage on the test object. E_{total} is the resultant electric field in the discharge defect being the vector sum of all the electric fields present in the discharge gap. When the resultant electric field becomes equal to or bigger than the PD inception stress, E_{inc}, a discharge can occur provided a seed electron is available to initiate the electronic avalanches. $E_{res(N)}$ and $E_{res(P)}$ can be termed the crossover residual electric fields that are responsible for stress enhancement in the discharge gap resulting in the zero-crossing PDs and the rabbit ear shape of the PDPRP. The crossover residual electric field is a function of how much residual charge is retained on the insulation surface of the discharge area which in turn is a function of the defect geometry and the discharge area surface conductivity. The extent of the rabbit ear is therefore dependent on the defect geometry as well as the ageing effects of PD on the discharge area [20].

In the present work, the deeper ring-cut defects in the cable terminations are more favourable to retaining crossover residual charge than the tramline and semicon feather and therefore exhibit more enhanced rabbit ear feature as depicted in Figure 5 (a) and (b). In the semicon feather defect, the geometry is less favourable to trapping of the residual charge compared to the ring-cut and tramline defects that are essentially cavities. Consequently the pulses, like corona [4], [5], are significantly displaced from the zero crossings and occur around the crest and troughs of the excitation voltage, and moreover the PDPRPs do not have the rabbit ear-like features.

The unique relationship between defects and the corresponding PDPRP in power cable terminations suggests possibilities of automatic defect recognition using PD classification techniques. More work may however be necessary to check out on how environmental conditions such as temperature variations may influence the PDPRP. It would also be interesting to know whether the distinct PDPRP could still be recognized in cases where the termination has more than one defect.

Conclusions

Some installation defects in heat shrink terminations on MV XLPE power cables can survive high potential tests but cause partial discharges that progressively degrade the insulation and eventually lead to

premature cable failure. Experimental tests and measurements in the present work have shown that each typical defect such as ring-cut, tramline and semicon feather give distinct phase-resolved-patterns that are essentially invariant whether the test voltage is VLF or power frequency. The PD inception voltage however is lower at VLF than at power frequency. Furthermore with power frequency excitation voltage, partial discharges tend to be generally bigger than at VLF voltage. The findings suggest possibilities of automatic recognition of unknown defects as part of after installation tests of power cable terminations using PD diagnosis techniques at either VLF or power frequency test voltages.

Acknowledgement

This study was supported by the National Research Foundation (NRF), Eskom and the Department of Trade and Industry (DTI), through the direct funding of the University of the Witwatersrand's High Voltage Research group. For this particular research, the authors would like to thank PTSI and Aberdare Cables for their contribution to this work through training, donations of termination material and the cables, as well as technical support throughout this research. Furthermore, the authors would like to thank B&W Instrumentation and Electrical and RWW Engineering for their donation of additional cables.

References

[1] W. Vahlstrom, "Strategies for field testing medium voltage cables", *IEEE Electrical Insulation Magazine*, Vol. 25, No.5, pp. 1-17, 2009.

[2] H. E. Orton, "Diagnostic testing of in-situ power cables - an overview", *IEEE/PES Transmission and Distribution Conference and Exhibition: Asia Pacific*, Yokohama, Japan, Vol. 3, pp. 1420-1425, 2002.

[3] *Guide for Field Testing and Evaluation of the Insulation of Shielded Power Cable Systems Rated 5 kV and Above*, IEEE Std 400-2012, 2012, pp. 1-54.

[4] *Recognition of discharges*, Cigré, Electra, No. 11, pp. 61-98, 1969.

[5] E. Gulski, "Computer-aided measurement of partial discharges in HV equipment", *IEEE Transactions on Electrical Insulation*, Vol. 28, No.6, 969-983, 1993.

[6] *Guide for Field Testing of Shielded Power Cable Systems Using Very Low Frequency* (VLF) (Less than 1 Hz), IEEE Std 400.2, 2013, pp. 1-49.

[7] W. Hauschild and E. Lemke, *High-Voltage Test and Measuring Techniques*, Springer-Verlag Berlin Heidelberg, 2014.

[8] E. Gulski, J. J. Smit, F. J. Wester and P. N. Seitz, "Transmission power cables PD detection at Damped AC voltages", *IEEE International Symposium on Electrical Insulation*, Indianapolis, Indiana, USA, pp. 462-465, 2004.

[9] R. Miller and I. A. Black, "Partial Discharge Measurements Over the Frequency Range 0.1 Hz to 50 Hz" , *IEEE Transactions on Electrical Insulation*, Vol. EI-12, No. 3, pp. 324-333,1977.

[10] R. Miller and I. A. Black, "Partial discharge energy measurements on electrical machine insulation when energised at frequencies between 0.1 Hz and power frequency", *IEEE Transactions on Electrical Insulation*, Vol. EI-14, No. 3, pp.127-135, 1979.

[11] E. Gockenbach and W. Hauschild, "The selection of frequency range for high-voltage on-site testing of extruded insulation cable systems", *IEEE Electrical Insulation Magazine*, Vol. 16, No.6, pp. 11-16, 2000.

[12] F. J. Wester, E. Gulski and J. J. Smit,"Detection of partial discharges at different AC voltage stresses in power". *IEEE Electrical Insulation Magazine*, Vol. 23, No. 4, pp. 28-43, 2007.

[13] R. Bodega, P. H. Morshuis, M. Lazzaroni and F. J. Wester, "PD recurrence in cavities at different energising methods". *IEEE Transactions on Instrumentation and Measurement*, Vol. 53, No. 2, pp. 251-258, 2004.

[14] C. Forssen, and E. Edin, "Partial discharges in a cavity at variable applied frequency Part 1: Measurements". *IEEE Transactions on Dielectrics and Electrical Insulation*, Vol. 15, No. 6, pp. 1601-1609, 2008.

[15] A. Cavallini and G. C. Montanari, "Effect of supply voltage frequency on testing of insulation system", *IEEE Transactions on Dielectrics and Electrical Insulation*, Vol. 13, No. 1, pp. 111-121, 2006.

[16] L. Niemeyer, "A generalized approach to partial discharge modeling ", *IEEE Transactions on Dielectrics and Electrical Insulation*, Vol. 2, No.4, pp. 510-527, 1995.

[17] F. Gutfleisch and L. Niemeyer, "Measurement and simulation of PD in epoxy voids", *IEEE Transactions on Dielectrics and Electrical Insulation*, Vol. 2, No.5, pp. 729-743, 1995.

[18] *High voltage test techniques - Partial discharge measurements*, IEC std. 60270, 2000.

[19] D. Pepper, "PD-measurements on typical defects on XLPE-insulated cables at variable frequencies," *10th International Symposium on High Voltage Engineering (ISH)*, Montreal, Canada, 1997.

[20] C. S. Kim, T. Kondo and T. Mizutani, "Change in PD pattern with ageing", *IEEE Transactions on Dielectrics and Electrical Insulation*, Vol. 11, No. 1, pp. 13-18, 2004.



Daniel Fynes-Clinton was born in Johannesburg, South Africa in 1991. He received the B. Sc. degree in electrical Engineering from University of Witwatersrand in the year 2013. He is currently studying at the same university and is pursuing the M. Sc. degree in electrical engineering. The work presented in this paper forms a large portion of his masters research report. His research interests include high voltage testing and new developments in electronics.



Cuthbert Nyamupangedengu was born in Zimbabwe. He received the Bachelors honours degree in electrical engineering from the University of Zimbabwe in 1994. At the University of the Witwatersrand, Johannesburg, in 2004, he was awarded the M.Sc. Engineering (with distinction) and in 2011, the Ph.D. He is an associate professor at the University. Before moving to the University of the Witwatersrand, Cuthbert was an engineer in the Zimbabwe Electricity Supply Authority from 1995 to 2005 in various capacities mainly in power system planning and development. His passion is research on development and diagnosis of high voltage insulation.